BRNO UNIVERSITY OF TECHNOLOGY

VYSOKÉ UČENÍ TECHNICKÉ V BRNĚ

CENTRAL EUROPEAN INSTITUTE OF TECHNOLOGY BUT

STŘEDOEVROPSKÝ TECHNOLOGICKÝ INSTITUT VUT

THE INFLUENCE OF MODIFIED TiO_2 NANOTUBES ON BIOINTERFACIAL INTERACTION

VLIV MODIFIKOVANÝCH TiO_2 NANOTRUBIČEK NA INTERAKCE NA BIOROZHRANÍ

DOCTORAL THESIS
DIZERTAČNÍ PRÁCE

AUTHOR — **Ing. Ondřej Bílek**
AUTOR PRÁCE

SUPERVISOR — **Mgr. Zdenka Fohlerová, Ph.D.**
ŠKOLITEL

BRNO 2021

ABSTRAKT

Nanotrubičky oxidu titaničitého v průběhu posledních let nabyly na významu v poli biomedicíny. Jakožto biokompatibilní nanostrukturovaný povrch nachází potenciál pro své uplatnění především v oblasti implantačních aplikací. Teoretická část této práce je tak věnována různým přístupům pro syntézu TiO_2 nanotrubiček, jejich modifikacím a aplikacím v biomedicíně. Experimentální část pak pojednává o nanotrubičkách oxidu titaničitého, které jsou připraveny z titanu metodou jednokrokové anodické oxidace v organickém elektrolytu. Jako výchozí materiály jsou používány křemíkové disky s naprášenou vrstvou titanu a titanové folie. Zprvu amorfní nanotrubičky jsou žíháním převedeny na svou krystalickou podobu, a následně modifikovány selenovými a stříbrnými nanočásticemi. Připravené struktury jsou zkoumány z hlediska povrchových vlastností a biologických interakcí s vybranými tkáňovými kulturami (MG-63, NIH-3T3) a bakteriemi (*E. coli, P. aeruginosa, S. aureus)*. V závěru experimentální práce jsou stručně porovnány výsledky selenových a stříbrných nanočástic. Hlavním cílem této práce je rozšířit znalosti týkající se bio-rozhraní tvořeným adherentními buněčnými liniemi, bakteriálními buňkami a nanostrukturovaným povrchem tvořeným TiO_2 nanotrubičkami dekorovanými selenovými a stříbrnými nanočásticemi.

KLÍČOVÁ SLOVA: TiO_2 nanotrubičky, anodická oxidace, selenové nanočástice, stříbrné nanočástice, antibakteriální aktivita, cytokompatibilita, povrchové modifikace

ABSTRACT

Over the past few years, titanium dioxide nanotubes have become increasingly important in biomedicine. As a biocompatible nanostructured surface, it finds the potential for its application especially in the field of implant applications. The theoretical part of this thesis, therefore, deals with options for TiO_2 nanotube preparation, and their use as a biomedical material. The review of conducted studies includes bare, surface-modified and doped nanotubes. The experimental part discusses titanium dioxide nanotubes, which are prepared from titanium by a one-step anodic oxidation method in an organic electrolyte. Titanium-sputter-deposited silicon wafers and titanium foils are used as a substrate. The initially amorphous nanotubes are annealed, and subsequently modified with selenium and silver nanoparticles. The prepared structures are studied in terms of surface properties, and biological interactions with selected tissue cells (MG-63, NIH-3T3) and bacteria (*E. coli, P. aeruginosa S. aureus*). The final part of experimental work is dedicated to brief comparison of selenium and silver nanoparticle modified TiO_2 nanotubes. The main aim of this thesis is to extend the knowledge regarding the bio-interface formed by adherent cell lines, bacterial cells, and selenium/silver modified TiO_2 nanotubes.

KEYWORDS: TiO_2 nanotubes, anodic oxidation, selenium nanoparticles, silver nanoparticles, antibacterial activity, cytocompatibility, surface modifications

BIBLIOGRAPHIC CITATION:

BÍLEK, O. *The influence of modified TiO_2 nanotubes on biointerfacial interaction.* Brno: Brno University of Technology, Central European Institute of Technology BUT, 2021, 109 p., Supervisor: Mgr. Zdenka Fohlerová, Ph.D.

DECLARATION

I certify that the work presented in this thesis was performed independently, under the supervision of Mgr. Zdenka Fohlerová Ph.D. All technical literature and other sources of information are properly cited in the text and listed in reference list.

Brno…… …….

(author's signature)

ACKNOWLEDGEMENTS

First, I would like to thank my supervisor, Mgr. Zdenka Fohlerová Ph.D. Under her leadership I acquired both my bachelor's and master's degree, and now I am (hopefully) on my way to acquire a Ph.D. It has been a long journey, and if I were to describe it, it wasn't a sunny walk on a nicely paved road. It was more like adventurous journey through freshly ploughed land, grown fields, deserts, thick forests and sky-high mountains. At several points I felt too heavy to continue. I doubted my very own decisions, that were made on this journey. I even thought about making it stop and quit. I believe it was not easy for you either. I am truly grateful, for you walking me through this mess without dumping me in the nearest river, or simply leaving me by the road. And now, finally, here we are. With this, I thank you from the bottom of my heart, for your valuable advice, methodological and pedagogical support. I thank you for your patience, for correcting my bad ideas, and approving the good ones. To put it simply, I thank you for your guidance through all my studies.

Next, I would like to thank all my colleagues from our group for their fruitful discussions that always helped me move in the right direction. I thank them for their smiles that helped me make it through the day and keep it positive. I would like to namely thank Tomáš Lednický for his Chinese-food days where the best-spicy-soup-ever-made put a smile on my face and calmed my mind, and for his table tennis games that helped me relax when I was unable to focus. I would like to thank Martina Gaňová for companionship and chemical expertise in innovation of laboratory exercises as well as each year of teaching of Electronics and biosensors

Last, but not least, I would also like to thank my family and friends. There are too many names to be mentioned, and not enough space, so I decided not to write any specific names. To you all - I know that at times, sharing your time with a PhD candidate might have felt slightly stressful. Not all days were sunny, nor just cloudy. Some of our shared days felt like they were filled with storms. But even though there were harsh times, you always helped me find a nice, dry, warm place, where we could stay and enjoy ourselves, have fun, and forget about the rain, lightning, and thunder. Thanks to you and your care, at the dawn of each new day, I was able to continue walking my PhD path and struggle, trying to reach the finish line with all my might. With this, I would like to express how truly thankful I am for having such a wonderful, supporting family, thanks to which I am able to stand in the place, where I currently am. I thank you for your vast patience and support, it shall never be forgotten.

Table of Contents

1. Introduction

Thanks to the rise of nanotechnologies over the last few years, nanomaterials are increasingly becoming more common in in everyday parts of or lives. These nanomaterials bring new possibilities to a wide range of different areas – be it the electronics, textile, mechanical, chemical, automotive or healthcare industry. However, hand-in-hand with the trend of technological development goes a significant increase in demands placed on used materials.

This trend applies to materials used in medicine as well. Today's requirements for biomaterials are way more demanding than in the past. Through long-time practice and research, we reached a better understanding of faults carried by materials used for hard tissue replacements. And the rapid progress in nanotechnology finally enabled us to approach the problem from a different perspective and mimic native tissue environment through modifications of individual surface features, such as surface chemistry or topography. These individual aspects can significantly change the interface formed between material surface and tissue cells or bacteria. As a result, we can observe different (bio)responses in terms of, for example, cell adhesion, viability, metabolism, differentiation, and antibacterial activity.

The necessity for the development of novel biomaterials, as well as improvement and enhancement of current ones, stems from the diversity of their applications. Surfaces need to be prepared wisely, with careful consideration for targeted tissue. For example, materials for hard tissue replacements should be favourable for bone cells. On the other hand, it would be inconvenient if implantable devices (that are meant to be removed) would actively ingrow into host tissue. Such a material would be considered unsuitable and inappropriate for this application. The problem is, we currently do not possess sufficient knowledge about fundamental cell-surface interactions between an already extensive range of cell types and variously micro/nanostructured surfaces prepared with a tremendous number of materials.

In order to achieve this knowledge, a lot of basic research focused on fabrication and characterization of individual nanosurfaces needs to be done. In our case, we decided to focus on one single attractive nanomaterial - TiO_2 nanotubes – modified with selenium and silver nanoparticles with variable features (concentrations, stabilizers). TiO_2 nanotubes themselves seem like a promising start, as these can considerably improve cell adhesion, growth, and differentiation[1-3] and could be possibly used as a drug delivery system[4]. Thus, we aim to add another piece to the puzzle revealing the cell-surface interactions with TiO_2 nanotube-based nanomaterials. Hopefully, if we understand their properties and their possible modifications in context with formed cell-surface biointerfaces, we could utilize them when designing implants or medical devices of the future.

2. State of the art

Ever since the first effort to fabricate nanotubular titanium dioxide back in 1984,[5] titania nanotubes gradually became a point-of-interest nanomaterial. Over time, it found potential use in various fields, including technical applications - e.g., photocatalysis, solar cells, electrochromic devices, gas sensing, anti-corrosion surfaces, self-cleaning surfaces - and biomedical applications – e.g., as device/implant coatings and drug or payload delivery systems.[6-8] It is true that some of the mentioned applications are not bound only to nanotubular TiO_2. In fact, bulk titanium dioxide already possesses chemical inertness, corrosion resistance, stability, and biocompatibility.[7] However, with nanofabrication, we can further enhance and improve the performance of TiO_2. In the field of biomedical engineering, this can be, in theory, used to tailor the surface in accordance with required cell-surface interactions based on a detailed design and specific needs of the targeted tissue.[9-14]

Over the past years, many in vitro and in vivo studies demonstrated that cell-surface interactions are highly dependent on nanotube characteristics, such as, e.g., length, diameter, shape, and crystal phase.[7] Subsequent studies focused on optimizing and further modifying TiO_2 nanotubes to promote/demote targeted features, such as antibacterial activity, cell adhesion, proliferation, differentiation, or metabolism.[6-8] However, to achieve desired results additional modification can be necessary in some cases. Improved biological properties can be achieved through modification with specific bioactive compounds, such as, e.g., hydroxyapatite or bone morphogenetic protein 2.[15] Additional improvement in antibacterial activity can be achieved through modification with antibiotics (e.g., vancomycin and gentamycin),[16,17] or metal/metal oxide nanoparticles (e.g., Se, Ag, Au, ZnO).[18-21] Nonetheless, an increase in antibacterial activity can, in some cases, lead to a decrease in biocompatibility.[22] Therefore thorough optimization is necessary, and toxicity towards tissue cells must be taken into consideration when designing biomaterials.

In the first part of this “state of the art” section, general options and possibilities for TiO_2 nanotube preparation and modification will be discussed. The second part will be devoted to a review of the research conducted in the field of TiO_2 nanotubes in biomedicine.

2.1. TiO_2 nanotube fabrication

There are numerous ways to prepare TiO_2 nanotubes. For the sake of clarity, we divided fabrication approaches into three main groups - template-assisted methods, hydro/solvothermal methods, and anodic oxidation methods.

2.1.1. Template-assisted methods

Summary

The first group consists of methods using templates as a stepstone for nanotube formation. A common template can be made of e.g., ordered alumina surface. The TiO_2 can be subsequently deposited into the template, to form a nanotubular structure.[8] To provide an example, the first recorded attempt in history utilized electrodeposition of TiO_2 from $TiCl_3$ solution into a prepared alumina template.[23] The filling of the alumina template is ordinarily followed by heat treatment. Subsequently, a selective dissolution of alumina follows. As a result, TiO_2 nanotubes are formed. A simplified illustrative scheme can be found in Figure 1. This technique is not limited to fabrication of nanotubular shapes. Different structures, such as nanowires, nanocolumns, nanorods, and other shapes, can also be fabricated.[8]

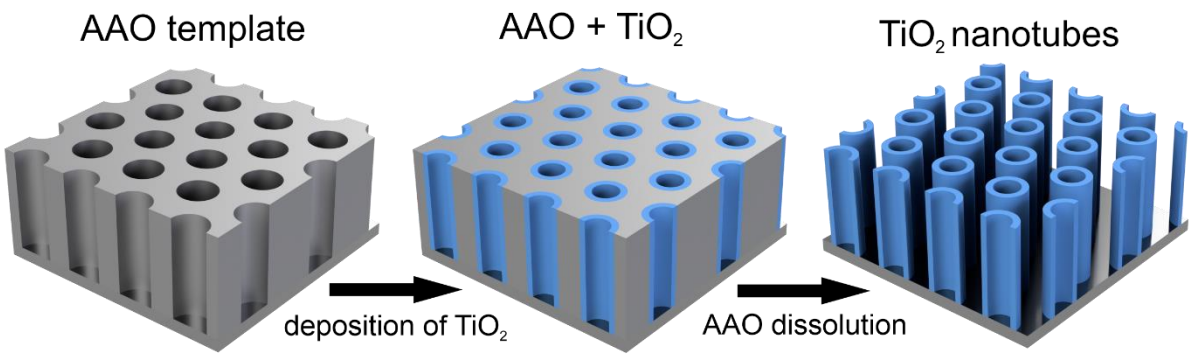

Figure 1: Illustrative drawing of template-assisted TiO_2 nanotube fabrication. *Porous anodic aluminium oxide (AAO) is used as the template.*

Templates

The currently most common template material is porous anodic aluminium oxide (AAO). The main reason for its use dwells in its easy fabrication and tunability. It consists of nanopores in a hexagonal pattern with high uniformity. As of today, the interpore distances can range between 10 and 500 nm, with aspect ratios far beyond 1 000. The preparation techniques are also well established and thus exhibit high reproducibility. Thanks to the uncomplicated fine-tuning of its surface topography, it can be used to prepare TiO_2 nanotubes with specific dimensions (diameter and length). The final nanotubular shape can be therefore modified directly by a change in the structure of the template The prepared TiO_2 nanotube product can be a free-standing film with a variable degree of order, a membrane, or a "powder" based on the selected fabrication process. In addition to AAO, there are other suitable template materials, such as, e.g., ZnO nanorods, MWCNTs, TiO_2 (and other) membranes or rod-like micelles, that can be used for TiO_2 nanotube fabrication.[8,24,25]

Template filling

Common filling approaches include electrodeposition, sol-gel techniques, and atomic layer deposition. Each path has some advantages and disadvantages. While considering electrodeposition, we have to bear in mind that alumina is actually an electrical insulator, and thus the pore bottom possesses a high resistance. Therefore, the pore bottom has to be thinned prior to electrodeposition itself. This can be achieved through, e.g., wet chemical etching of alumina with a phosphoric acid solution. Subsequently, a pulsed current can be used to overcome the remaining resistance of the pore bottom and fill our template. Another approach would be to remove the barrier layer on the pore bottom in its entirety. This, however, results in a porous through-hole structure. This structure can be subsequently coated with conductive metals, such as, e.g., gold or platinum, and therefore it can be used for conventional electrodeposition, e.g., direct current electrodeposition. The second mentioned approach is sol-gel technique filling. This method employs hydrolysis reactions of Ti-alkoxide, $TiCl_4$, TiF_4 precursors, and subsequent condensation reactions. As a result, a Ti-O-Ti chain is developed, which can further hydrolyse to TiO_2. The third and last technique is a method of its own, atomic layer deposition. During past years, it repeatedly attracted attention as it is very precise, and its possibilities are vast. As the name suggests, it enables us to coat up one atomic layer at a time repeatedly. It cycles exposure to precursors (for TiO_2 nanotubes, $TiCl_4$ can be used) with purging and hydrolysis steps. As a result, a highly controlled surface can be acquired. To finally obtain the nanotubular shape, the removal of the used template is necessary. Alumina templates can be selectively dissolved by wet chemical means, e.g., dipping them into an aqueous NaOH solution or Chromic-Phosphoric acid of suitable concentration and temperature. [6-8]

2.1.2. Hydrothermal methods

Summary

The first hydrothermal synthesis of TiO_2 nanotubes was achieved in 1998 by Kasuga et al.[26] It is important to note that hydrothermal methods, in opposition to other approaches, usually yield single nanotubes or clusters of nanotubes that are “free” and are not standing nor ordered. Usually, their diameters are small (e.g., 2-20 nm), and their length can reach several micrometers. The standard preparation technique includes alkaline treatment of TiO_2 precursor (e.g., anatase) at higher temperatures. The treatment can last up to several days. To finish up, the treated substrates are washed with low molarity aqueous acid solution. Before further use, the resulting powdered nanotubes have to be filtered and dried. This technique can be used to fabricate other structures, such as nanofibers or ribbons. [6-8] A simplified scheme of hydrothermal nanotube preparation is displayed in Figure 2.

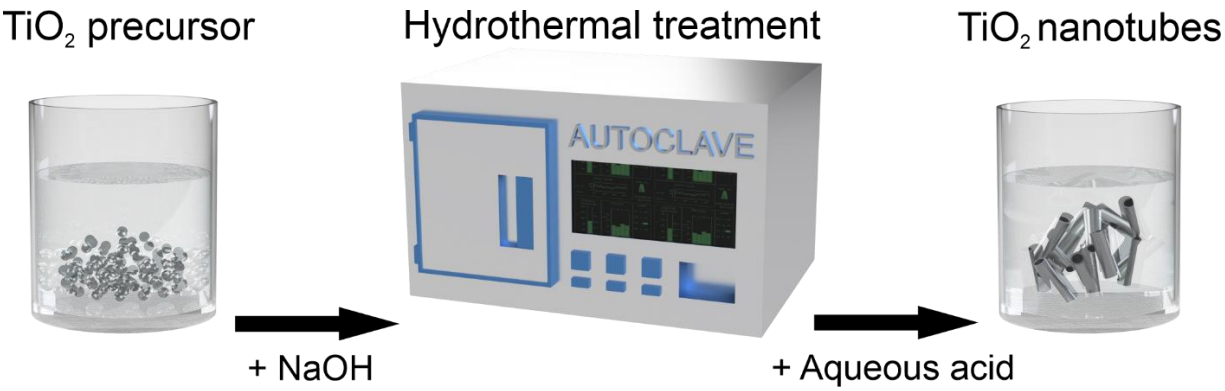

Figure 2: Illustrative drawing of hydrothermal TiO_2 nanotube fabrication. *Autoclave is used for the hydrothermal treatment in this scheme.*

The treatment of a precursor

There is a selection of precursors that can be used for TiO_2 nanotube fabrication. It can be either rutile, anatase, commercial P-25, or amorphous TiO_2. The selected precursor is usually heated in NaOH solution with higher molarity (4-20 mol/L). The temperature can reach between 100 and 180 °C. However, for some fabrication techniques, this temperature might be insufficient. In that case, the NaOH can be switched to KOH, which can sustain slightly higher temperatures up to 200 °C. The thermal treatment can be carried, for example, in an autoclave. The synthesis itself is facilitated with an increase in NaOH concentration and temperature. After the treatment, the resulting powders are usually washed with water and an aqueous HCl solution. Once the pH of the washing solution drops below 7, the powder can be filtered and dried. [6-8]

Tuning of the nanotube features

Prepared nanotubes usually have smaller diameters (2-20nm) consistent along the whole nanotube. Their length can reach up to several micrometers, and can have open-ended morphology. Their final shape is influenced by two main factors – fabrication conditions and the size and structure of used precursors. However, it can be generally said that higher temperatures and larger substrates tend to result in longer nanotubes. Prepared nanotubes, however, lean towards agglomeration. This can be dealt with by their dispersion in aqueous solutions. Under the right conditions, hydrothermal methods can be used to fabricate nanotubes with atomic-sheet-range wall thickness. [6-8]

2.1.3. Anodic oxidation

Summary

The first successful fabrication of anodic TiO_2 nanotubes dates back to 1984.[27] This work was carried by Assefpour-Dezfuly et al. In comparison to other shown methods, it can be easily used for the fabrication of ordered standing TiO_2 nanotubular surfaces directly from metal titanium. Briefly, a voltage is applied to substrate titanium in a suitable electrolyte, with an inert counter electrode present. As the reaction proceeds, a nanostructured TiO_2 layer is formed (Figure 3) Altering the fabrication process parameters, such as applied voltage, reaction time, and properties of used electrolytes (composition, temperature, and pH), can enable us to tune the final morphology of the fabricated surface. The process can last from minutes to days. The diameter of prepared tubes can range from 10 to 500 nm, with the wall thickness from 2 to 80 nm and their length ranging from hundreds of nm up to 1000 µm. However, fabricated nanotubes are mostly V-shaped, meaning their diameter is largest on their top and decreases towards the nanotube bottom. On the other hand, the fabrication process is relatively cheap. In addition to aluminium and titanium, it can be used to fabricate nanostructures from other transition metals, including, e.g., Hf, Zr, Fe, Nb, V, W, Ta, Co, and Si. Interestingly, it can be also used for nanostructured alloys that meet specific criteria - such as standard implant Ti, Al, and V based alloy. However, this technique is not limited to fabrication of the nanotubes – compact oxide, bamboo nanotubes, nanolaces, and both ordered and disordered porous structures can be obtained. [6-8]

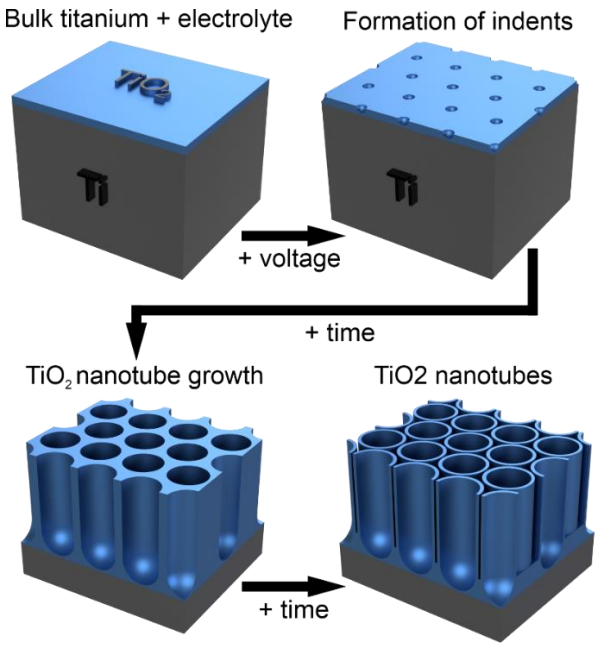

***Figure 3: Illustrative drawing TiO_2 nanotube fabrication through anodic oxidation**. Bulk titanium is used for the subrate. A thin layer of TiO_2 forms naturally on titanium when exposed to air. This layer is usually very thin.*

Formation mechanism

Anodic oxidation is a well-established industry electrochemical process used for "coating" the metal substrate with compact or porous oxides of the same metal. The fabrication can be carried in an electrochemical cell with an inert cathode (e.g., platinum or carbon) and substrate metal anode. The whole reaction proceeds under a suitable voltage. In the case of TiO_2 nanotubes that are made directly from titanium, there are three dominating processes: electrochemical oxidation of titanium (Ti→ TiO_2), the electrical field induced TiO_2 dissolution, and chemical dissolution of Ti induced by the presence of suitable ions (e.g., F^- or Cl^-). The balance between the individual components is critical, as it directs the course of fabrication. The General process can be described by the following equations:[6,8]

$$M \rightarrow M^{z+} + ze^- \qquad \text{(Eq.1)}$$

$$M + \frac{z}{2}H_2O \rightarrow MO_{\frac{z}{2}} + zH^+ + ze^- \qquad \text{(Eq. 2)}$$

$$M^{z+} + solv \rightarrow M^{z+}_{solv} \qquad \text{(Eq. 3)}$$

$$zH_2O + ze^- \rightarrow \frac{z}{2}H_2 + zOH^- \qquad \text{(Eq. 4)}$$

These four equations can be interpreted as follows. First, upon applying sufficient potential metal M is oxidized to M^{z+} while z electrons are being released into the electrolyte (Eq.1). At this point, it can either form an oxide (Eq.2) or get dissolved into the electrolyte (Eq 3). As a counter reaction, hydrogen gas is formed on the cathode (Eq. 4). The result is determined by the balance between dissolution and oxide formation. [6,8]

To make these equations more relatable and practical, let us discuss them in context with fabrication technique used in this dissertation thesis. The reaction proceeds in an electrolyte consisting of ethylene glycol, NH_4F, and a small amount of H_2O in a two-electrode setup.

$$Ti \rightarrow Ti^{4+} + 4e^- \qquad \text{(Eq.1")}$$

$$Ti + 2H_2O \rightarrow TiO_2 + 4H^+ + 4e^- \qquad \text{(Eq. 2")}$$

$$TiO_2 + 6F^- + 4H^+ \rightarrow [Ti\,F_6] + 2H_2O \qquad \text{(Eq. 3a")}$$

$$Ti^{4+} + 6F^- \rightarrow [Ti\ F_6]^{2-} \qquad \text{(Eq. 3b")}$$

$$4H_2O + 4e^- \rightarrow 2H_2 + 4OH^- \qquad \text{(Eq. 4")}$$

As we can see in Equations 1" through 4", upon applying sufficient potential the titanium can form a compact oxide layer (Eq. 1" and 2") whilst hydrogen gas forms on the cathode (eq. 4"). As the oxide layer grows, it becomes harder for the TiO_2 to grow. The uneven electric field helps F- ions accumulate on sites with a higher electric field present upon the grown TiO_2 layer. At this point, local dissolution of TiO_2 occurs, and small indents are formed (eq. 3a" and 3b"). The decrease of oxide thickness in the location of indents increases the electric field density, and indents slowly become pores and consequently form a nanotubular structure.[8,28,29]

All of the abovementioned can be observed in the course of anodic oxidation through changes in current density. For example, a curve characteristic to fluoride-based electrolytes can be found in Figure 4. There are three general parts that can be observed in this Figure. In the first part, the current density drops thanks to the growth of the barrier oxide layer. In the second part, the current density slowly rises as the nanotubular indents form. In the third, and last part the current density stabilizes as the self-ordered nanotubular structure is grown. [7]

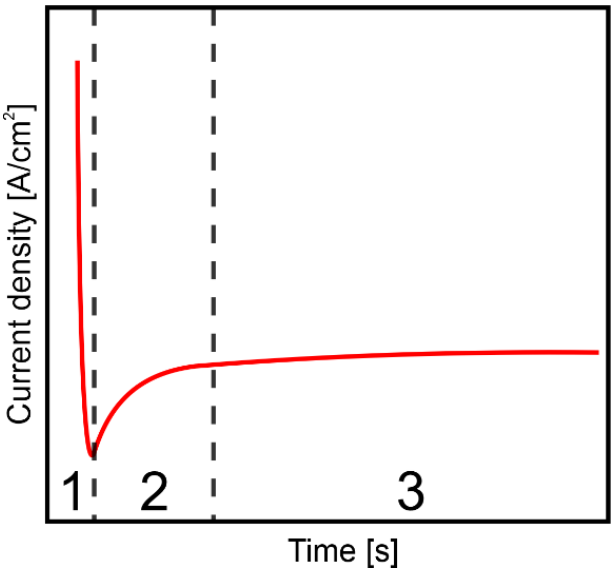

Figure 4: Example curve describing the current density/time dependency observed upon the growth of TiO_2 nanotubes. *This curve is characteristic for fluoride-containing electrolytes.*

Due to the nature of nanotube growth mechanism, their inner diameter is V-shaped (Figure 5) along their length – meaning it is biggest on the top and gets smaller towards their bottom.[7,29]

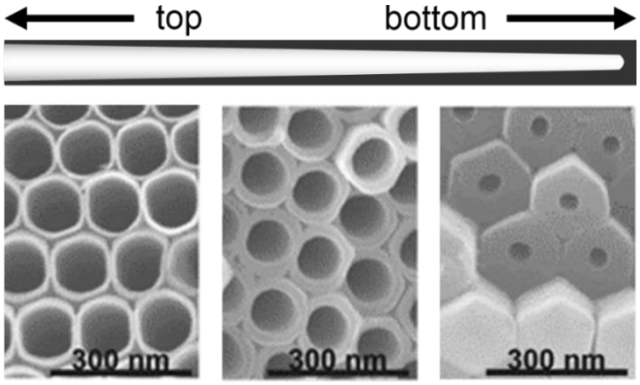

***Figure 5: Cross-section of the nanotube profile**. Adapted and modified from[30]*

Anodic oxidation can be carried in a single step with mentioned two-electrode setup, as shown in illustrative design (Figure 6). However, it can get more complex with three electrodes and two or more consequent anodization steps. Additional steps can lead to significantly smoother and more distinguished topographies with higher organization levels.[7]

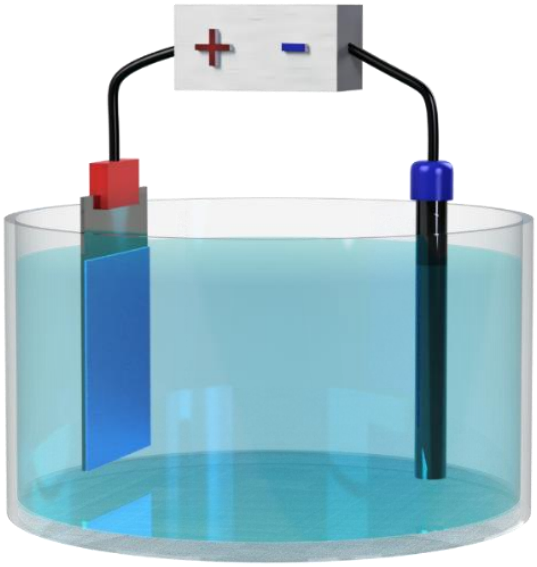

***Figure 6: Illustrative design of simple 2-electrode electrochemical anodization cell.** Titanium foil (+, anode) and an inert or anode (-, carbon, platinum, etc.)*

The effect of anodization conditions

Substrate titanium

As it was mentioned before, one of the most significant advantages of anodic oxidation is that it can be carried directly with the metal substrate, meaning any bulk titanium, such as titanium rod, sheet, or foil, is acceptable. However, the result is variable, based on substrate properties. Purity of used titanium, surface roughness, and substrate modification (e.g., nano-imprinting, focused ion beam micropatterning, or grinding/polishing) can notably affect

the result. In fact, in most bio-focused cases, some kind of pre-treatment (at least polishing) might seem necessary. In the other case, fabricated nanosurface can suffer from deteriorated arrangement and orientation of formed nanotubes (Figure 7) as well as the presence of surface artifacts caused by impurities – which can significantly affect the performance of the fabricated surface. Even though this technique uses directly titanium, it is not limited to bulk metal. In some cases, it might be desirable to work with a highly defined thin titanium film. Such a substrate can be prepared by deposition of titanium onto a supporting substrate. E.g., a silicon wafer can be sputter-deposited with a smooth titanium layer with high purity and uniform thickness. Such a surface has the potential to lead to highly uniform and organized TiO_2 nanotubes with specified length. However, the prerequisite for this to work is the presence of sufficient thickness of TiO_2 substrate. With overly thin layers, no nanotubular structures can be observed.[6-8,30]

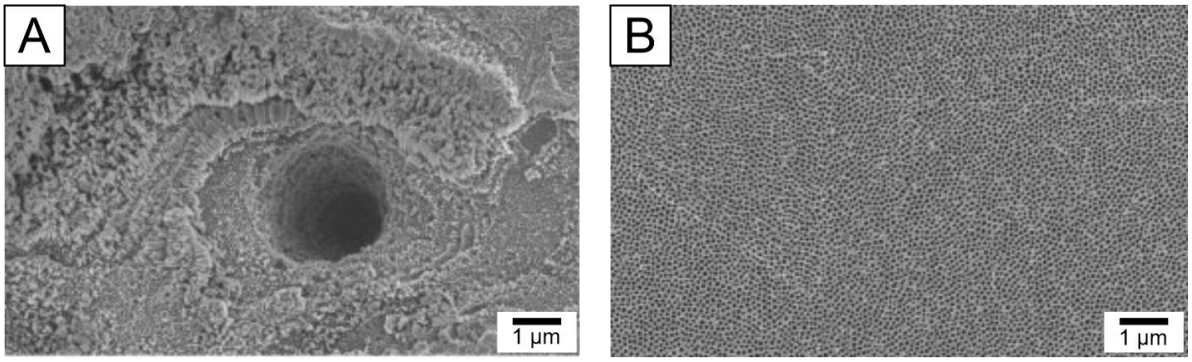

Figure 7: TiO_2 nanotubes prepared from polished (A) and non-polished (B) surfaces. *Polished surfaces yield more organized surfaces. Adapted from [31]*

The electrolyte

The choice of electrolyte is an important part of fabrication. Its composition, concentration, and pH can significantly affect acquired nanostructures. There are four main electrolyte groups that are commonly used for TiO_2 nanotube fabrication via anodic oxidation. The first group consists of aqueous solutions with hydrofluoric acid as its base. The pH of such electrolytes is relatively low. TiO_2 nanotube arrays fabricated with this electrolyte group tend to be less organized and relatively short (approx. 500nm maximum). The second group could be called "the buffered electrolytes". It utilizes the addition of weaker acids (e.g., KF). Also, the pH of such electrolyte is adjusted (either weakly acidic or neutral). The resulting TiO_2 nanotube arrays exhibit higher organization degrees and can grow to notably larger lengths (approx. 5 µm). The third group consists of polar organic electrolytes, such as, e.g., glycerol, dimethylsulfoxide, or ethylene glycol (used in this dissertation thesis) enriched with fluoride-containing compounds (e.g., NH_4F, KF, or NaF) and a tiny amount of water. This kind of electrolyte can produce substantially longer TiO_2 nanotubes (100 µm and more). In organic electrolytes, it is vital to maintain a balance between applied voltage, fluoride

concentration, and the amount of water. It can be generally said that higher water content and/or high hydrodynamic flow of electrolytes can impair both the organization and achievable length of acquired nanotubes. Getting under 2% of water dramatically improves the self-organization of fabricated nanotubes. The fourth and last group are electrolytes that could be called "fluoride-less electrolytes". As the name implies, these do not contain any fluoride ions. Most of them are aqueous and involve compounds such as perchloric acid, hydrochloric acid, or hydrogen peroxide. The role of fluoride ions can be substituted by chloride ions, chrome ions, bromide ions, or perchlorate.[7,8]

Anodization time

The anodization time is also an essential variable in anodic TiO_2 nanotube fabrication. The time interval has to be sufficiently long. If the time interval is too short, the anodic oxidation can be stopped before it reaches the growth stadium of nanotubes. If that is the case, the fabrication can result in either no observable change, a compact oxide layer or a porous layer.[31] Once it reaches a critical value, nanotubular structures can be observed. From this point, it can be generally said that an additional increase in the anodization time results in longer TiO_2 nanotubes, with no effect on nanotube diameter whatsoever. The length of nanotubes then steadily increases proportionally with anodization time, until it eventually stabilizes and a steady state is achieved.[7,8,32]

Applied voltage

The applied voltage is another crucial parameter determining the final shape of fabricated nanotubes. [33] Three general scenarios can occur while selecting the applied voltage. The applied voltage can be too low. In this case, a compact oxide layer is formed. As could be expected, the other extreme is when the applied voltage is too high. In this case, a porous structure without any observable nanotubes is formed. Finally, in the third and most favourable scenario, a fitting voltage that falls into the effective range is applied. This "effective range" of voltage can range from V_{min} to V_{max}. The dependency could be generally described as follows. The fabrication produces a smaller nanotube diameter towards V_{min} and larger nanotube diameters as it approaches values closer to Vmax. The effective interval is specific for the used electrolyte and its current composition. For instance, the effective interval of organic electrolytes can range from units to hundreds of volts.[7,8,34]

Temperature

It can be generally said that electrolyte temperature affects the speed of nanotube growth – both in terms of length and wall thickness. This is the cause because it directly influences the oxide growth rate. [35] It has been shown that with the appropriate temperature, both the internal and external diameters of produced nanotubes can be affected.[4, 6]However, if the aim is to prepare stable TiO_2 nanotube arrays, a room temperature can be considered optimal. [7,8]

By carefull selection of all the above-discussed parts of the experimental setup, we are enabled to modulate the TiO_2 fabrication process and tune the resulting features of the designed TiO_2 surface. This can be used to specifically target desired physical and physicochemical features accordance with desired application – be it for biomedical[36] or industrial applications. Under specific conditions, we can acquire various structures – e.g., compact TiO_2[6], nanopores[36] or various nanotubular TiO_2 structures (Figure 8). [7,8,37-40]

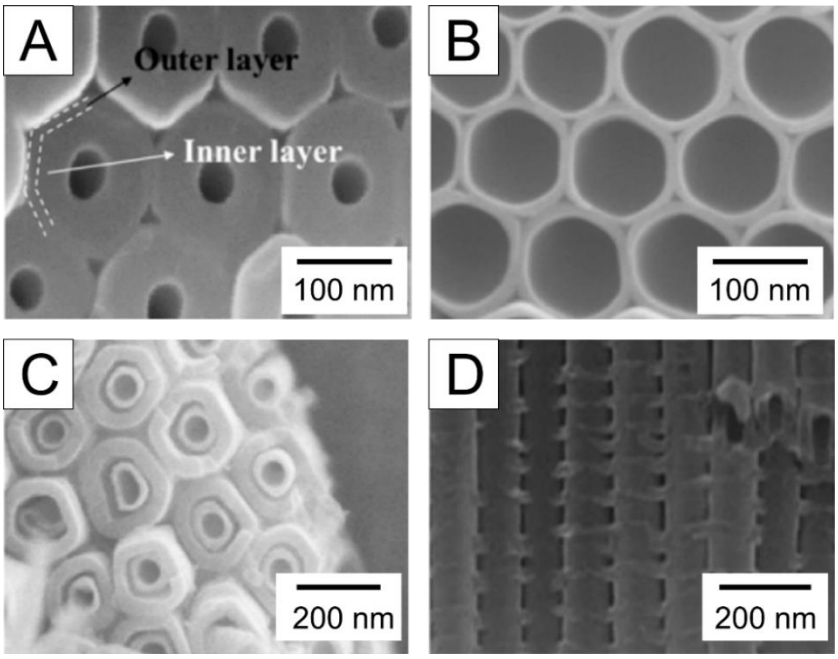

Figure 8: Different nanotube morphologies. *Double-walled[41] (A), single walled[41] (B), tube-in-tube[8] (C) and bamboo[40] (D) nanotubes*

2.2. TiO_2 nanotube modification

Even though there is a whole variety of nanotubular TiO_2 surfaces, there are some shortcomings to their applications, and thus, their performance might not be adequate for the intended use. Therefore, through past years there has been an effort to improve their performance through various modifications further. These enhancements are used to deliver better performance in a specific way, such as e.g., a shift of photocatalysis towards visible spectra, enhancement of specific cell response, heightened biocompatibility, or increased antibacterial activity. For clarity, we divided modification options into three categories: annealing, doping and surface modifications (Figure 9).

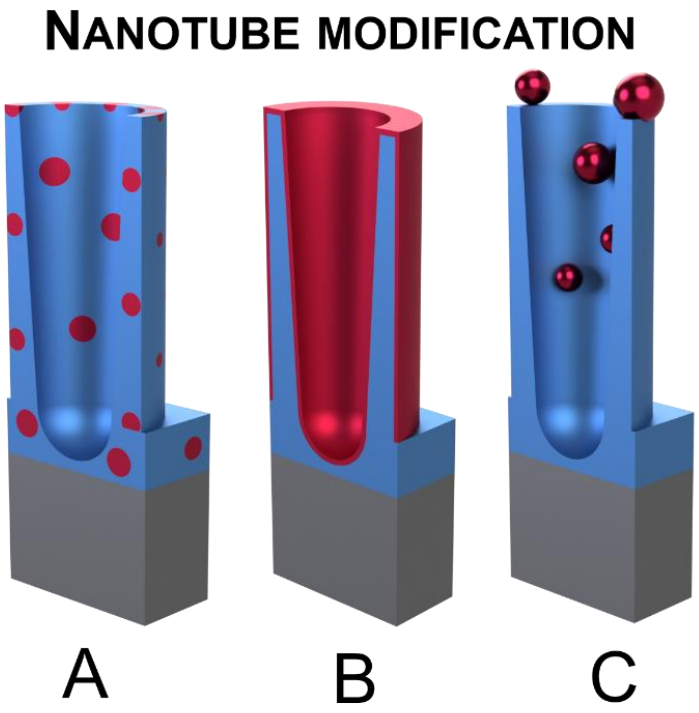

Figure 9: Nanotube modifications. *An illustrative drawing depicting doping (A), and example surface modifications - thin film coatings(B) and nanoparticle decoration (C)*

2.2.1. Annealing

It has been shown that the crystal structure of formed oxide can influence some properties of TiO_2 nanotubes.[42] However, as-formed anodic TiO_2 nanotubes are amorphous. The transformation into crystal phases (anatase or rutile) can be carried through annealing under specific conditions. The main factors influencing the result are temperature and atmospheric composition. Generally, it can be said that lower annealing temperatures (above 300 °C) yield anatase, and as the temperature rises (above 500 °C), the rutile phase appears. With higher temperatures (above 600 °C), the rutile phase becomes dominant. Above a critical temperature (around 800 - 900 °C), fabricated nanostructures start to collapse. This temperature is, however, dependent on nanotube type and fabrication design. The heating rate has to be chosen carefully, as it can change the morphology of the fabricated surface. As for the conductivity (lowest resistance) and photoelectric properties, the annealing temperature of about 400 °C seems like the best choice.[7,8,43]

2.2.2. Doping

Doping is another approach that can be used for the modulation of TiO_2 nanotube properties. It utilizes the introduction of other elements directly into TiO_2 lattice, be it in the form of ions or atoms. Common doping procedures include, for instance, treatment of either growing or final TiO_2 nanotubes in solution or melt of doping agents, thermal treatments or fabrication in atmospheres containing dopant gas, or high energy ion implantation. In the case

of anodic oxidation, a suitable doping element can be added directly into the source titanium, forming a titanium-based alloy. If an alloy with suitable composition is formed, it can be directly used for the fabrication of anodic TiO_2 nanotubes. The doping element is, therefore, embedded straight into the TiO_2 lattice. This approach can be used in industrial applications – e.g., to improve their photoresponse towards visible light or their electrical properties – as well as in biomedical applications. Doped TiO_2 nanotubes can be divided into three groups based on used dopants– metal-doped TiO_2 nanotubes, non-metal-doped TiO_2 nanotubes, and co-doped TiO_2 nanotubes. The group of metal-doped nanotubes includes metals, such as Nb, Fe, Cu, Cr, Zr, Zn, and V. [44-47] The non-metal-doped nanotube group includes non-metals, such as, for example, N, B, C, S, I.[48-50]. Third group consists of combined doping agents, such as e.g., N-Ta, N-Nb, C-N-Ni.[7,8,51-54]

A particular approach called self-doping can also be employed. As the name suggests, it does not introduce any foreign element. In the case of titanium, it includes the formation of Ti^{3+} and oxygen vacancies through various means. Self-doped TiO_2 can exhibit enhanced performance in the field of photocatalytic activity. The presence of Ti^{3+} and oxygen vacancies is also a feature observed in black TiO_2, which is a photocatalyst with superior properties in environmental applications that repeatedly attracted attention for its superior visible light absorption.[55]

2.2.3. Surface modifications

Surface modifications are another viable approach for modulation of TiO_2 nanotube properties that is in a way related to doping methods. It employs additional functional substances that are, in this case, introduced onto the fabricated surface (its top layer). These additional layers can take the form of thin films, monolayers, nanoparticles or various other nanostructures.[6,8]

Lately, thin-film coatings introduced through atomic layer deposition became a well-established treatment for TiO_2 nanotube modification. The use of atomic layer deposition with TiO_2 nanotubes has its challenges. It was a difficult task to achieve uniform coatings because of their high aspect ratios. However, individual aspects of atomic layer deposition and their effect on deposition on high aspect ratio nanostructures were thoroughly studied. Therefore, nowadays the additional functional layer introduced through atomic layer deposition can exhibit high uniformity and be fine-tuned through careful design of the deposition process. A big advantage is that it can proceed with an atomic layer precision due to the nature of the deposition process. The resulting properties of the modified surface are influenced by the character of the added functional layer. Among the materials used for this technique, we can find elements such as Pd, Pt, Al, W, and compounds, such as ZnO, Al_2O_3, Ta_2O_5, Co_3O_4, or CdS [56-59]

Another approach that also covers the whole fabricated surface is modification through the attachment of defined organic monolayers. These can be attached, for example, by self-assembly from liquid or gaseous phases. Through them, we can tailor surface characteristics, such as, e.g. wettability, charge transfer or biological interactions. Defined organic monolayers can be used directly for surface modulation but can also serve as anchor molecules in case of dye-sensitized TiO_2 solar cells (e.g., n-octadecylphosphonic acid), or linker molecules for multiple-stage functionalized surfaces (e.g., 3-aminopropyltriethoxysilane - abbrev. APTES). APTES is also considered a bioactive linker used to promote protein adhesion to oxide surfaces in implant applications.[6,8]

The other side of the barricade consists of techniques that utilize nanoparticles. There is a whole bunch of nanoparticle types and mechanisms used for this kind of modification. Common approaches include, for example, electrodeposition, adsorption, precursor hydrolysis, UV-assisted photocatalytic reduction, ultra-high vacuum evaporation, or chemical reduction.[6-8] Among the decoration agents, we can find oxide nanoparticles, such as WO_3, Cu_2O, Fe_2O_3, ZnO, NiO, Bi_2O_3 or TiO_2[60,61], metal nanoparticles, such as Ag[62], Au, Pd, and Pt, metalloids, such as Se but also quantum dots[63], such as CdS, CdSe and PbS. Likewise, other nanostructures, such as, e.g., nanowires, can be used for surface modification.[64]

Up to this point, all of the presented knowledge about fabrication and modification of TiO_2 nanotubes was general and included their applications in various fields. The nature of this dissertation thesis is, however, inclined towards their biomedical applications. So, henceforth, we will discuss titania nanotubes in both their pristine and modified forms as a biomedical material.

2.3. TiO_2 nanotubes for biomedical applications

One might ask: “Why TiO_2 nanotubes and biointerfacial interactions?” The motivation stems from the widespread use of titanium and its alloys in the field of everyday medicine. Currently, we can find them in orthopaedical, dental, and cardiovascular implants and implantable medical devices.[54] Despite their broad use, several issues can degrade their performance. These shortcomings include insufficient antibacterial activity[65] (which can lead to bacterial biofilm formation) and inadequate biocompatibility.[66] In most cases, we use surfaces that are not micro-/nanostructured, which means they are prone to the fibrous tissue growth. The formation of the fibrous layer weakens the bond between the bone and the implant.[13,66] As a consequence, the loosening of the implant and risks associated with it can become a serious threat.

During past years, many strategies were introduced to overcome these issues and improve the desired cell-surface interface.[2,13,67-77] It has been pointed out in several studies that attributes such as surface chemistry, topography, protein adsorption, and wettability

significantly influence the cell-surface interface,[9-14] resulting in different, e.g., cell adhesion[70,78], viability[77,78], metabolism[78,79] , differentiation,[79-83] or antibacterial activity.[19,21,84-86] Among the studied materials, the use of TiO_2 nanotubes repeatedly attracted attention. Since we are able to grow TiO_2 nanotubes on both bulk titanium and some of its alloys, it seems like an accessible way to enhance its properties and improve their performance.[9-14] At the same time, we can use surface modifications to adjust its properties further. It needs to be stressed out that even though their biomedical-field potential is vast and, apart from coatings, can include, novel drug delivery systems and advanced tissue engineering, their actual biomedical applications are in an extremely early stage.[8]

The following passage will summarize the findings in the field of biointerfacial interactions of TiO_2 nanotubes. To make this section more clear, the data are divided into three parts – bare TNTs, surface modified TNTs, and doped TNTs.

2.3.1. Bare TiO_2 nanotubes

Through time, the interactions between various cells and bare TiO_2 nanotubes were thoroughly investigated. Various studies have reported improvement in cell adhesion, growth, and differentiation in comparison to non-structured surfaces.[1-3,13,87] Some results were coherent, others yielded conflicting results. However, it can be generally said that it has been confirmed the diameter of TiO_2 largely affects the cell viability and shapes the resulting cell-surface interface. [79,87,88]

The first effort in this field dates back to 2007,[88] when Park et al. tested mesenchymal stem cells grown on nanotubes with diameters ranging from 15 to 100 nm. Diameters above 50 nm induced apoptosis, but the smallest 15 diameters significantly promoted adhesion, proliferation, and differentiation. What more, the osteogenic differentiation has deteriorated on the largest 100nm diameter. [88] In 2009, Oh et al.[87] reported conflicting results. Their TiO_2 nanotubes with diameters above 70nm induced osteogenic differentiation, and their small nanotubes improved only adhesion. After this, other factors such as residual fluorides, TiO_2 crystal phases, surface pre-treatment were closely studied, with results inclining towards the former research conducted by Park et al.[89,90]

Similar diameter-dependent behaviour was observed for osteoblasts and osteoblast-like cells. Generally, it can be said that osteoblasts preferred larger diameters. However, the specific number is hard to state, as conflicting results were reported. Oh et al.[31] reported that nanotubes with approx. 100nm outer diameter and 70nm inner diameter significantly increased the number of adherent cells (by 300 - 400 %) compared to flat titanium. Zhang et al.[91] reported that the performance of 170 nm TiO_2 nanotubes was promising. On the contrary, Yu et al.[92] reported yet another result that claimed that in terms of adhesion, larger diameters (100 and 120nm) performed worse than flat titanium. In terms of proliferation, it

seems like larger diameters perform better (even the 100 and 120nm groups), but the ALP activity and mineralization were suppressed on these larger diameters.

Analogous behaviour has been observed in other cell types. Human adipose-derived stem cells (hASCs) preferred the nanotube diameter of 70 nm. This study, carried by Lv et al. [93] examined both in vivo and in vitro performance, reaching the conclusion it performs better than sandblasted, large grit, acid-etched implant surface (SLA). Smith et al.[94] studied dermal fibroblasts and epidermal keratinocytes are grown on 70 – 90 nm nanotubes. The indicated decrease in keratinocyte coverage reached 92%, while the increase in fibroblast coverage was approximately 40%. Overall, the adhesion, proliferation, and differentiation of keratinocytes were damaged, while the same was promoted for fibroblasts. Peng et al.[95] studied aortic endothelial cells and aortic vascular smooth muscle cells. The outcome of this study is indicating that the growth of endothelial cells can be promoted while demoting the proliferation of vascular smooth muscle cells. It needs to be said that this is actually the desired effect since the proliferation of vascular smooth muscle cells is often connected with their de-differentiation and some unpleasant health implications (restenosis).

There is a number of studies targeting interactions with other cells, proteins, and other bio-targets. Smith et al.[96] studied the hemocompatibility of TiO_2 nanotubes. Their results showed elevated protein adsorption together with platelet adhesion and activation. In the same paper they admitted that this response could be modified through a change in nanotube characteristics. Later, Li et al.[97] studied TiO_2 nanotube membranes. From their plasma recalcification experiment, it can be assessed that these membranes have superior hemocompatibility. Kulkarni et al.[98] have categorized TiO_2 nanotubes as a promising interfacial blood-contacting material. It is also worth mentioning that TiO_2 nanotubes have been proven to boost hydroxyapatite growth (compared to flat TiO_2 surface),[99] and stimulate the Collagen type 1 expression.[100]

From all these studies, it can be said that cell cultures can prefer a specific nanotube diameter, and through careful design, the resulting cell-surface interface can definitely be affected in a positive way. Therefore, when used right, nanostructuring the TiO_2 into the form of nanotubes can bring some improvement into the resulting cell-surface interface. It should also be noted that the diameter-dependent behaviour is probably not specific solely to TiO_2. To explain, a study was carried, that has shown a similar observed behaviour for both TiO_2 and ZrO_2 nanotubes.[101]. Nevertheless, other factors, such, as e.g. the technique used for sample fabrication, purity of used chemicals, and crystalline phase, should not be disregarded.

A brief list of works and their highlights can be found in Table 1.

Table 1: Bare TiO_2 nanotube-oriented example studies. *Authors, studied nanotube diameters, objects of study and study highlights are included.*

Author	Nanotube diameter /other structures	Object of study	Highlights
Park et al.[88]	15, 20, 30, 50, 70 and 100 nm	Mesenchymal stem cells (rat)	15nm – promoted adhesion, proliferation, and differentiation 100nm – induced apoptosis
Oh et al.[87]	30, 50, 70 and 100 nm	Mesenchymal stem cells (human)	30nm – promoted adhesion 70 and 100nm – induced osteogenic differentiation
Park et al.[90]	15, 20, 30, 50, 70, and 100 nm.	Mesenchymal stem cells (human) Osteoblast-like cells	Above 70nm – severely impaired differentiation, reduced proliferation and migration
Oh et al.[13]	70nm	MC3T3-E1 pre-osteoblast	Increase in adherent cells by 300-400%
Zhang et al.[91]	50nm, 170nm and 400 nm mesopores	Primary osteoblasts (Sprague-Dawley rats)	170nm – increased adhesion speed
Yu et al.[92]	20, 50, 70, 100 and 120 nm	MC3T3-E1 pre-osteoblast	100 and 120 nm – impaired adhesion, spreading, ALP activity and mineralization. The adhesion was even worse than non-anodized titanium 20-70nm – good adhesion 70 – 120 nm - increased proliferation

Longwei et al.[93]	50, 70, and 100 nm	Human adipose-derived stem cells (hASCs)	Superior osteogenic differentiation
Smith et al.[94]	70 - 90 nm.	Dermal fibroblasts (human) Epidermal keratinocytes (human)	Increase in dermal fibroblast and a dramatic decrease in epidermal keratinocyte adhesion, proliferation and differentiation.
Peng et al.[95]	30 nm	Aortic endothelial cells (bovine) Aortic vascular smooth muscle cells (mouse)	Promoted proliferation of endothelial cells, decreased vascular smooth muscle cells
Smith et al.[96]	70 – 90 nm	Whole blood (human)	Increased blood clotting kinetics
Li et al.[97]	80 nm	Human endothelial cells ECV304	Excellent hemocompatibility
Tsuchiya et al.[99,100]	100nm	Simulated body fluid	Significant increase in apatite formation
Wilmowsky et al.[100]	30nm	*In vivo* pig frontal skull	Enhanced osteoblast function

2.3.1. Surface-modified TiO_2 nanotubes

The most common biomedical-related motivation for surface modifications of TiO_2 nanotubes can be divided into three groups. First, the antibacterial activity of TiO_2 nanotubes is unsatisfactory, and the formation of biofilm is a real threat, so the enhancement of antibacterial activity is desired. Second, cell-surface interactions do not proceed as intended, thus a modification improving cell-surface interface is applied. As for the third and last group, the nanotubular shape calls for use as a novel payload or drug delivery system. In some cases, these categories can overlap as some substances can affect several characteristics of TiO_2 nanotubes.

Among the most common antibacterial surface modifications, we can find extensively studied silver nanoparticles. These have been here with us for quite some time and have already found their place in relatively common parts of our lives – including cosmetics, clothing, medicine, and many other applications.[6] Silver nanoparticles are notoriously famous for their antimicrobial properties,[102] and thus, attempts executed in order for antibacterial activity enhancement are definitely in place. Das et al.[103] prepared nanotubular TiO_2 surface modified with silver nanoparticles. They implied that it showed significant antibacterial activity while maintaining surface biocompatibility. Lan et al.[85] claimed that silver nanoparticles decorated on TiO_2 nanotubes did not promote only antibacterial activity but also enhance surface biocompatibility. These claims are kind of confusing because many studies showed that silver nanoparticles are toxic to mammalian cells, and can induce apoptosis even in non-cytotoxic doses.[22] Nevertheless, the study of silver-modified TiO_2 nanotubes is a current and deeply researched topic.[19,85,104-107]

Lately, selenium nanoparticles have attracted attention. As a trace element naturally present in the human body, selenium plays an important role in cancer regulation and oxidative damage protection.[108,109] It has also been reported to carry several interesting traits including antibacterial[18,84,110,111], anti-cancer [70,84] and anti-inflammatory[18,112] activity. Thanks to these unique traits, selenium nanoparticles became alluring for various applications including oncology[70,84], regenerative medicine[113] and tissue engineering[18,110,114-116]. Hopefully, these interesting properties can be imparted to TiO_2 nanotube surfaces. Chen et al.[84] studied selenium-deposited TiO_2 nanotubes with chitosan coating. Their surface showed superior antibacterial and anti-cancer activity. However, there were no visible selenium nanoparticles in the images supplied for this study, even before the spin-coating with chitosan. Also, these effects could be attributed solely to chitosan, which exhibits both antibacterial[117] and anti-cancer[118] activity by itself. A few years later, Liu et al. [18] investigated selenium nanoparticle decorated TiO_2 nanotubes, this time with visible selenium nanoparticles. They reported that fabricated surfaces exhibited both antibacterial and anti-inflammatory properties. There are, however, many other chemical substances and compounds that are suitable for the

enhancement of antibacterial activity. Among the other used substances, we can find e.g., ZnO,[21,119] Ag_2O,[120] Au[20,121], and strontium nanoparticles[83]

A list of relevant nanoparticle-oriented example works, and their highlights can be found below, in Table 2.

Table 2: Antibacterial-activity-oriented example studies. *Authors, studied nanotube diameters, modifying agents, objects of study and study highlights are included.*

Author	Nanotube diameter / modifier	Object of study	Highlights
Das et al.[103]	100 nm Silver nanoparticles	Osteoblasts (human, Hob) *Pseudomonas aeruginosa*	99.99% reduction of P. aeruginosa Enhanced proliferation TNTs>Ag-TNTs>flat Ti
Lan et al.[85]	25, 50 and 100 nm Silver nanoparticles	Fibroblasts (human, MRC-5) *Staphylococcus aureus*	Inhibition of S. aureus growth Diameter-dependent behaviour observed 25nm – promoted adhesion and proliferation of fibroblasts
Gunputh et al.[104]	116 nm Silver nanoparticles Approx. 100 nm	*Staphylococcus aureus*	Significant antibacterial activity
Esfandiari et al.[105]	50 and 100 nm 40, 30, 20, 18, 16 and 12 nm silver nanoparticles	*Escherichia coli*	100nm TNTs with 20 nm AgNPs – highest antibacterial activity
Mei et al.[19]	80 nm Implanted silver ions	Epithelia-like cell (Tca-8113) Fibroblast-like cell (HT1080) *Porphyromonas gingivalis* *Actinobacillus actinomycetemcomitans*	Examined lower surface Ag content performs better in early stage. Investigated higher surface Ag content has long-term effect with performance towards fibroblasts and epithelial cells comparable to nonmodified TNTs

Lan et al.[107]	25, 50 and 100 nm Silver nanoparticles	Nasal Epithelial Cell (human, HNEpC) *Pseudomonas aeruginosa*	Ag-decorated 25nm – best biocompatibility out of all modified samples, inhibited growth of P. aeruginosa 100nm – both TNTs and Ag-TNTs exhibited bad biocompatibility
Chen et al.[55]	110 nm Selenium nanoparticles chitosan	Osteoblasts (neonatal rat calvaria) Cancerous osteoblasts	Both antibacterial and anticancer activity confirmed
Liu et al. [73]	125-150 nm 20-100 nm selenium nanoparticles	Macrophages (RAW 264.7) *Escherichia coli* *Staphylococcus aureus*	Significantly decreased number of bacteria on all Se-TNT samples With increasing selenium content, macrophage activity decreased
Liu et al.[21]	70nm ZnO nanoparticles	Bone mesenchymal stem cells (Sprague Dawley rats) *Streptococcus mutans* *Porphyromonas gingivalis*	Higher ZnO concentrations promoted antibacterial activity Lower ZnO concentrations performed comparably to non-modified TNTs Stem cell proliferation was impaired with higher concentrations, but was preserved with one specific concentration, that was suggested as optimal.

Yao et al.[119]	50nm ZnO nanoparticles	Macrophages (RAW 264.7) *Staphylococcus aureus*	Inhibited proliferation and viability of S. aureus Decreased macrophage response – weaker immune reaction
Gao et al. [120]	80 nm Ag_2O nanoparticles	Pre-osteoblastic cells (mouse, MC3T3-E1 subclone 14) *Escherichia coli* *Staphylococcus aureus*	Antibacterial activity higher than 97% Improved osteoblast spreading, proliferation and differentiation
Li et al. [121]	80 nm Gold nanoparticles	*Escherichia coli* *Staphylococcus aureus*	Antibacterial ratio above 80%
Yang et al. [20]	100 nm 15nm gold nanoparticles	Bone mesenchymal stem cells (rat, rBMSCs) *Staphylococcus aureus* *Escherichia coli*	Promoted adhesion and proliferation of stem cells Slight antibacterial activity
Zhao et al.[83]	30 and 80 nm Strontium coat	Mesenchymal stem cells (Sprague-Dawley rats)	Induced osteogenic differentiation

The second group includes coating with various compounds with the focus on cell-surface improvement. It has been presented by Yang et al. [122] that, to some extent, even the diameter-dependent behaviour of TiO_2 nanotubes can be overcome with pre-adsorbed proteins. Lai et al.[15] introduced bone morphogenetic protein onto TiO_2 nanotubes in order to investigate the effect of the resulting surface on the differentiation of mesenchymal stem cells. As a result, they reported they observed a synergistic effect of BPM2 and TiO_2 nanotubes, that promoted the differentiation of used cells. Bauer et al.[123] investigated the effect of both BMP2 and an epidermal growth factor (EGF) in their study and reported that the size-induced apoptosis can could be prevented by adsorption of suitable proteins. Park et al.[124] inspected the effect of BMP2 coated onto 15 and 100 nm TiO_2 nanotubes, claiming that the differentiation towards osteogenic or chondrogenic lineages can be directed by the selection of the appropriate nanotube diameter.

Growth factors are, however, not the only functional layer type of interest. A whole subgroup could be defined by functional layers targeted at superior osseointegration. One of the most important factors for this process is hydroxyapatite. Kar et al.,[125] and later Kodama et al.,[126] have successfully coated hydroxyapatite onto TiO_2 nanotubes. Parcharoen et al.[127] also studied hydroxyapatite formation on TiO_2 layers with the conclusion that I can significantly improve adhesion between hydroxyapatite, and both modified implant and surrounding bone. Some other researchers did not proceed in this direct way. For example, Ma et al. [128] studied the role of TiO_2 nanotube precalcification on hydroxyapatite formation. The bioactivity of precalcified TiO_2 nanotubes was reported as superior, compared to nonmodified nanotubes. Interestingly, an additional thin ALD-deposited TiO_2 layer can enhance the cell growth on TiO_2 nanotubes.[129]

Modifications of wettability also seem like an interesting way of cell-surface interface optimization, as it is well known that the contact angle can influence observed interactions. Shifting the wettability from superhydrophilic to superhydrophobic in the study by Bauer et al.[130] caused the nanotubes to perform independently of the studied nanotube diameter. Even though the adhesion of mesenchymal stem cells was enhanced, this effect was only brief, as it faded after three days. In another study, carried by Yang et al.,[131] the effect of superhydrophobicity granted exceptional hemocompatibility, successfully resisting the adhesion and activation of thrombocytes.

A line-up of example studies using proteins, growth factors, hydroxyapatite and wettability modifications together with their highlights is presented in Table 3.

Table 3: Proteins, growth factors, hydroxyapatite, and wettability modifications example studies. *Authors, studied nanotube diameters, modifying agents, objects of study and study highlights are included.*

Author	Nanotube diameter /modifier	Object of study	Highlights
Yang et al. [122]	30 and 100 nm Collagen type 1 fibronectin	Osteoblasts	The cell response is directed by the adsorbed protein layer Adsorption of proteins can overcome the diameter-selective behaviour
Lai et al.[15]	30, 60 and 100 nm Polydopamine conjugated bone morphogenetic protein 2	Mesenchymal stem cells (rat)	The effect of BMP2 and TiO_2 nanotubes is synergistic, promoting their differentiation
Bauer et al. [123]	15 and 100 nm Epidermal growth factor Bone morphogenetic protein 2	Mesenchymal stem cells (rat)	Prevention of apoptosis inferred by specific nanotube diameter through EGF introduction
Park et al.[124]	15 and 100 nm Bone morphogenetic protein 2	Mesenchymal stem cells (rat) Primary chondrocytes (new-born mouse)	The differentiation lineage can be directed through TiO_2 nanotubes modified with BMP2
Parcharoen et al.[127]	60-100 nm Hydroxyapatite nanocrystals	Simulated body fluid	Hydroxyapatite coated TiO_2 nanotubes can improve the bond between implant and surrounding bone.

Ma et al.[128]	70 nm Precalcified	Hydroxyapatite formation	Superior formation of hydroxyapatite on precalcified surfaces
Motola et al.[129]	12 and 15 nm ALD TiO_2 layer	Lung fibroblast (human, WI-38) Osteoblast-like cells (human, MG-63) Neuroblastoma (human)	Coating enhanced growth of all cell types. Thinner layer (only 5 ALD cycles) performed significantly better
Bauer et al.[130]	15,20,30,50,70 and 100nm superhydrophobic	Rat mesenchymal stem cells (4-week-old Wistar rats, bone marrow)	Effect of superhydrophobicity prevails over nanotube diameter Cell adhesion enhanced in short term
Yang et al.[131]	80 nm UV-irradiated (hydrophilic) PTES methanolic solution (hydrophobic)	Platelet rich plasma	Superhydrophobic TiO_2 nanotubes showed excellent hemocompatibility, resisting adhesion and activation of platelets.

The third group includes approaches that use nanotubes as containing capsules. These can be used as drug/payload delivery carriers. Among the drugs, we can find antibiotics, such as, e.g., vancomycin[16] or gentamicin[17,68] but also melatonin,[132] and N-acetyl cysteine.[133] The payload can be made of nanoparticles. As Shrestha et al.[134] have presented, Fe_3O_4 nanoparticles can be encapsulated. By their use, we can be enabled to guide them to the point of interest magnetically. The current problem of this application dwells in insufficient control over the release times of carried payload. To address this issue, nanotube caps and release mechanisms are being studied. These can include light-sensitive, pH, temperature-sensitive, radiofrequency, ultrasound or magnetic drug delivery, and biodegradable polymer caps.[135,136]

A brief list of payload delivery studies and their highlights can be found in Table 4.

Table 4: Payload delivery system example studies*. Authors, studied nanotube diameters, modifying agents, objects of study and study highlights are included.*

Author	Nanotube diameter /modifier	Object of study	Highlights
Zhang et al.[16]	80 nm Vancomycin	Sprague Dawley rats *Staphylococcus aureus*	Significantly improved biocompatibility and microbial activity both *in vivo* and *in vitro*
Popat et al.[17]	80 nm Gentamicin	Pre-osteoblastic cells (newborn mouse, MC3T3-E1 subclone 14) *Staphylococcus epidermis*	Effective decrease in number of initially adhered bacteria and improvement of cell adhesion and proliferation.
Kumeria et al.[68]	100 nm Gentamicin PLGA Chitosan	Osteosarcoma (HOS) *Staphylococcus epidermis*	Significant antibacterial activity was observed with chitosan, that got even stronger when combined with gentamicin.
Lai et al.[132]	70 nm Melatonin	Mesenchymal stem cells (Wistar rats)	Enhanced cell adhesion, spreading, proliferation and osteoblastic differentiation
Lee et al. [133]	50 nm N-acetyl cysteine	Osteoblast like cells (MC-3T3-E1)	Enhanced cell viability

2.3.1. Doped and alloy-based TiO_2 nanotubes

The last category includes TiO_2 nanotubes that contain a foreign substance embedded directly into the TiO_2 lattice. This can be achieved either through fabrication directly from suitable Ti alloys, as mentioned in the chapter about anodic oxidation, or by subsequent enrichment of already fabricated TiO_2 nanotubes.

Among the former, we find titanium implant alloys, such as e.g. Ti-6Al-4V,[137,138] Ti-6Al-7Nb,[137,138] Ti26Nb13Ta4.6Zr,[138] and Ti-15Mo.[139] with the motivation for currently-applied material enhancement. However, specific purpose-designed alloys also find their place here. Amidst them, we find alloys such as TiZr[140,141] for cell growth scaffolds, TiTa[142] for bimodal self-organized surfaces, NiTi[143] for enhanced corrosion resistance Ti35Nb[144] for enhanced bioactivity, or Ti35Nb0.1Ag[145] for promoted antibacterial activity, and so on. The main advantage of this approach is the straightforward nature of doped TiO_2 nanotube synthesis, which does not require any additional steps. However, as was mentioned before, not all alloys are suitable for this kind of treatment, and thus, the alloy composition needs to be carefully considered.[146]

The latter usually includes two steps – TiO_2 nanotube fabrication and subsequent doping step. For example, in the study conducted by Yeniyol et al.[147], the doping step included electrochemical treatment under constant voltage and yielded Ag-doped TiO_2 nanotubes with enhanced antibacterial activity against selected periodontal pathogens. T Studies carried by Liu et al.[148] (N) and Hou et al.[149] (Ag) employed ion implantation for the doping process, leading to improvement in cytocompatibility and antibacterial activity, respectively. Zhang et al.[150] doped TiO_2 nanotubes with strontium through subsequent hydrothermal treatment.

A brief list of example works concerning doped and alloy-based TNTs and their focus can be found in Table 5.

Table 5: Alloy-based and doped TiO_2 nanotube example studies. *Authors, used alloys/dopants and the focus of presented studies are included*

Author	Alloy/doped TNTs	The focus of study
Macak et al.[137]	Ti-6Al-7Nb Ti-6Al-4V	The process of nanotube fabrication applied to biomedical alloy that is currently in use.
Tsuchiya et al.[138]	Ti-6Al-4V Ti-6Al-7Nb Ti-29Nb-13Ta-4.6Zr	Nanotube fabrication using three distinct biomaterial alloys, determination of resulting morphology.
Oliveira et al.[139]	Ti-15Mo	Preparation of nanotubular surface from standardized biomaterial Ti-Mo alloy.
Grigorescu et al.[140]	Ti-50Zr	Two-step anodization process for TiZr nanotubular surfaces. Biocompatibility assessment with osteoblast-like cells (MG-63)
Minagar et al.[141]	Ti-50Zr	Fabrication of mixed oxide TiO_2-ZrO_2-$ZrTiO_4$ nanotubes by anodic oxidation of TiZr alloy.
Tsuchiya et al.[142]	Ti-13Ta Ti-25Ta Ti-50Ta Ti-80Ta	Study of nanostructured surfaces fabricated from various TiTa alloys. Formation of nano porous/nanotubular surfaces. Analysis of bimodal self-organization.

Hang et al.[143]	NiTi	Preparation of Ni_2O_3 doped TiO_2 nanotubes via electrochemical anodization. Estimate of apatite formation. Wettability evaluation.
Ding et al. [144]	Ti-35Nb	Fabrication of nanotubes and their *in vitro* biocompatibility evaluation using mesenchymal stem cells.
Taipina et al. [145]	Ti-35Nb-0.1Ag Ti-35Nb-5Ag	Enhancement of Ti-35Nb antibacterial activity. Pre-osteoblast (MC3T3-E1) cytocompatibility appraisal. Antibacterial activity against *E. coli*
Yeniyol et al.[147]	TiO_2 nanotubes Ag nanoparticle doped	Modification of fabricated TiO_2 nanotubes (Ti foils). Testing of antibacterial properties against *A. actinomycetemcomitans*, *C. rectus*, and *T. forsythia*.
Liu et al.[148]	AO TiO_2 nanotubes N+ ion implanted	Preparation of N+ doped TiO_2 nanotubes and evaluation of its cytotoxicity (L-929 fibroblasts) and antibacterial activity (*E. coli*)
Hou et al.[149]	AO TiO_2 nanotubes Ag ion implanted	Fabrication of Ag doped TiO_2 nanotubes and analysis of its activity against *S. aureus*
Zhang et al.[150]	AO TiO_2 nanotubes Sm/Sr doped	Production of Sm/Sr doped TiO_2 nanotubes with subsequent *in vitro* biocompatibility evaluation (MC3T3-E1) and antibacterial performance assessment (*S. aureus, E.coli)*

3. Aims of Thesis

Based on the current state of the art, we decided to focus on the study of cell behaviour on selenium and silver nanoparticle modified TiO_2 nanotube surfaces in order to better understand their cell-surface interactions in nanoscale.

1. **Biointerface of selenium-nanoparticle decorated TiO_2 nanotubes:**

Selenium nanoparticle have attracted attention for their antibacterial, anti-inflammatory, and anti-cancer properties and it maintains relatively low off-target cytotoxicity.[18,84] Here we introduce the fabrication, characterization and cytocompatibility of titanium oxide nanotube surface decorated with various surface densities of chemically synthesized selenium nanoparticles. Due to the absence of more complex reports regarding the interaction of such a surface with mammalian cells and bacteria, we studied mutual effect of selenium nanoparticles and TiO_2 nanotubes on antibacterial properties against *E. coli* and viability of osteosarcoma MG-63 cells and non-cancerous NIH/3T3 fibroblasts.

2. **Biointerface of silver nanoparticle decorated TiO_2 nanotubes with different nanoparticle stabilizers:**

Enhanced antibacterial properties of TiO_2 nanotubes (TNTs) and silver nanoparticles (AgNPs) have attracted much attention in biomedicine. The antibacterial properties of nanoparticles depend, among others, on the functionalization layer of the nanoparticles. However, the more complex information about the influence of different functionalization layers on antibacterial properties of nanoparticle decorated surfaces has been missing. Here we prepared the array of TNTs decorated with AgNPs having different functionalization layers such as polyvinylpyrrolidone, branched polyethyleneimine, citrate, lipoic acid, and polyethylene glycol. To assess the antibacterial properties, the viability of Gram-positive (*Staphylococcus aureus*) and Gram-negative bacteria (*Escherichia coli* and *Pseudomonas aeruginosa*) has been performed.

4. The antibacterial and anti-cancer properties of Se-nanoparticle decorated TiO_2 nanotube surfaces

The widespread use and persisting negative properties of some metallic biomaterials for tissue engineering or surgical instruments aimed research to modulate the surface characteristics of biomaterials into the form with desired functional surface properties. The rapid progress in nanotechnology enabled us to approach and mimic the tissue environment via surface modifications including chemistry, topography or roughness that can significantly change the interface between individual material and tissue cells or bacteria and thus, results in different responses in cell adhesion, viability, metabolism, antibacterial or anti-inflammatory activity. Nanostructuring of titanium film into the form of nanotubes (TNTs) has attracted great attention for improving cell adhesion, growth, and differentiation. Further, many approaches were subsequently introduced to enhance the antibacterial activity through the loading the nanotubes with various antibiotics or their decoration/doping with various nanoparticles, including gold, silver, and zinc oxide. Other addressed the biocompatibility through coating with bioactive compounds, such as PLGA, chitosan, hydroxyapatite, or growth factors. Recently, treatment of bio-surfaces with selenium attracted attention. Selenium is an important element that plays crucial role in preventing cancer and protecting cells from oxidative damage. It has been reported to exhibit antibacterial, anti-cancer and anti-inflammatory properties that make selenium interesting for many biomedical applications. In our work, we introduced the fabrication of TiO_2 nanotubes of 50 nm in diameter via anodic oxidation of titanium layer deposited on silicon wafer. Nanotubes were decorated with chemically synthetized selenium nanoparticles of diameter ~90 nm. We prepared three samples having different number of nanoparticles per area. Designed films were characterized with contact angle measurement, SEM, XPS and AFM techniques. Further, we studied the antibacterial properties such surfaces against *E. coli* and viability of osteosarcoma MG-63 cells and non-cancerous NIH/3T3 fibroblasts.

4.1. Materials and methods

Sputter deposition of titanium

Titanium films with thickness of 500 nm were deposited onto 100mm P-type silicon wafers covered with approx. 1 μm of thermal silicon dioxide. Ion-Beam Sputter Deposition System (BESTEC) equipped with three-grid radio frequency-induced coupled plasma Kaufman ion-beam source (Kaufman & Robinson–KRIÒ, Inc., USA) were used for the deposition process.

Fabrication of nanotubes via anodic oxidation

TiO_2 nanotubes were fabricated from Si wafer sputter-deposited with 500 nm of titanium. The fabrication was carried through single-step electrochemical anodization in ethylene glycol-based electrolyte. Conventional two-electrode setup was used. Shortly, the electrochemical anodization was performed with a voltage ramp with the step of 1 volt per second in the electrolyte solution of ethylene glycol ($C_2H_6O_2$, p.a., Penta, CZ), 1.2 wt% ammonium fluoride (NH4F, Sigma Aldrich, DE) and 2 vol% of deionized water (Millipore Corp., USA, 18,2 MΩ). The maximum voltage was set to 15 V. After reaching the maximum set voltage, the value was maintained until the current dropped to zero. Samples were thoroughly rinsed with deionized water, dried with a stream of nitrogen and subsequently annealed in a vacuum furnace at 450 °C for 3 hours, with the heating ramp of 5 °C per minute.

The setup consisted of anodization cell filled with electrolyte, with a crocodile clamp jawed onto innox tube and a needle as electrical connections.

Preparation of selenium nanoparticles and Se-NP surface decoration

Selenium nanoparticles were prepared according to protocol inspired by the previous study carried by Liu et al.[18] Source solution was prepared by mixing 3 mL 100 mmol L^{-1} L-glutathione (Sigma-Aldrich) and 3 mL of 100 mmol L^{-1} sodium selenite (Sigma-Aldrich). To initiate the reaction by bringing the pH to alkaline region, NaOH was added. Adjustment of nanoparticle amount decorated onto the surface was done through dilution of source solution. The volumes of added ultrapure water were 9 mL for low, 6 mL for medium, and 3 mL for high nanoparticle concentration. The formation of nanoparticles manifested as a change in color of the solution. The transition proceeded from transparent to clear red. After the solution turned red, 100 μL of acquired nanoparticle suspension was introduced onto prepared TiO_2 nanotube surfaces, where they were incubated for 20 minutes. After that, samples were rinsed several times, soaked in ultrapure water to remove non-adsorbed particles, and named TNTs, Se-Low, Se-Medium, and Se-High. Prior to further use, modified surfaces were sterilized with UV irradiation for 15 minutes. Simplified scheme of the whole process can be found in Figure 10.

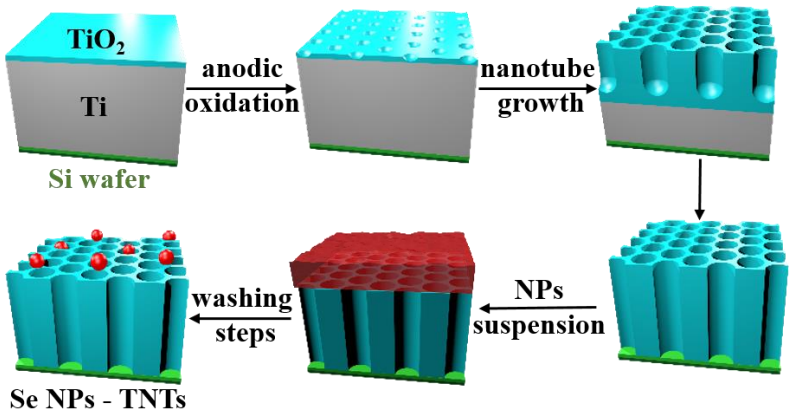

Figure 10: Simplified scheme displaying general process of specimen fabrication. *Samples were fabricated through anodic oxidation of sputter-deposited titanium. Selenium nanoparticles were adhered from prepared suspension.*

Characterization of nanostructured surfaces

The wettability of samples was measured at room temperature by determination of water contact angle of 5 µL water drop introduced on sample surface after UV irradiation (Phoenix 300, Surface & Electro Optics Co.,Ltd, KOR). Contact angle was evaluated using tangent line method 2 (higher angles) and trigoniometric functions method (lower angles) implemented in software Surfaceware 8. The surface morphology and nanoparticles size were characterized with scanning electron microscope (SEM, Mira II, Tescan, CZ) and the roughness was calculated by atomic force microscopy in dry non-contact mode (AFM, NanoWizzard3, JPK). Chemical composition of samples was determined with X-ray photoelectron spectroscopy (XPS, AXIS Supra, Kratos Analytical Ltd, UK). The XPS spectra were analyzed by a peak fitting software (CasaXPS version 2.3.18PR1.0) provided by SPECS GmbH (Berlin, Germany). Raw data were processed by the subtraction of a Shirley background for secondary electrons and element peak fitting was used to estimate the relative element molar fraction. The integral of the peak was divided by a relative sensitivity factor (R.S.F.), which is characteristic for each element. Finally, the concentration profile of selenium released from the surface was determined with inductively coupled plasma mass spectrometry (ICP-MS). Decorated samples were immersed into 3 mL of ultrapure water for 15 days. At selected points in time, ultrapure water was collected, samples dried with a nitrogen stream and subsequently immersed into fresh ultrapure water.

Cell culture

The cancerous MG-63 cells and non-cancerous NIH/3T3 cells were maintained in complete Dulbecco's Modified Eagle's medium (DMEM) supplemented with 10% fetal bovine serum (FBS), 2 mmol L^{-1} L-glutamine, and 5% penicillin/streptomycin (50 U mL^{-1} and 50 µg mL^{-1}) at 37°C in a humidified 5% CO_2 incubator. Cells were harvested by trypsinization with 0.25% trypsin-EDTA solution at 75% confluency and seeded with a defined density onto the sterile samples placed in a polystyrene microplate.

Cell adhesion and viability

The adhesion of MG-63 and NIH/3T3 cells onto selenium-nanoparticle decorated TiO_2 and onto the control (bare TiO_2 nanotubes) was qualitatively evaluated from images taken by an optical microscope (Axio Imager M2m, Zeiss). All samples were placed in a 24-well plate and used as the surface for cell seeding at a density of $1 \cdot 10^3$ cells per area. The images of cells were taken at 3 hours. Viability of MG-63 cells was measured with XTT assay and evaluated on days 1, 2, and 6 after the seeding; the initial cell density was $1 \cdot 10^3$ cells per area. Briefly, the cells were incubated for a defined period of time and then gently washed twice with pre-heated phosphate buffer saline (PBS). The mixture of 100 µL culture medium and 50 µL of tetrazolium dye (XTT, 1 mg mL^{-1} in DMEM and 25 µmol L^{-1} PMS in PBS) was added into each well containing the samples and incubated 2 hours in CO_2 incubator. 100 µL of solution were transferred from each well into a new 96-well plate and the absorbance was measured at 450 nm with a microplate spectrophotometer (Beckman Coulter Paradigm).

Tests of antibacterial activity

Antibacterial properties of selenium nanoparticle decorated nanotubes were evaluated through the bacterial viability assay with gram-negative *E. coli*. Non-decorated nanotube surface was used as a control. The samples were rinsed with water and sterilized with UV for 15 minutes before each experiment. Briefly, 50 µL of bacterial suspension was spread onto the surface and incubated 4 hours at 37 °C. Subsequently, adhered bacteria were washed out with phosphate buffer saline (PBS) and collected bacterial suspension was diluted 100 times with PBS. Bacteria cultured plates were prepared using agar, yeast extract, NaCl, and tryptone. 200 µL of the diluted solution was inoculated on prepared agar plates and incubated for 24 hours at 37 °C and 80% humidity. Agar plates were then photographed, and colony-forming units were calculated (CFU mL^{-1}).

Statistical analysis

Mean values and standard deviations of obtained data were calculated. Statistically significant differences ($p < 0.05$) were confirmed using Student's t-test. All shown data are expressed as the mean ± standard deviation.

4.2. Results and discussion

4.2.1. Surface characterization

Selenium NPs decorated TiO_2 nanotubes were fabricated via anodic oxidation of titanium layer deposited on silicon wafer followed by the adsorption of chemically synthesized selenium nanoparticles. Fabrication of nanostructured surface resulted in TiO_2 nanotubes with the diameter of 51.72 ± 5.55 nm (Figure 12C) and length of 500 nm (Figure 12B). The size distribution of their diameter can be found in Figure 11B The surface was decorated with spherical selenium nanoparticles (Figure 12A) of 88.93 ± 6.87 nm in size, which is

significantly more than nanotube diameter. Thus, the nanoparticles covered the top of the nanotubes at Se-Low (Figure 12D), Se-Medium (Figure 12E) and Se-High (Figure 12F) samples corresponding to number of 3.2 ± 1.14 (low), 9.1 ± 1.20 (medium) and 18.5 ± 2.37 (high) particles per 4 μm^2, respectively.

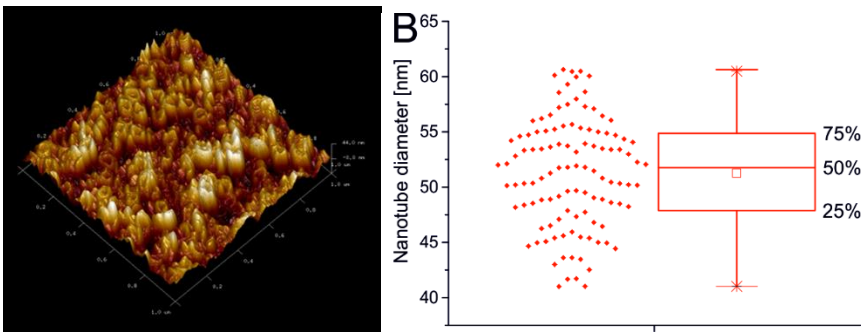

Figure 11: AFM of bare TiO_2 nanotubes(A) and their diameter size distribution (B). *Individual tube tops can be observed.*

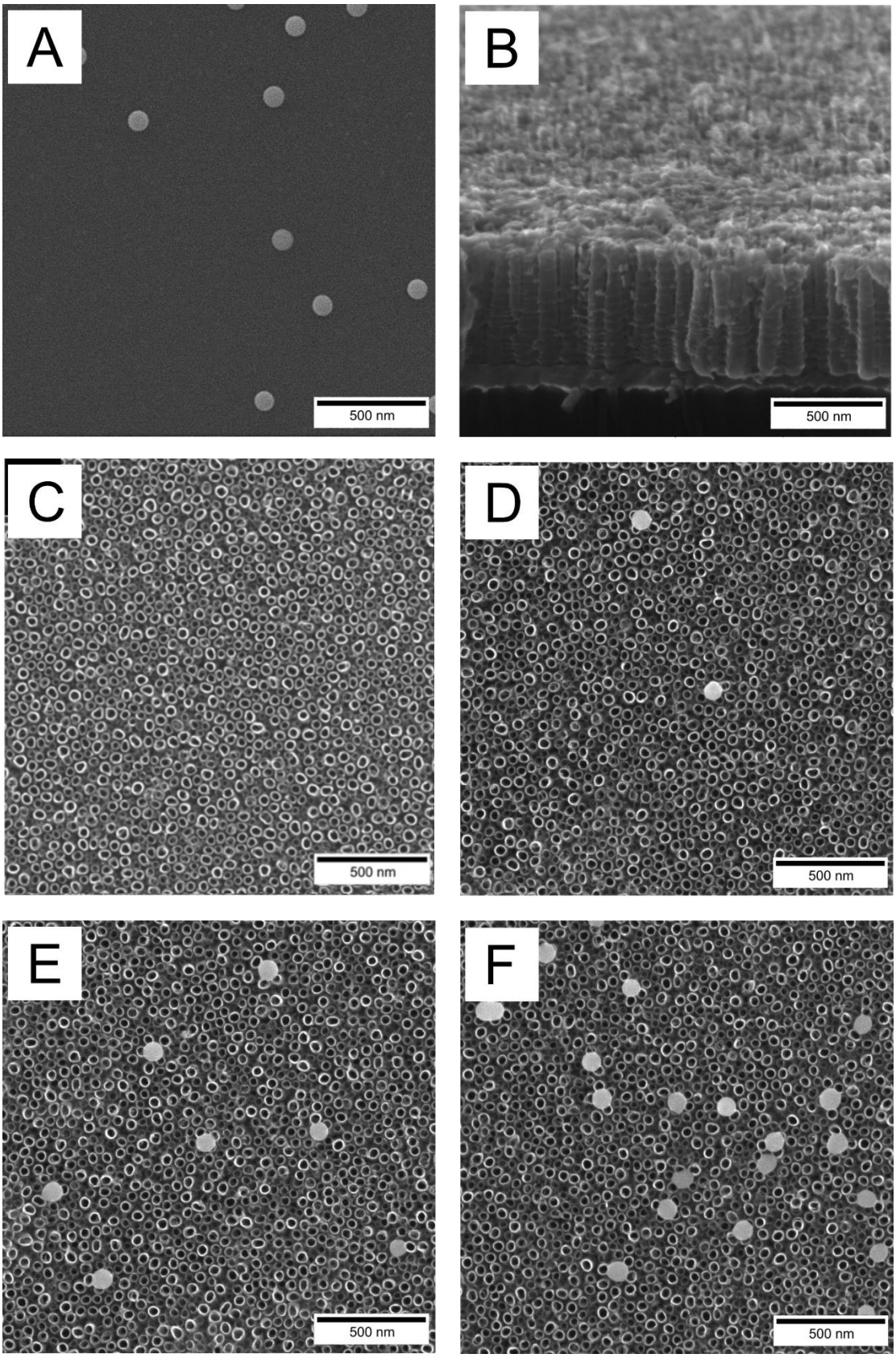

Figure 12: SEM images of prepared surfaces. *Selenium nanoparticles (A), side view of TiO_2 nanotubes (B), their top view (C), and samples with low (D), medium (E) and high (F) nanoparticle surface densities.*

SEM analysis also revealed that both the number of decorated nanoparticles and the diameter of nanotubes are consistent over the surface of each sample. AFM analysis further showed the increase in root mean squared (RMS) roughness of samples with an increasing number of nanoparticles decorated onto TiO_2 nanotubes. The RMS value ranged from 16.6 nm to 24.1 nm. The AFM of bare TiO_2 nanotubes can be seen in Figure 11A. The X-ray diffraction of bare TNTs showed peaks of titanium, anatase, rutile, and silicon peak (data not shown). The presence of the titanium peak implies that not all the titanium was transformed into the oxide. The presence of anatase and rutile peaks signifies the success of transformation from amorphous to crystalline phase through annealing at high temperature.

Measurement of UV-treated TNTs wettability revealed a significant difference between decorated and non-decorated TiO_2 nanotubes. The contact angle of bare annealed nanotubes was ~20°. Selenium-decorated nanotubes were more hydrophobic with values ~48°. The difference between individual nanoparticle surface densities was ~1.5° each. (Figure 13) It was reported previously, that selenium nanoparticles could slightly increase the contact angle of TiO_2 surfaces.[151] This effect apparently persisted even after the UV irradiation.

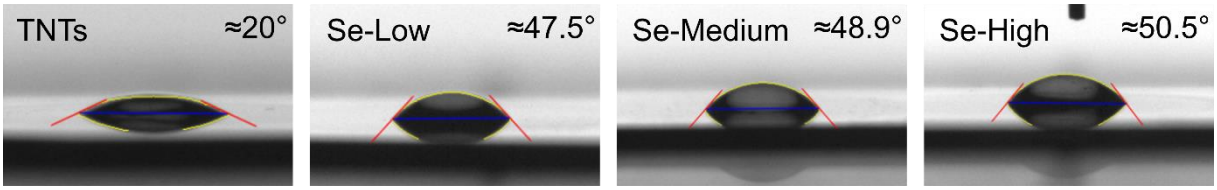

Figure 13: Wettability of prepared surfaces after UV treatment. *Decorated surfaces exhibited significantly higher contact angles.*

X-ray photoelectron spectroscopy of selenium decorated TiO_2 nanotubes was done to confirm the presence of selenium in the samples (Figure 14). There was no significant change in bonding states of Ti2p and O1s after the decoration with nanoparticles. The XPS quantitative analysis of selected elements was summarized in Table 6. The percentage of selenium Se3d proportionally increased with the increasing number of decorated selenium nanoparticles. We also observed a peak corresponding to the presence of sulphur. The sulphur peak was observed for all nanoparticle decorated samples even after multiple washing steps and 24 hours immersion in ultrapure water. It could correspond with the adsorption of glutathione, or other product of reaction containing sulphur on the fabricated surface.

Table 6: XPS analysis of selenium decorated TiO_2 nanotubes. *Relative percentage of selected elements calculated from narrow spectra*

	TNTs [%]	Se-Low [%]	Se-Medium [%]	Se-High [%]
O1s	55,93	56,12	55,89	51,92
Ti2p	12,75	11,69	11,98	11,11
C1s	31,31	32,19	31,76	35,24
Se3d	0,00	0,08	0,46	1,73

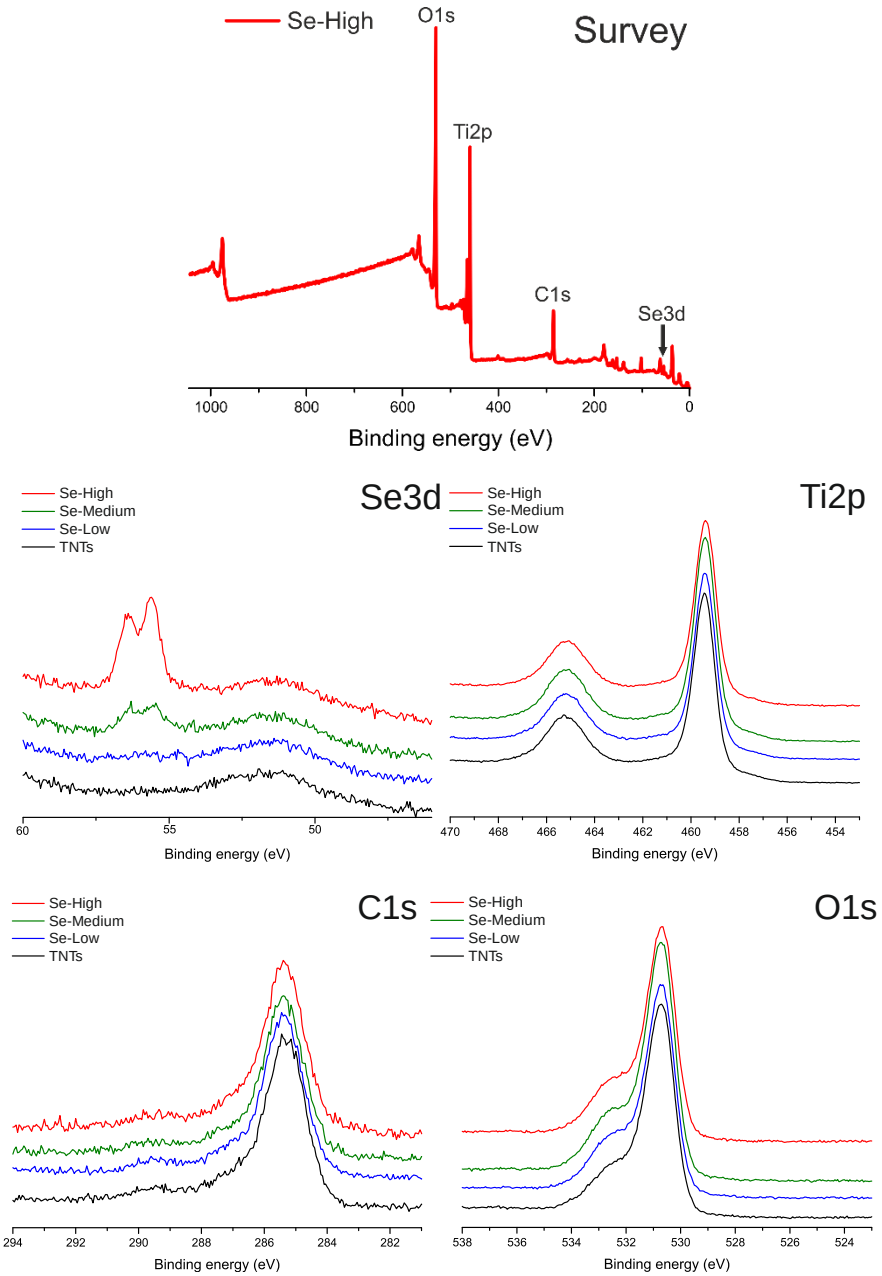

Figure 14:XPS graphs*. Narrow spectra of Se3d, Ti2p, C1s and O1s. Spectra were used to calculate relative percentage of selected elements.*

The ICP-MS analysis introduces powerful and sensitive technique capable of detecting metals and several non-metals at concentrations as low as one part in 10^{15} (part per quadrillion, ppq). We used this technique to obtain the release profile of selenium from the nanotube surface. The analysis showed the release rate of selenium at maximum tens of ppb (Figure 15). The biggest contribution to the total release was during the first 24 hours. The absolute value was highly dependent on the amount of initially decorated selenium nanoparticles. Over the time, the released amount of selenium steadily decreased. After the experiment, samples were repeatedly analyzed with SEM. No significant decrease in the number of nanoparticles was observed. Further, the release rate was significantly lower than in research done by Liu et al.[18] In their case, authors attributed the cytotoxicity to the gradual release of selenium. In our case, it is questionable whether such a low concentration of selenium can inflict toxicity, either for bacteria or tissue cells. We believe that there is another mechanism of toxicity via the interaction of the cell membrane with a combination of nanoparticle and nanotube properties, nanoparticle size, and the number of nanoparticles decorated on nanotubes.

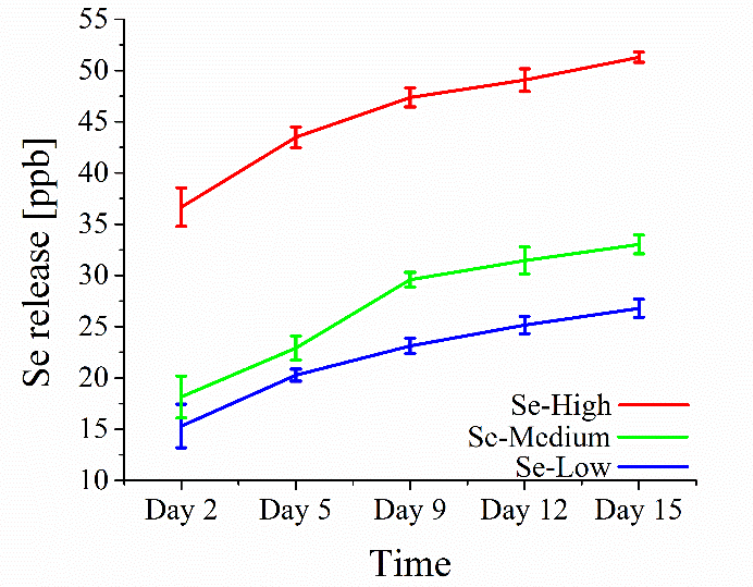

Figure 15:The cumulative release profile of selenium acquired by ICP-MS. *Initial amount of selenium nanoparticles significantly influenced total overal release.*

4.2.2. Antibacterial properties of selenium-nanoparticle decorated TiO_2 nanotubes

To prevent the adhesion and proliferation of pathogenic bacteria on biomaterials, we rely on coatings with antibiotics, biocidal agents, or antibacterial nanoparticles. Selenium nanoparticles are well-known for their antibacterial properties to a wide range of bacteria, even if the mechanism of action is still unknown. [152] It has been reported by Tran et al.[110]

that selenium nanoparticles inhibited the growth of gram-positive *Staphylococcus aureus*. Liu et al.[18] incorporated these nanoparticles into TiO_2 nanotubes to enhance the antibacterial activity of surface to *Escherichia coli* with 50% efficiency compared to bare TNTs in 24 hours. Our assay revealed that compared to bare nanotubes, selenium-nanoparticle decorated nanotubes exhibited significantly enhanced antibacterial properties (Figure 16). The short 4-hour time interaction of the bacteria with the surface was efficient to decrease the number of *E. coli* colonies for Se-Low and Se-High approximately 60% and 90%, respectively. We have confirmed antibacterial properties of selenium nanoparticle decorated TiO_2. Since the release mentioned above was so low, the question is how it was caused. Selenium is known to be non-adhesive, anti-proliferative, and membrane damaging for some bacteria.[18,110,115,153] Also, both selenium nanoparticles and TiO_2 carry negative charge at physiological pH, which could be repulsive for a negatively charged membrane of *E. coli*. [154]

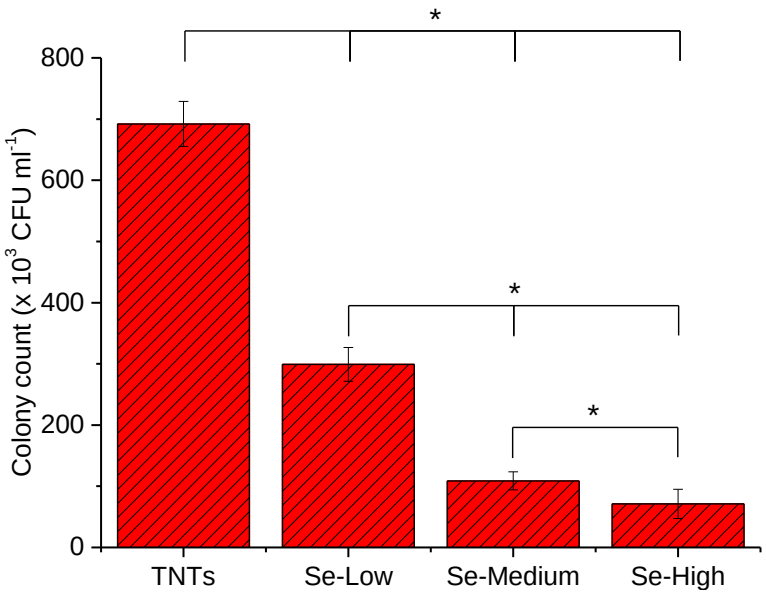

Figure 16: Bacterial assay of viability expressed as colony forming units. *The antibacterial activity was compared with undecorated TNTs. * indicates significant difference between compared samples (p=0.05)*

4.2.3. Viability assay of NIH/3T3 and MG-63 cells

Adhesion plays a fundamental role in cell development, differentiation, communication and migration, and during the pathogenesis of a wide range of diseases, including cancer [155], osteoporosis[156], and atherosclerosis.[157] The strength of cell adhesion is a crucial consideration in biomaterial design and development. On the other hand, selenium is known to be involved in anti-cancer activity while protecting the benign cells.[70,84,109,158] Thus we studied the effect of selenium nanoparticle decorated TiO_2 nanotubes on adhesion and proliferation of cancer (MG-63 cells) and normal (NIH/3T3 cells) cells. The adhesion and morphology of both cell lines were qualitatively evaluated by taking DIC images 3 and 24

hours after cell seeding, as shown in Figures 17 and 18. The NIH/3T3 cells adhered onto TNTs and Se-Low sample surface with fibroblastic well spread elongated morphology. Se-Medium surface showed a little deterioration in cell morphology turning the elongated morphology to rounded shape but still well adhered. The NIH/3T3 cells on Se-High surface were completely round in shape with obvious apoptotic cells (Figure 18). The unfavourable conditions reflecting the change in cell morphology resulted in a lower number of attached cells. A similar effect was observed for adhesion and morphology of cancerous MG-63 cells (Figure 17). These cells at day 1 attached to the control and Se-Low surfaces but exhibited more rounded shape compared to the noncancerous cells (Fig 18). Cell adhesion experiment demonstrated that selenium nanoparticle decorated TiO_2 nanotubes caused unfavourable conditions for cancer MG-63 and normal NIH/3T3 cells, particularly at Se-Medium and Se-High TNTs surface, compared to the control TNTs and Se-Low surface. In order to know whether these microscopic observations were not done by the slow adhesion rate, we performed proliferation assay by measurement of cellular activity using XTT assay.

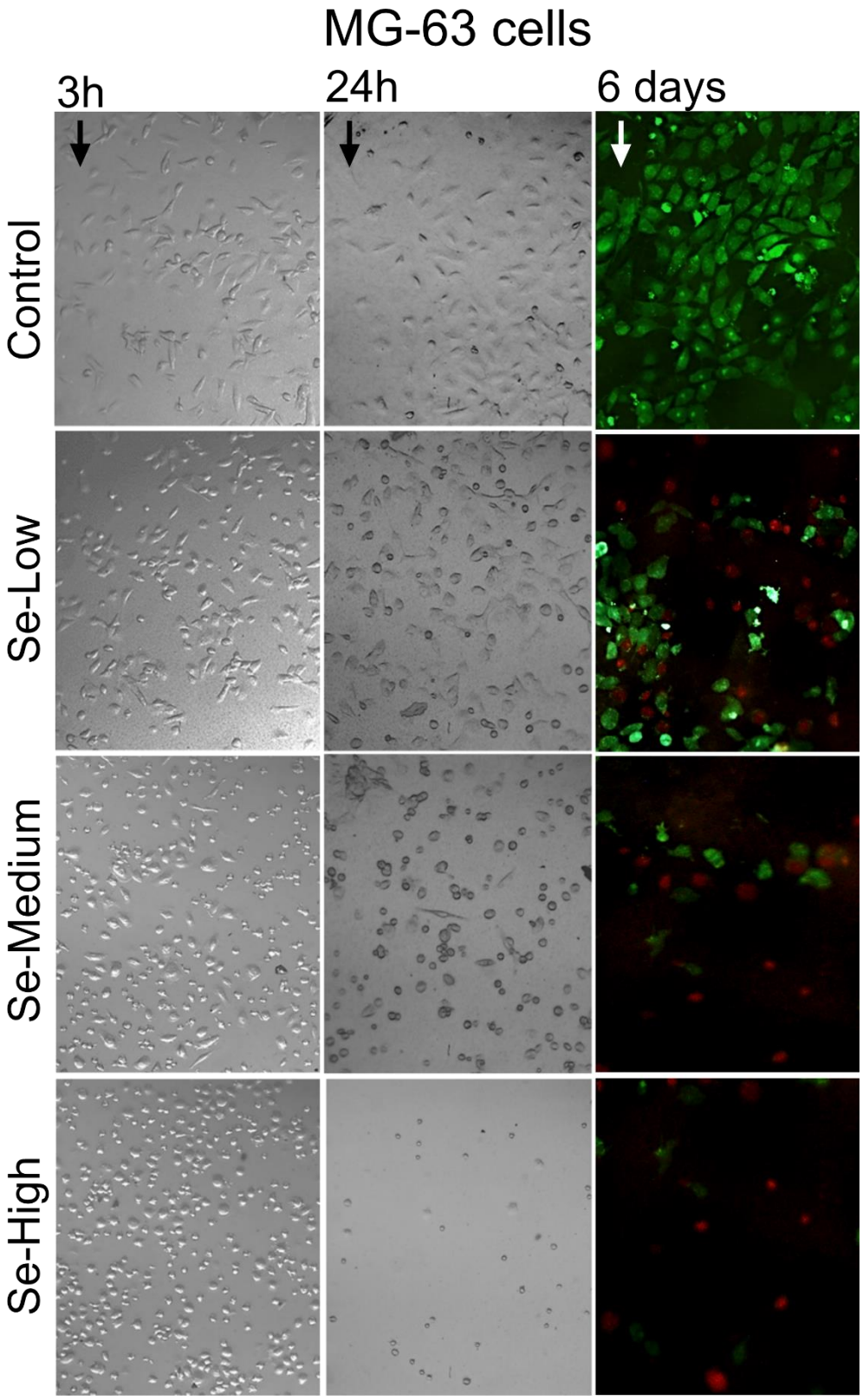

Figure 17: DIC images of adhesion and morphology of MG-63 (cancerous) cells. *Cells were cultured on prepared selenium nanoparticle decorated TiO_2 nanotubes. Photographs were taken after 3 and 24 hours.*

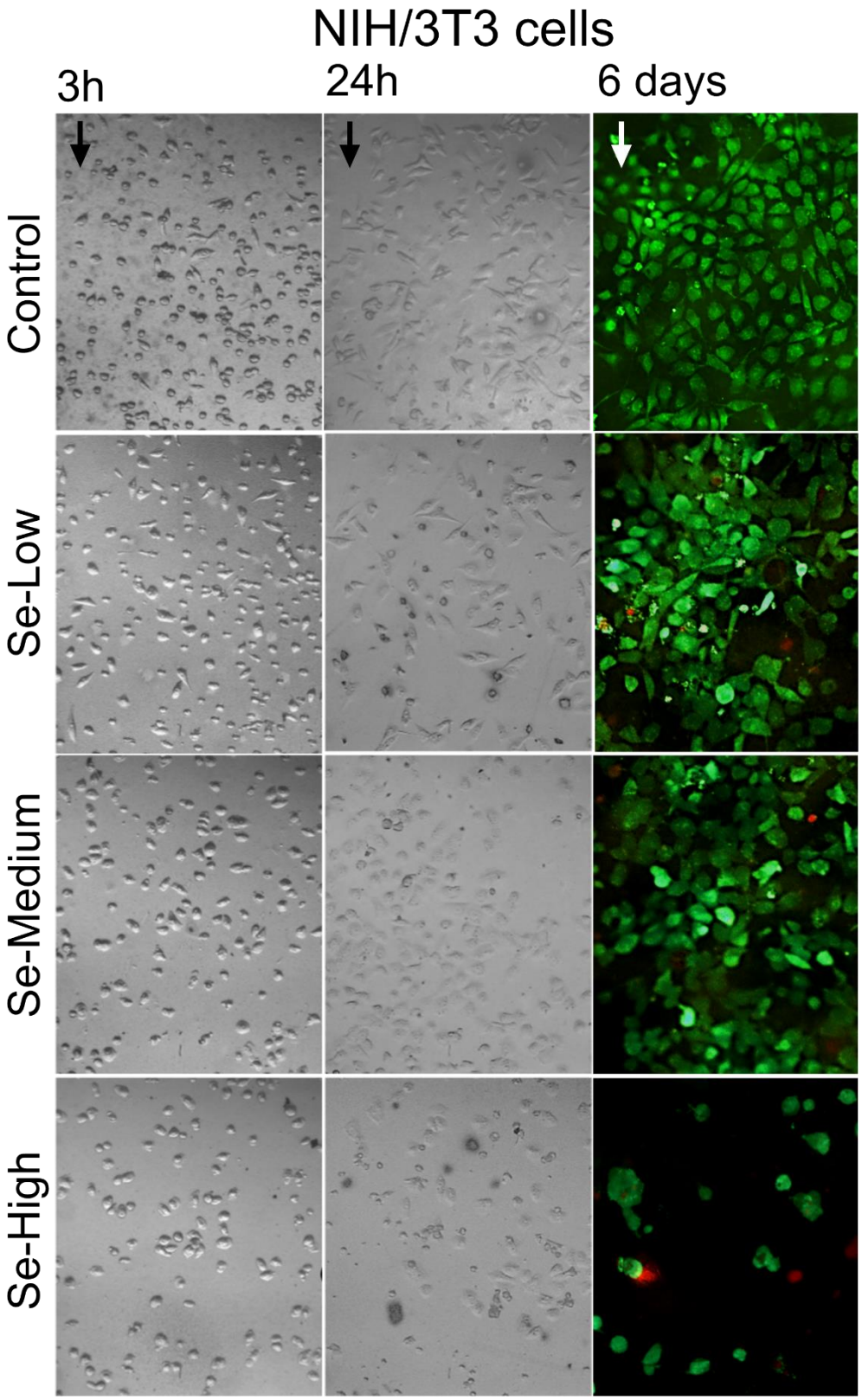

Figure 18: DIC images of adhesion and morphology of NIH/3T3 cells. *Cells were cultured on prepared selenium nanoparticle decorated TiO_2 nanotubes. Photographs were taken after 3 and 24 hours*

Our results with NIH/3T3 cells suggested that there was no significant difference in proliferation rate at day 1 and 2 for Se-Low and Se-Medium TNTs surfaces compared to the control group (Figure 19A). At day 6, XTT assay showed an increased proliferation rate of NIH/3T3 cells. The values measured at this day had decreasing tendencies towards a higher number of decorated selenium nanoparticles. This can be attributed to slower adhesion, activity, or proliferation of cells on such surfaces. The proliferation rate of NIH/3T3 cells cultured on Se-High TNTs surface was significantly decreased at day 1, 2 and 6. It came out from the smaller initial number of cells adhered on Se-High surface as observed with adhesion assay and suggested that this amount of decorated selenium nanoparticles was not compatible with the adhesion and proliferation of noncancerous NIH/3T3 cells. Similar results were obtained for cancerous MG-63 cells (Figure 19B). The unfavourable effect was much stronger at Se-Medium surface compared to the noncancerous cells and maximal at Se-High surface. From our results it is apparent that MG-63 cells did not adhere well onto selenium decorated surfaces and when adhered, they did not increase activity or proliferation rate since no significant change in absorbance was observed at day 6 compared to day 1 and 2. Finally, we did live/dead staining of both cells to check the viability of cells at the day 6. The images (Figure 18) confirmed our quantitative results obtained from the proliferation test. The cancerous cells gradually detached the selenium decorated surface and compared with the control, mostly dying cells occurred attached the surface (Fig 17, red colour). Fibroblasts showed significant decrease in a number of adhered cells on Se-High surface and a few dying cells on Se-Medium surface which again supported our results from proliferation assay (Figure 18).

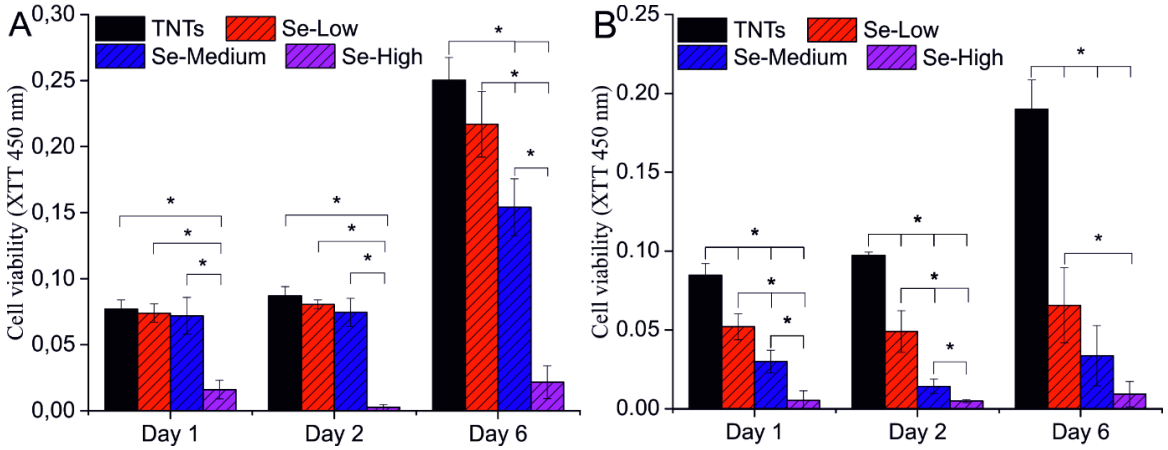

Figure 19: XTT viability assay of NIH/3T3 (A) and MG-63 (B) cells. *Cell cultures were seeded on TiO_2 nanotubes decorated with various surface densities of selenium nanoparticles. * indicates significant difference between compared samples (p=0.05)*

Our observation is consistent with other similar report of Chen et al.[84] in which the selenium nanoparticles released from TiO_2 nanotubes and diffused through the chitosan layer, decreased adhesion and viability of cancerous osteoblasts. Other reports suggesting selenium as a promising and favourable for noncancerous cells[70,84] was not confirmed in our experiments since the Se-High TNTs surface was significantly suppressing the noncancerous NIH/3T3 cells adhesion and viability. To conclude these results, the exact mechanism that makes the anti-cancer action of selenium work is still a subject of research as well as much work must be done regarding the influence of selenium towards noncancerous cells. However, selenium nanoparticle decorated TiO_2 nanotubes can be promising biomaterial surface for tissue engineering since the mechanisms of action combining the antibacterial selenium nanoparticles and nanostructured TiO_2 surface is still unknown.

5. Effect of nanoparticle stabilizers on antibacterial activity of silver nanoparticle decorated TiO_2 nanotubes

The antimicrobial properties of nanoparticles depend on the surface charge, nanoparticle size, shape, and surface coating (stabilizers/functional layers). Lately, the role of nanoparticle surface coatings became more apparent. To date, colloidal nanoparticles with different surface coatings have been synthesized and evaluated for their antibacterial efficiency. The silver nanoparticles introduce the most reported nanoparticles with the natural antibacterial properties. The NPs size and shape and the topography of the nanostructured surface can effectively modulate the antibacterial properties. In our work, the array of ~50 nm diameter TiO_2 nanotubes has been fabricated *via* anodic oxidation of polished titanium foil. The nanotubes were decorated with commercial silver nanoparticles of ~50 nm diameter. Nanoparticles were functionalized by polyvinylpyrrolidone, branched polyethyleneimine, citrate, lipoic acid and polyethylene glycol. Ag-decorated TNT arrays were characterized by scanning electron microscopy, atomic force microscopy and X-ray photoelectron spectroscopy. To assess the antibacterial properties, the adhesion and viability of Gram-positive (*S. aureus*) and Gram-negative bacteria (*E. coli* and *P. aeruginosa*) were performed.

5.1. Materials and methods

Polishing of titanium foils

Raw 0.125 mm thick titanium foil sheets (GoodFellow, 0.125 mm, 99.6+%, annealed) were cut to pieces of appropriate sample size. Guillotine shears were used to minimize the foil bending. Cut pieces were degreased in acetone and isopropyl alcohol. Degreased samples were fixated onto 30mm stubs. Used stubs were moved to semiautomated grinder/polisher Tegramin 30 for further processing. In groups of six, future samples were polished with fabric disks (Struers, MD-Dur and MD-Nap) and diamond suspensions (9μm, 3 μm, 1 μm). Before further use, polished samples were cleaned with acetone and isopropyl alcohol.

Fabrication of nanotubes via anodic oxidation

TiO_2 nanotubes were fabricated from polished titanium foil (GoodFellow, 99.6+%, annealed). The fabrication was carried through single-step electrochemical anodization in ethylene glycol-based electrolyte. Conventional two-electrode setup was used. Similarly to previous experiment, the electrochemical anodization was performed with a voltage ramp with the step of 1 volt per second in the electrolyte solution of ethylene glycol ($C_2H_6O_2$, p.a., Penta, CZ), 1.2 wt% ammonium fluoride (NH4F, Sigma Aldrich, DE) and 2 vol% of deionized water (Millipore Corp., USA, 18,2 MΩ). Further process optimization was necessary after switching the substrate. Desired nanotube features were the closest with

samples anodized at 30V, thus, it was used as maximum voltage applied to polished titanium foils. After reaching the maximum set voltage, the value was maintained until reaching set time limit. Subsequently, the samples were thoroughly rinsed with deionized water, dried with a stream of nitrogen and annealed in a vacuum furnace at 450 °C for 3 hours, with the heating ramp of 5 °C per minute.

The fabrication setup consisted of two crocodile clamps. One jawed onto the innox tube, and the other jawed directly into prepared sample, submerged in container filled with electrolyte.

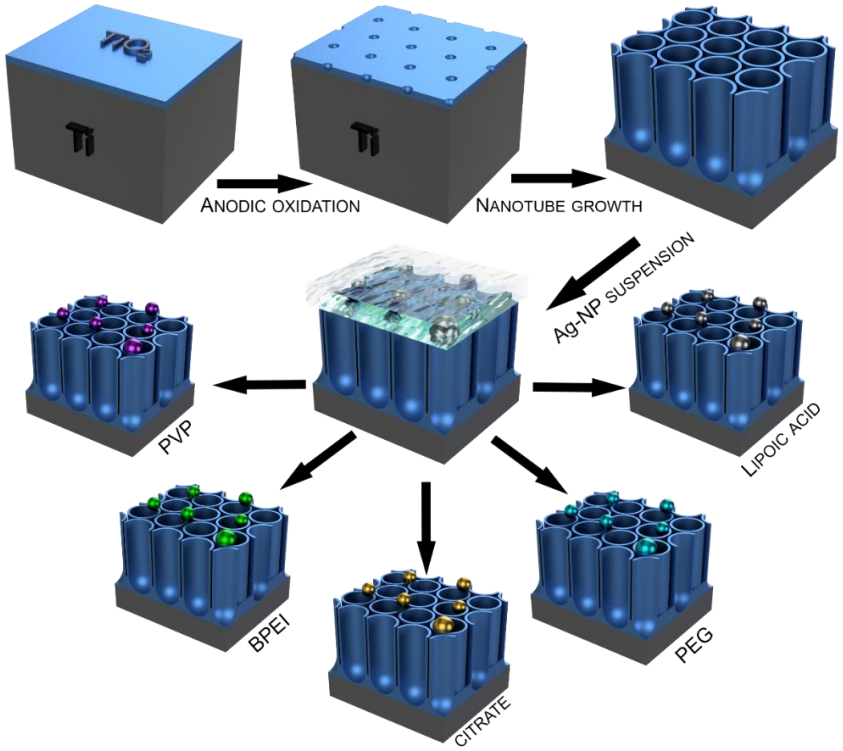

Figure 20: Simplified scheme displaying the process of Ag-decorated TiO_2 nanotube sample fabrication. *Samples were fabricated through anodic oxidation of titanium foil. Silver nanoparticles were adhered from solutions with variable dilution*

Decoration of TNTs with Ag-NPs

The array of TiO_2 nanotubes was decorated with commercial silver nanoparticles functionalized with polyvinylpyrrolidone (PVP), citrate, branched polyethyleneimine (BPEI), polyethylene glycol (PEG), and lipoic acid (Sigma-Aldrich; 0.02 mg mL^{-1} stock solutions) as depicted in simplified scheme in Figure 20. Because different nanoparticles exhibited different degree of adsorption rates onto the TiO_2 nanotubes, we optimized the dilution of stock solution for each nanoparticle to achieve the same number of nanoparticles per surface area. Then, 15 µL of diluted nanoparticle suspension was dropped onto the heated TNTs

surface until drying. Decorated samples were rinsed five times in deionized water and soaked in ultrapure water to remove any un-adsorbed nanoparticles.

Characterization of nanostructured surfaces

The morphology of AgNPs-TNTs array was characterized with scanning electron microscope (SEM, Mira II, Tescan, CZ), surface roughness was analyzed using atomic force microscopy (AFM) in dry non-contact mode (SPM, Dimension Icon, Bruker), and X-ray photoelectron spectroscopy has been used to analyse surface chemistry (XPS, AXIS Supra, Kratos Analytical Ltd, UK). XPS spectra were analyzed by a peak fitting software (CasaXPS version2.3.18PR1.0) provided by SPECS GmbH (Berlin, Germany).

Bacterial cultures and SEM microscopy

Bacterial strains of S. aureus (CCM 4223), E. coli (CCM 3954), and P. aeruginosa (CCM 3955) were purchased from the Czech Collection of Microorganisms (CZ). After overnight cultivation at 37 °C on blood agar, the strains were diluted in Mueller Hinton broth (Oxoid, UK) to the concentration of 1 × 106 CFU mL^{-1} (where CFU is colony-forming unit), measured by optical density at 600 nm (OD600). To image the bacteria on the TNTs surface using the SEM microscopy, 2 mL of bacterial suspension was dropped on TNTs (control) and AgNPs-TNTs array and incubated at 37 °C for 5 hours. Then, the samples were three-times gently washed with sterile physiological solution. Bacteria were fixated in 2% glutaraldehyde for 1 hour. The dehydration step was performed using graded ethanol concentration of 30%, 50%, 70%, 80%, 90%, 95% and 100%, one time for each and twice in 100% for 15 min each. Dried samples were coated with a 10 nm thick gold layer in order to achieve a better contrast of bacteria.

Tests of antibacterial activity

Live/dead fluorescence staining was performed in order to image and count the live and dead bacteria on the silver nanoparticle-decorated TiO_2 nanotube surfaces. Samples were rinsed with sterile ultrapure water and left to dry in sterile conditions. The dried samples were subsequently placed in sterile 12-well plate, bathed in 2 mL of bacterial inoculum, and incubated for 24 hours at 37 °C. After the incubation, samples were washed five times with sterile saline. The staining of bacteria with Live/Dead BacLight Bacterial Viability and Counting Kit (Thermo Fisher Scientific) was performed as recommended by the manufacturer. The samples were observed by inverted fluorescence microscope Olympus IX71 (Olympus, Japan) at a magnification of 20×. Captured images were analyzed with ImageJ software. The contrast, brightness, and the displayed range (max, min) were adjusted with the brightness/contrast tool until individual bacteria became clearly visible. The area occupied by red (or green) colour was selected using the colour threshold and calculated using the measurement module. The value in pixels was divided by the total number of pixels present in the analyzed image, and the area of bacterial coverage (in percentage) specific for live and dead bacteria was calculated.

Antibacterial properties of silver nanoparticle decorated nanotubes were also evaluated via colony counting method. A bacterial inoculum with a density of 108 CFU mL^{-1} was prepared as the stock solution. Samples were rinsed in sterile water and 100 µL of bacterial suspension was spread onto the surface, followed by 4 hours' incubation at 37 °C. Subsequently, the samples were gently rinsed in PBS and adhered bacteria were de-attached by vortexing and sonication. Collected bacterial suspension was diluted 100 times with PBS. The 200 µL of diluted solution was inoculated on agar plates and incubated for 24 hours at 37 °C and 80% humidity. Bacteria colonies were then counted and colony forming unit was calculated (CFU mL^{-1}).

Statistical analysis

Mean values and standard deviations of obtained data were calculated. Statistically significant differences ($p < 0.05$) were confirmed using Student's t-test. All shown data are expressed as the mean ± standard deviation. Coverage values are calculated from 5 images with the area of 558.7 × 419 µm per each sample and bacterium. Colony counting method was performed in a duplicate.

5.2. Results and discussion

5.2.1. Characterization of TNTs and AgNPs–TNTs surface

TiO_2 nanotubes decorated with silver nanoparticles were fabricated *via* single-step anodic oxidation of titanium foil, followed by adsorption of commercially available silver nanoparticles of similar diameter but having a different functionalization layer (PVP, BPEI, citrate, PEG and lipoic acid). TNTs array without nanoparticles was taken as a control. SEM image analysis of nanostructured surface resulted in highly ordered TNTs with a diameter of 51.11 ± 5.77 nm as depicted in Figure 21.

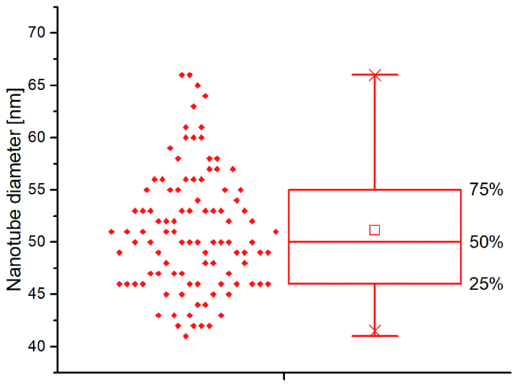

Figure 21: Boxplot of nanotube sizes. *Diameters were measured from SEM images.*

The surface roughness of the undecorated TiO_2 nanotubes was characterized using AFM. Figure 22A shows the 3D morphology of TNTs. The surface roughness measured by AFM was approximately 24.34 nm. In order to confirm the uniform distribution of Ag nanoparticles on the TNTs surface, several independent SEM images were evaluated for the number of nanoparticles per scanned area. The analysis of SEM images confirmed the decoration of TNTs surface with 3 – 4 nanoparticles on the area of 4 μm2 for each of differently functionalized Ag nanoparticles (Figure 22B and C). The size of nanoparticles of ~50 nm also guaranteed their deposition on the top of nanotubes.

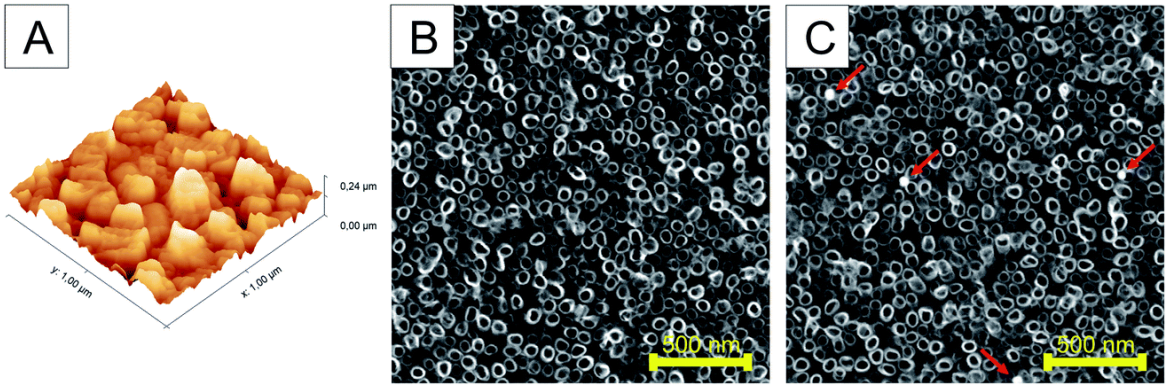

Figure 22: AFM image showing root-mean-square (RMS) surface roughness of TNTs and SEM images of bare(B) and decorated TiO_2 nanotubes(C). *The nanoparticles are indicated by arrows.*

The presence of silver nanoparticles and chemical composition of TiO_2 surface for bare- and silver-modified samples was investigated by X-ray photoelectron spectroscopy (XPS). In Figure 23A, a typical XPS survey of the TiO_2 surface after AgNPs decoration is shown. The survey shows the Ti, C, O and Ag signals, indicating that silver nanoparticles are adsorbed on the TiO_2 nanotubes. Four main elements, i.e. Ti 2p, O 1s, C 1s and Ag 3d were quantitatively analyzed in details and XPS data is summarized in Table 7. Data shows that samples did not differ significantly in their compositions and chemical state of elements. All the samples possessed high carbon level on the surface in the range of 31–33%, which could be attributed to used electrolyte, or/and adsorbed CO_2 from the air. The silver content ~0.2% was indicated for all AgNPs decorated samples and no silver peak was observed for bare nanotubes. Similar Ag values on all samples also indicate that nanotubes were coated with nanoparticles evenly.

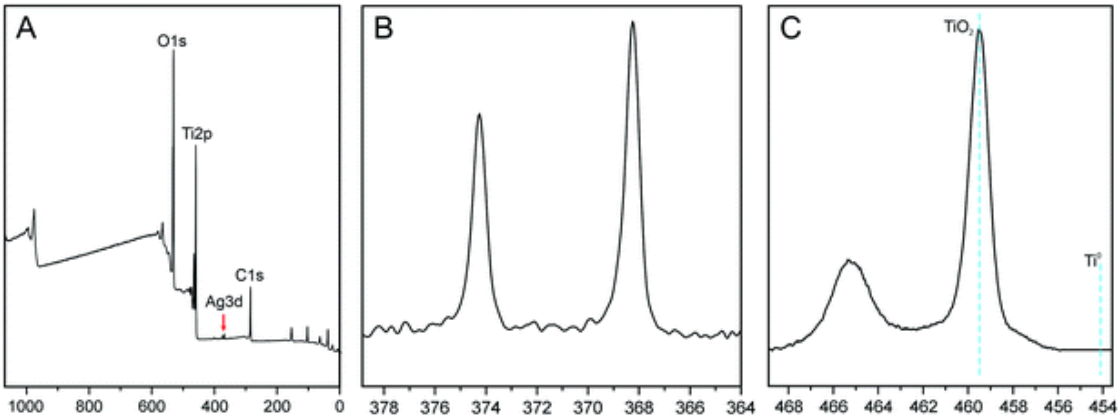

***Figure 23: XPS spectra**. Survey of TiO_2 nanotubes decorated with AgNPs (A), high resolution Ag 3d spectra (B) and high-resolution spectra Ti 2p (C).*

***Table 7: XPS analysis of bare-(control) and AgNPs decorated TiO_2 nanotubes.** Relative percentage of selected elements calculated from narrow spectra*

	BPEI [%]	Citrate [%]	Lipoic [%]	PEG [%]	PVP [%]	Control [%]
O 1s	51.42	50.28	50.74	51.49	51.29	51.07
Ti 2p	16.95	16.02	15.66	16.75	15.98	16.42
C 1s	31.44	33.5	33.41	31.56	32.52	32.51
Ag 3d	0.19	0.19	0.19	0.20	0.21	0,00

The characteristic high resolution XPS spectra of the Ag 3d region is shown in Figure 23B. The signals at binding energies of 368 eV and 374 eV were corresponding to the 3d5/2 and 3d3/2 orbits of Ag0 (metallic silver). The nanoparticles are not oxidized, as no further peaks at lower BE energy were needed for the fit. Additionally, high resolution XPS spectra of the Ti 2p is shown in Figure 23C. The Ti 2p3/2 peak has a maximum at 459 eV which can be assigned to TiO_2. There is no contribution from metallic Ti (BE = 453.8 eV) which could be attributed to a thickness of oxide layer (> 10 nm).

5.2.2. Antibacterial properties of AgNPs-TNTs surfaces

The array of TiO_2 nanotubes has been previously found to exhibit antibacterial action in a certain extent compared to the flat surface but it still has been clearly insufficient for use as an antibacterial surface. On the other hand, the silver nanoparticles exhibited strong antimicrobial performance against wide spectra of microorganisms.[159] Although the mechanism of their antimicrobial action is not clearly understood, several mechanisms have

been proposed. Those include the continual release of silver ions, disruption of the bacterial envelope, deactivation of respiratory enzymes, and generation of intracellular reactive oxygen species; consequently, cell death occurs.[160,161] The antimicrobial activity of nano-sized silver particles was also found size- and shape-dependent, one of the reasons could be that different morphologies provide different areas to interact with bacteria and thus results in different antibacterial efficiency. In accordance with most reported data, the smallest-sized spherical AgNPs (<50 nm) were more efficient to kill G− bacteria as compared to larger spherical AgNPs. Moreover, nanoparticles are usually stabilized in solution with a wide spectrum of chemicals such as citrate, polyvinylpyrrolidone etc. A few stabilization agents and/or functional layers of nanoparticles have been previously reported to affect the cell–surface interaction resulting in different antibacterial action.[162,163] Since the nanoparticle stabilizers have not been extensively investigated for their antibacterial action of adsorbed nanoparticles, here we compared five different NPs stabilizing agents by the decoration of AgNPs on TNTs nanotubes. The synergistic antibacterial activity was evaluated for three bacteria such as *E. coli*, *P. aeruginosa* and *S. aureus*.

Adhesion and viability assay of G⁻ bacteria

The evaluation of the adhesion and viability of bacteria on AgNPs-TNTs surfaces, *E. coli* was chosen as a first representative model of Gram-negative bacteria. Some strains of *E. coli* are known for biofilm formation, which can be the source of persistent medical-device related infections.[164,165] SEM microphotographs (Figures 25A and B) shows *E. coli* growing and colonizing control TNTs surface. Live/dead images and image analysis of *E. coli* after 24 hours' incubation shows the antibacterial activity of AgNPs-TNTs depending on the variability of nanoparticle functionalization layers (Figure 24 and 25C). The bacterial nucleic acid was stained with two fluorescence dyes, SYTO9 and propidium iodide, respectively. Green stain SYTO9 is cell membrane permeant, thus is stains nucleic acids of viable cells. On the contrary, red stain propidium iodide is membrane impermeable, it is commonly used to detect dead cells in a population. However, when the DNA is exposed to both stains, propidium iodide shows higher affinity to intercalate DNA and it is able to replace SYTO9. Therefore, the red fluorescence signal is generally considered as dead cell and green signal as live cell.[166,167] The non-decorated TNTs surface (control) showed almost 40% of dead *E. coli* bacteria, whereas nanoparticle-coated TNTs exhibited enhanced antibacterial activity as it is shown in Figure 24. The live/dead ratio obtained from the image analysis determined the enhanced antibacterial activity of the sample as follows: TNTs > PVP > BPEI > citrate > PEG > lipoic acid (Table 8). The antibacterial activity of TNTs as control is in a good agreement with previous studies suggesting the antibacterial properties of annealed unmodified TiO_2 nanotubes.[168-170]

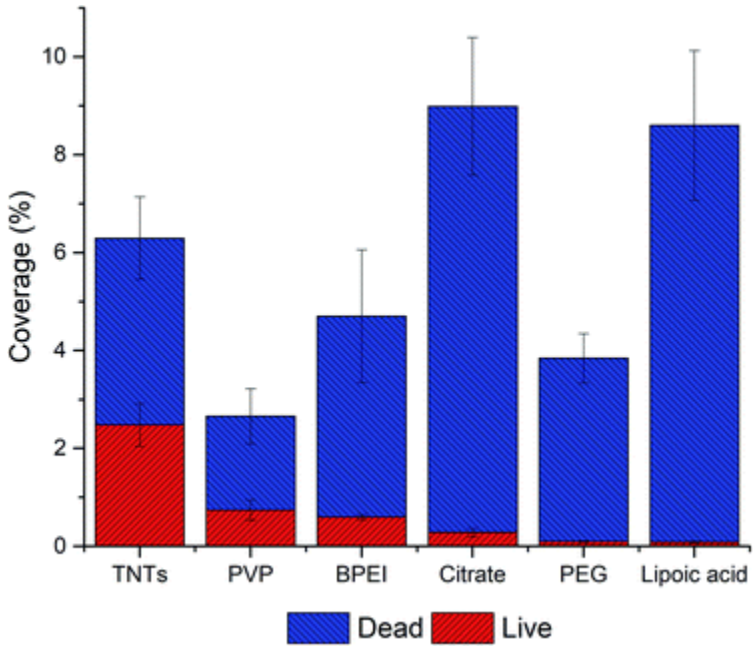

Figure 24: The adhesion and live/dead assay of* E. coli *on AgNPs-TNTs surfaces. *Data is expressed in % of total image area. All samples showed statistically significant difference (*p *< 0.05).*

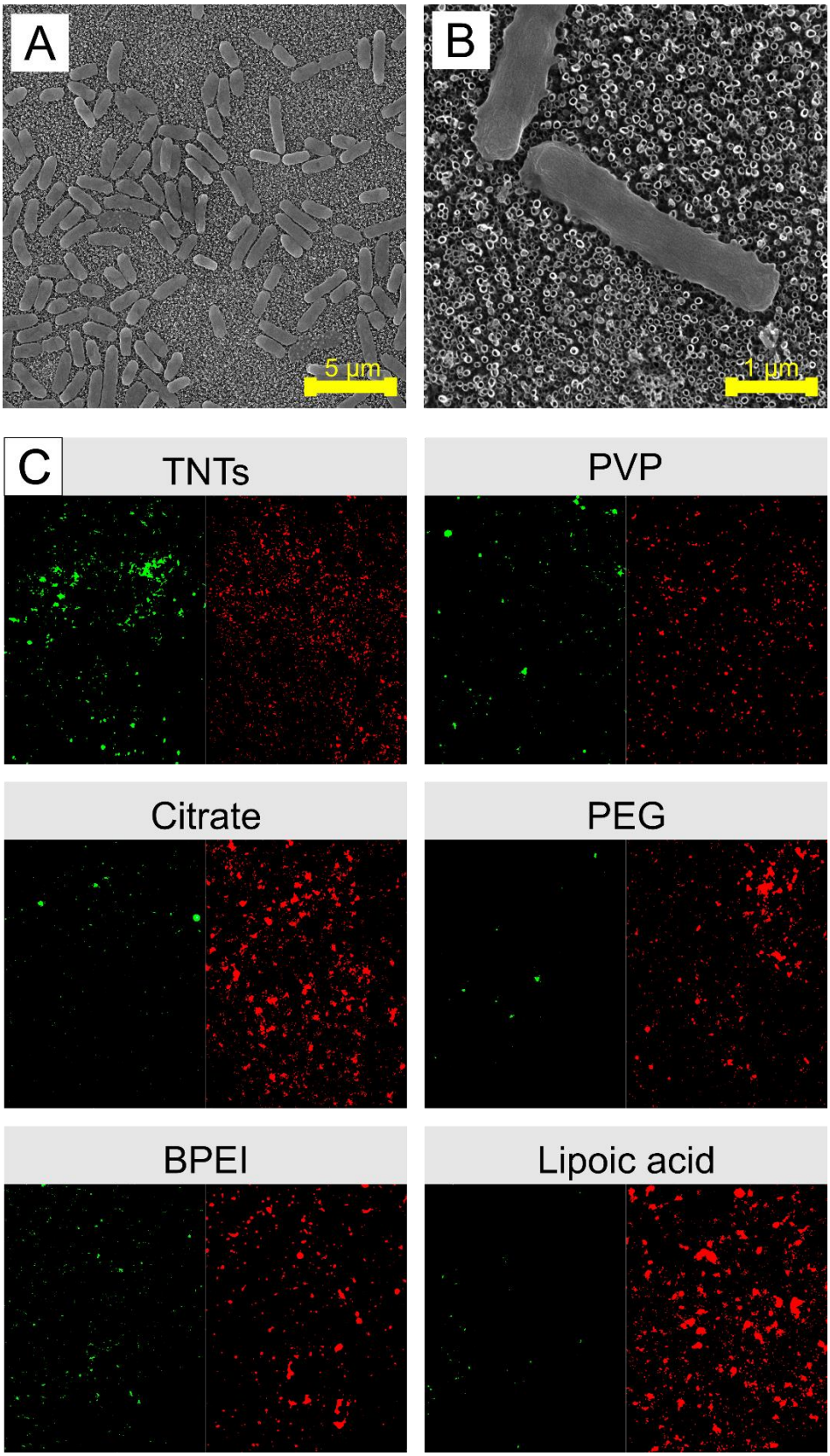

Figure 25: SEM image of E. coli grown on control TNTs surface (A) with bacteria detail (B) and Live/dead fluorescence staining of E. coli performed on differently functionalized Ag-NPs decorating TNTs nanotubes(C)*. (red color represents dead cells and green color represents live cells). Abbreviations: PVP (polyvinylpyrrolidone), BPEI (branched polyethyleneimine), PEG (polyethylene glycol).*

Table 8: The live/dead ratio of G− and G+ bacteria on TiO_2 nanotubes decorated with differently functionalized Ag-NPs. *Data were measured after 24-hour incubation*

	Live/dead ratio		
	E. coli	***P. aeruginosa***	***S. aureus***
TNTs	0.652 ± 0.012	1.161 ± 0.05	1.168 ± 0.003
PVP	0.381 ± 0.008	0.099 ± 0.011	0.926 ± 0.012
BPEI	0.151 ± 0.004	0.093 ± 0.001	1.021 ± 0.020
Citrate	0.033 ± 0.002	0.101 ± 0.013	2.457 ± 0.035
PEG	0.026 ± 0.001	0.009 ± 0.0002	0.447 ± 0.011
Lipoic acid	0.010 ± 0.001	0.019 ± 0.001	0.621 ± 0.008

Generally, Ag nanoparticles significantly enhanced the antibacterial properties of TNTs in term of the amount of dead *E. coli* bacteria. Especially, lipoic acid and citrate functionalized AgNPs-TNTs samples showed a very low value of live/dead ratio (Table 8). However, when considering the total coverage of the surface with *E. coli*, which corresponds with the adhesion of bacteria, "lipoic acid" and "citrate" samples showed significantly higher surface coverages compared to other samples. Contrary, the PVP sample showed the lowest total surface coverage but exhibited good bacteria survival. It is generally considered that the electrostatic interaction between negatively charged bacteria membrane and positively charged nanoparticles increases the antibacterial efficiency.[171] For instance, since the lipoic acid, citrate, and PVP have a negative charge at physiological pH,[172-174] the repulsiveness between negatively charged NPs and bacterial cells is supposed to dominate. However, a significantly high surface coverage on citrate and lipoic acid functionalized AgNPs–TNTs surface compared to PVP was observed. Further, the pKa value of TiO_2 is between 5.3–6.2.[175] It means that under the physiological pH, the surface is negatively charged, and thus it should also behave repulsively to bacteria. Contrary, when combining negatively charged TNTs and positively charged BPEI functionalized NPs, the surface coverage is lower than citrate, and lipoic acid functionalized AgNPs-TNTs surface. Thus, we did not find any correlation in bacteria adhesion depending on the surface charge and charge of bacterial membrane. It leads us to the conclusion that instead of electrostatic interaction, the topography and the chemical character AgNPs-TNT surfaces must be the key factor not only in cell–surface interaction and adhesion but also in viability of bacteria on such surfaces. The nanoparticles enhanced the antibacterial properties of TNTs, and more importantly, the nanoparticle functionalization layers significantly contributed to the antibacterial effect of AgNPs-TNTs surface against *E. coli*.

Further, we tested all samples against Gram-negative *P. aeruginosa*, which is also known for the biofilm formation. It is the second most common Gram-negative bacteria causing orthopedic implant infection[176] and multidrug resistance.[171] Figures 26A, B and C show the SEM image of *P. aeruginosa* on the control TNTs surface and live/dead staining of bacteria on AgNPs decorated TNTs with different nanoparticle functionalization layers, respectively.

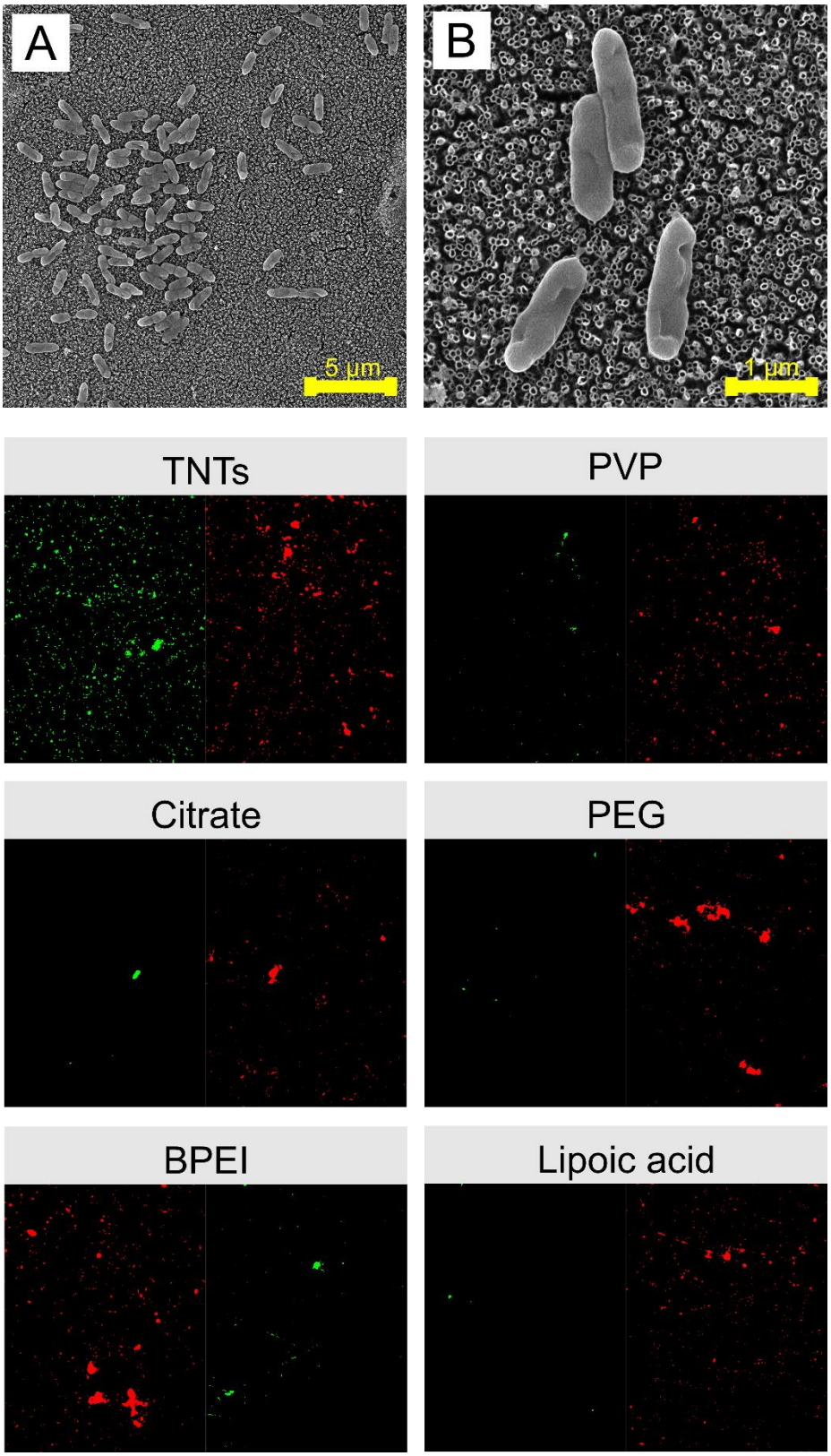

Figure 26: SEM images of P. aeruginosa adhered on control TNTs sample (A), bacteria detail (B) and Live/dead fluorescence images (C). P. aeruginosa *adhered on differently functionalized Ag-NPs decorated on TNTs nanotubes (red = dead cells; green = live cells). Abbreviations: PVP (polyvinylpyrrolidone), BPEI (branched polyethyleneimine), PEG (polyethylene glycol).*

The data from image analyses of live/dead staining of *P.aeruginosa* (Figure 27 and Table 8) showed a significant decrease in bacteria adhesion on NPs decorated TNTs compared to the control TNTs and also compared to the results obtained from *E. coli* experiment. Results can be attributed to several factors, including the charge repulsiveness, different composition of bacteria membrane, topography and chemistry of TiO_2 nanotubes and Ag nanoparticles.[177,178] These factors probably acted synergistically, as was demonstrated by our results. Additionally, the viability of *P.aeruginosa* on TNTs control was enhanced (~50%) compared to *E. coli* bacteria, and the lowest live/dead ratio has been found on PEG and lipoic acid samples which was also observed for *E. coli* bacteria. The similar live/dead ratio ~0.1 was calculated for PVP, BPEI, and citrate functionalized NPs.

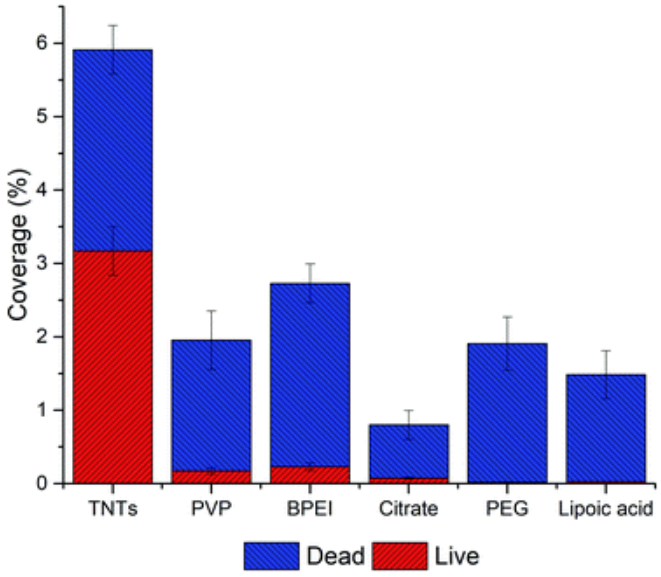

Figure 27: Adhesion and live/dead assay of P. aeruginosa on AgNPs-TNTs surfaces. *Data is expressed in percentage of total image area. All samples showed statistically significant difference (p < 0.05).*

Adhesion and viability assay of G+ bacteria

S. aureus was chosen as a representative bacterial model for the evaluation of the adhesion and viability of Gram-positive bacteria on AgNPs-TNTs surfaces. In comparison to *E. coli* and *P. aeruginosa*, the primary source of hospital-acquired infections dwells in already infected people. *S. aureus* is biofilm-forming bacteria on bones, heart valves, or implanted materials.[179] Results obtained from live/dead assay suggested that *S. aureus* adhered well on nanoparticle decorated TNTs surfaces as well as on the control TNTs (Figure 28). The bacterial coverage of surfaces with *S. aureus* (>32%) was several times higher than it was observed for Gram-negative bacteria (<9%). Moreover, the ratio of live/dead cells significantly increased, as shown in Figure 29 and Table 8. For instance, the citrate functionalized NPs decorating TNTs showed a two-folded increase in live/dead ratio compared to the control TNTs.

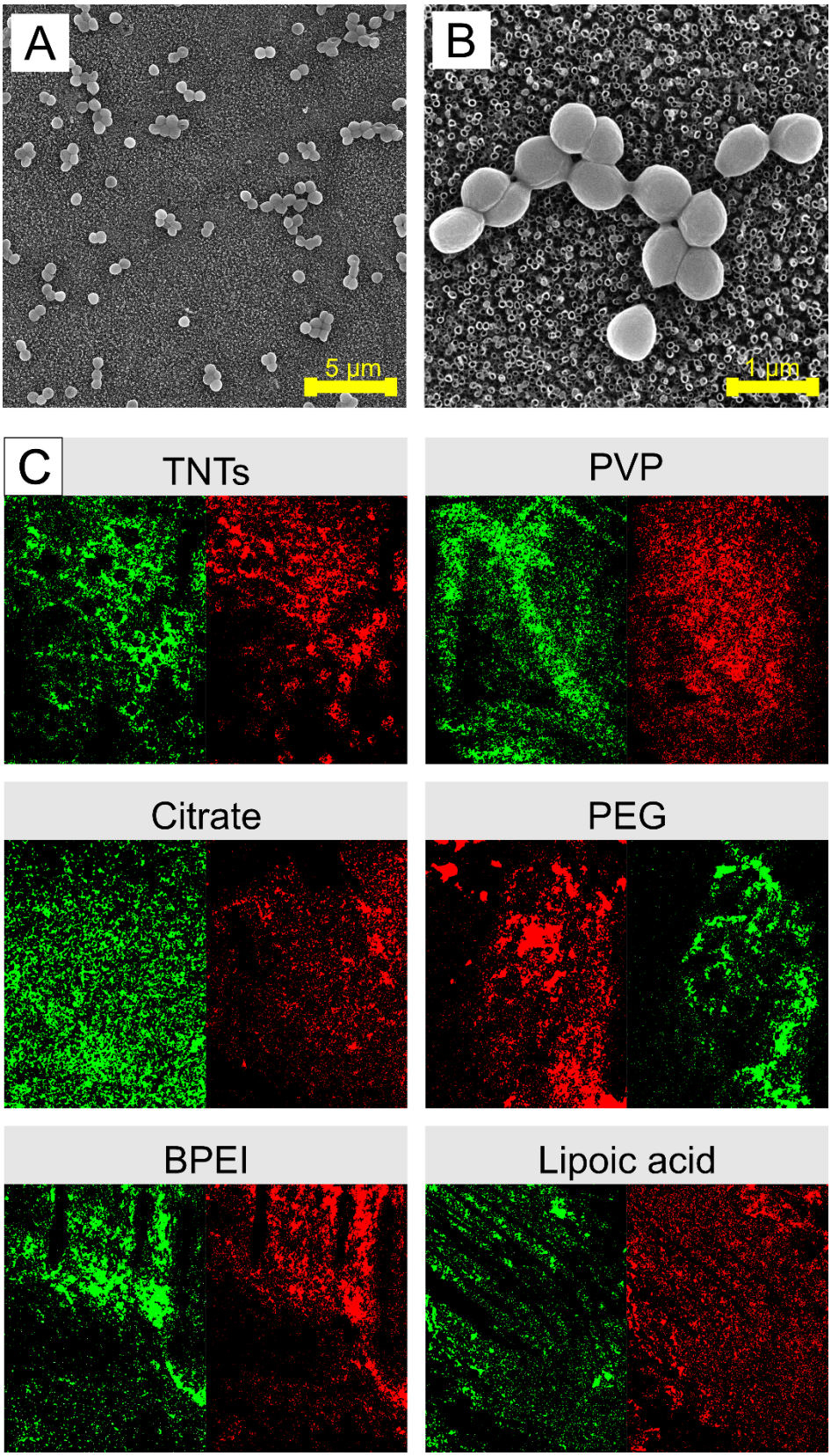

Figure 28 SEM images of* S. aureus *adhered on the control TNTs sample (A) with bacteria detail (B) and results of Live/dead fluorescence staining (C). S. aureus *performed differently on functionalized Ag-NPs decorated on TNTs nanotubes (red color represents dead cells and green color represents live cells). Abbreviations: PVP (polyvinylpyrrolidone), BPEI (branched polyethyleneimine), PEG (polyethylene glycol).*

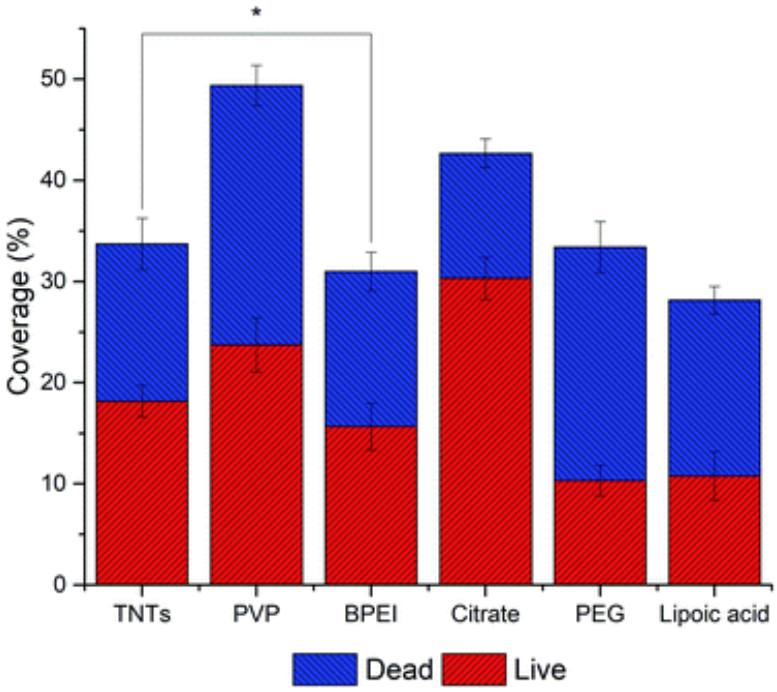

Figure 29: Adhesion and live/dead assay of* S. aureus *on AgNPs-TNTs surfaces. *Data is expressed in % of total image area. * indicates that there is no statistical significance (p > 0.05).*

The results demonstrated on *S. aureus* suggested that bacteria interact differently on AgNPs decorated TNTs surfaces as the increased adhesion and viability were observed compared to the G− bacteria. *S. aureus* was also more resistant to the character of NPs functionalized layers. To get better antibacterial properties of AgNPs-TNTs surface against *S. aureus*, the increased number of nanoparticles on TNTs nanotubes should be performed and tested. On the other hand, it is also possible to think about absolutely different design of antibacterial surface for such resistant G+ bacteria.

Colony counting assay of G^+ and G^- bacteria

Results from fluorescence staining showed the degree of bacterial adhesion after 24 hours and the living/dead cell ratio. Colony counting method performed in this work reflects the bacterial adhesion and viability after 4 hours' incubation of bacteria with AgNP-TNTs surfaces. Here, we performed colony counting assay for *E. coli* and *S. aureus* as representatives. Figure 30A shows data obtained for *E. coli* bacteria, in which the adhesion and viability of bacteria decreased as follows: TNTs ≥ BPEI ≥ PVP > citrate > PEG > lipoic acid. The viability of bacteria corresponds with live/dead staining obtained for 24 hours, where the portion of living bacteria had the similar trend. Different results could be observed for bacterial adhesion at 4 hours and 24 hours. The shorter time of interaction between bacteria and surface followed the trend of bacteria viability. However, it was significantly changed when *E. coli* was exposed to the surface for 24 hours, in which the adhesion was increased on citrate and lipoic

acid samples; although at the expense of more dead cells. The results obtained for *S. aureus* (Figure 30B) after 4 hours' incubation of bacteria on the samples showed increased adhesion and viability as follows: TNTs ≥ PVP > BPEI ≥ PEG ≥ lipoic acid > citrate. Here we can see that there is a significant difference of results obtained for two incubation times. The explanation for this observation could be that bacteria sense, adhere and grow on different surfaces with different speed.

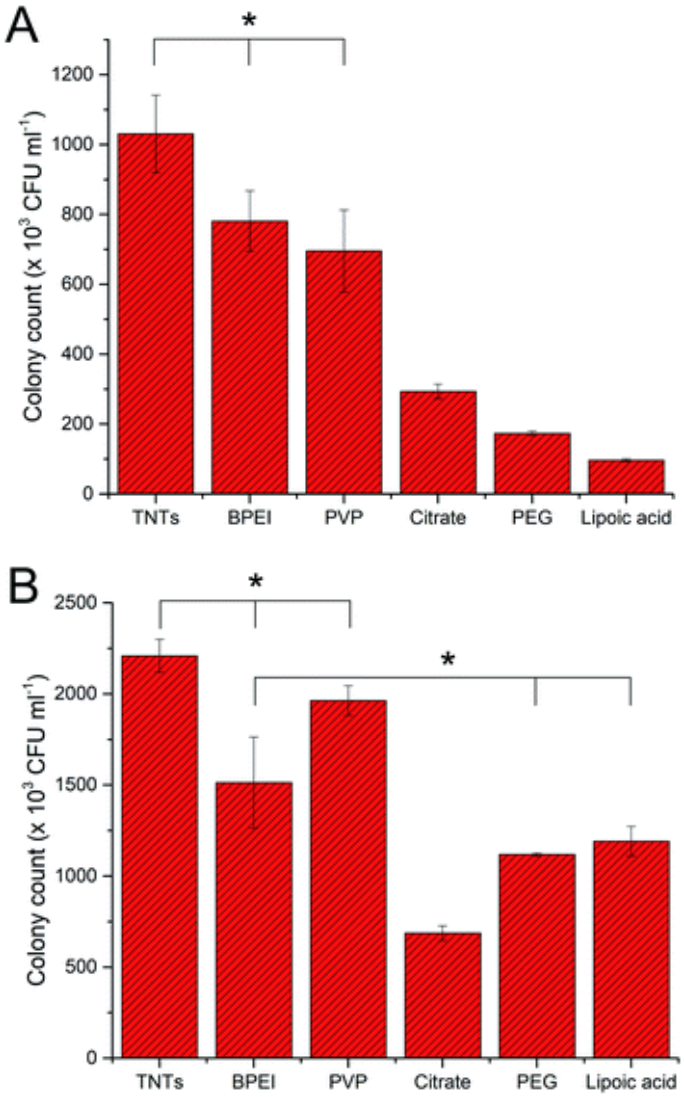

Figure 30: The graphs of colony counting experiments expressed in colony forming units for* E. coli *(A) and* S. aureus *(B). *Bacteria was exposed to surfaces for 4 hours, and the antibacterial effect was compared between individual samples. * indicates that there is no statistical significance.*

6. Discussion about antibacterial action of Ag and Se nanoparticles

Based on our obtained data acquired from colony counting experiments with a short 4-hour incubation period, we can compare the antibacterial activity of prepared selenium and silver nanoparticle decorated surfaces. There are three aspects that need to be considered:(i) fabricated nanotubes must be very similar in diameter, (ii) the number of nanoparticles per area must be comparable (iii) the reproducible protocol of antibacterial experiment (colony counting method) with the same bacteria (*E. coli)* expressed in relative numbers (%) to unmodified TiO_2 nanotube array. All of these requirements were met, and thus, we can use our experimental data to compare the relative antibacterial efficiency of our nanoparticle decorated surfaces. We analysed and compared data from Se-Low-TNTs (Se-Low in Chapter 4), BPEI-Ag-TNTs (BPEI in Chapter 5), and Lipoic-acid-Ag-TNTs (Chapter 5). Silver nanoparticle decorated surfaces were chosen by the degree of their antibacterial activity against *E. coli*, where Lipoic acid functionalized nanoparticles were the most effective and BPEI performed the worst effectiveness toward bacteria. Se-High-TNTs (Se-High in Chapter 4) with a significantly higher surface density of nanoparticles are included to stress the difference between the results. Bare TNTs were always used as a reference (100%).

Table 9: Average and median values of nanoparticles present on compared samples. *Number of NPs were calculated from SEM images.*

Sample	***Median value***	***Average number of nanoparticles***
Se-Low-TNTs	3.5	3.20 ± 1.14
BPEI-Ag-TNTs	3.0	3.16 ±0.69
Lipoic-acid-Ag-TNTs	3.0	3.20 ± 0.75
Se-High-TNTs	17	18.5 ± 2.37

From calculated results (Figure 31), it can be seen that the results are somehow curious. The most effective antibacterial activity showed Lipoic-acid-Ag-TNTs array. It effectivity is higher than for Se-High-TNTs array, which was decorated with more than five times higher number of nanoparticles. It was previously reported by Shi et al. [180] that lipoic acid exhibits antimicrobial activity. However, the authors suggested that the antimicrobial activity is only moderate. Thus, we can assume that the antibacterial activity of Lipoic-acid, silver nanoparticles, and TiO_2 nanotube work in a synergistic way. In the same experiment, the antibacterial effectivity of BPEI-Ag-TNTs was the worst among all tested samples. It could be assumed that the branched polyethyleneimine would also be able to enhance the

antibacterial activity of silver nanoparticle decorated TiO_2 nanotubes. As Wiegand et al.[181] studied various polyethyleneimines, and even though the antibacterial activity of linear polyethyleneimines was superior, the branched forms exhibited strong antibacterial activity against both *S. aureus* and *E. coli*.

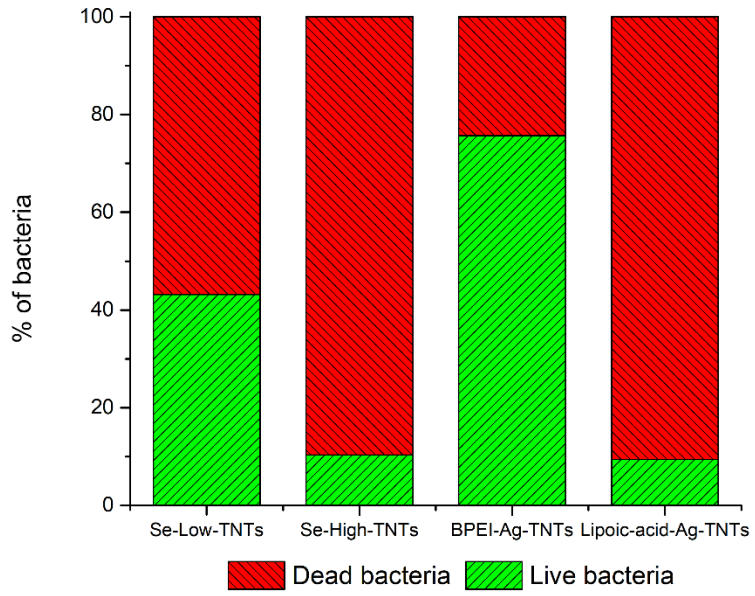

Figure 31: Relative antibacterial activity of selected silver and selenium decorated TiO_2 nanotubes. *Bare TNTs were always used as a reference (100%) for both experiments. The number of dead bacteria was calculated as 100% - live bacteria.*

Generally, it can be said that the antibacterial effectiveness of compared surfaces is as follows:
Lipoic-acid-Ag-TNTs > Se-High-TNTs > Se-Low-TNTs > BPEI-Ag-TNTs. The Lipoic-acid-Ag-TNTs surface showed the most promising antibacterial activity among our tested and compared samples and it can be expected that an increase in the number of decorated nanoparticles will lead to further improvement. Considering the currently very low silver content, even decreasing the population of bacteria to zero might be possible, as it was previously shown in an example with aminocellulose and acylase modified silver nanoparticles and *P. aeruginosa*.[182]

However, if we consider it from the biomaterial point of view, we have to bear in mind that silver nanoparticles have been shown to induce apoptosis even at non-cytotoxic levels.[22,183] One might complain that even the Se-High-TNTs were shown highly cytotoxic. However, the improvement carried by Se-Low-TNTs was also noticeable. Considering their other advantages, such as anti-cancer activity[70] and possible processing by cells, as it is a substance native to the body, selenium nanoparticles seem to have a better perspective for this kind of application.

7. Conclusions

TiO_2 nanotubular films are an exciting nanomaterial that has shown promise in various scientific fields, including biomedical applications. The effect of nanotube features, such as their shape, diameter, wall thickness, and length, has been extensively studied so that it could be adequately understood and applied. Even though improved responses towards selected cells were acquired, including enhanced adhesion, proliferation, and differentiation, through the time it has been shown that there are limits to their performance. Thus, much effort was put into research about their modifications, that could enable us to further improve their performance. Introduction of antibacterial nanoparticles, such as, e.g., silver, through surface decoration significantly improved the antibacterial activity of nanotubular TiO_2. However, obtained results were very conflicting, as in some cases, silver nanoparticles act strongly cytotoxic, and therefore, not suitable for biomaterial applications.

In this thesis, we studied the effect of the decoration with selenium and silver nanoparticles on the performance of fabricated TiO_2 nanotubes. Many optimizations were needed to prepare surfaces with similar nanotube diameters, and a relatively low and consistent number of nanoparticles to make these experiments at least slightly comparable.

In the first part of the experimental section of this thesis, selenium nanoparticle decorated TiO_2 nanotubes were fabricated and subsequently studied for their antibacterial and cytotoxicity activities. All samples decorated with selenium nanoparticles showed a different degree of antibacterial activity. The trend suggested that higher selenium nanoparticle numbers induced enhanced antibacterial effect. However, the samples with the highest number of decorated selenium nanoparticles were not compatible with MG-63 nor NIH/3T3 cells. With decreasing number of decorated selenium nanoparticles, the cytocompatibility with NIH-3T3 cells was increasing. However, even the lowest number of decorated selenium nanoparticles showed anti-cancer activity against MG-63 cells. Therefore, optimized, low selenium nanoparticle concentrations could be used to decrease the risk of bacterial infection, as well as it can be utilized in anti-cancer orthopaedic applications.

In the second part of the experimental section of this thesis, comparable numbers of silver nanoparticles (PVP, BPEI, PEG, Lipoic acid, Citrate functionalized) were decorated onto TiO_2 nanotubes to observe the effect of the nanoparticle stabilizing agent on the antibacterial activity of such surface. Prepared surfaces were tested against *E. coli*, *P. aeruginosa*, and *S. aureus*. In the colony counting experiment with *E. coli*, the most prominent effect was observed for TiO_2 nanotubes decorated with lipoic acid and polyethylene glycol functionalized silver nanoparticles. On the other side of the barricade, the worst performance was observed on TiO_2 nanotubes decorated with branched polyethyleneimine and polyvinylpyrrolidone functionalized nanoparticles. The contrast is massive, as the performance of branched polyethyleneimine was not statistically different from bare annealed

TiO_2 nanotubes, whereas the TiO_2 nanotubes decorated with lipoic acid functionalized nanoparticles decreased the number of *E. coli* by as much as approximately 90%. *E. coli* and *P. aeruginosa* were more susceptible to these antibacterial surfaces, as the number of adhered and viable *S. aureus* colonies was significantly higher. However, it should be stressed out that the effect of stabilization agents play a vital role in resulting antibacterial activity of silver nanoparticle decorated TiO_2 nanotubes and should be considered carefully and in accordance with purpose planned for designed silver nanoparticle decorated nanostructured surface.

In the third part, a brief comparison of selenium and silver modified TiO_2 nanotubes follows. From the obtained data, we can say that silver nanoparticle decorated TiO_2 nanotubes can perform both better and worse than selenium nanoparticles, based on used stabiliser. For instance, the antibacterial efficacy of surface decorated with lipoic acid functionalized silver nanoparticles was comparable to that of a surface with five times the number of selenium nanoparticles. This only highlights to what extent can the nanoparticle-bound stabilizing agents and functional layers affect the performance of decorated nanosurfaces.

To conclude it, from a TiO_2 nanotube biomaterial point of view, tested selenium nanoparticles synthesized from a precursor using glutathione bring enhanced antibacterial activity, anti-cancer properties, and the potential to be processed by the organism, as selenium is a substance native to the body. However, from the general antibacterial surface point of view, appropriately functionalized silver nanoparticles perform better. Further research in this field could be focused on topics like, for example, the effect of nanoparticle size, nanoparticle shape or nanotube geometry.

8. References

[1] BRAMMER, K. S. et al. Improved bone-forming functionality on diameter-controlled TiO2 nanotube surface. *Acta Biomaterialia*, 2009, sv. 5, č. 8, s. 3215-3223. ISSN 1742-7061.

[2] BRAMMER, K. S. et al. TiO2 nanotubes for bone regeneration. *Trends in Biotechnology*, 2012, sv. 30, č. 6, s. 315-322. ISSN 0167-7799.

[3] POPAT, K. C. et al. Influence of engineered titania nanotubular surfaces on bone cells. *Biomaterials*, 2007, sv. 28, č. 21, s. 3188-3197. ISSN 0142-9612.

[4] POPAT, K. C. et al. Titania Nanotubes: A Novel Platform for Drug-Eluting Coatings for Medical Implants? *Small*, 2007, sv. 3, č. 11, s. 1878-1881. ISSN 1613-6810.

[5] ASSEFPOUR-DEZFULY, M. et al. Oxide morphology and adhesive bonding on titanium surfaces. *Journal of materials science*, 1984, sv. 19, č. 11, s. 3626-3639. ISSN 1573-4803.

[6] ROY, P. et al. TiO2 Nanotubes: Synthesis and Applications. *Angewandte Chemie International Edition*, 2011, sv. 50, č. 13, s. 2904-2939. ISSN 1433-7851.

[7] FU, Y. a MO, A. A review on the electrochemically self-organized titania nanotube arrays: synthesis, modifications, and biomedical applications. *Nanoscale research letters*, 2018, sv. 13, č. 1, s. 1-21. ISSN 1556-276X.

[8] LEE, K. et al. One-dimensional titanium dioxide nanomaterials: nanotubes. *Chemical reviews*, 2014, sv. 114, č. 19, s. 9385-9454. ISSN 0009-2665.

[9] KASEMO, B. Biocompatibility of titanium implants: Surface science aspects. *Journal of Prosthetic Dentistry*, 1983, sv. 49, č. 6, s. 832-837. ISSN 0022-3913.

[10] TANG, L. et al. Surface chemistry influences implant biocompatibility. *Current topics in medicinal chemistry*, 2008, sv. 8, č. 4, s. 270-280. ISSN 1568-0266.

[11] MENZIES, K. L. a JONES, L. The Impact of Contact Angle on the Biocompatibility of Biomaterials. *Optometry and Vision Science*, 2010, sv. 87, č. 6, s. 387-399. ISSN 1538-9235.

[12] LAMERS, E. et al. The influence of nanoscale topographical cues on initial osteoblast morphology and migration. *European Cells and Materials*, 2010.

[13] OH, S. et al. Significantly accelerated osteoblast cell growth on aligned TiO2 nanotubes. *Journal of Biomedical Materials Research Part A*, 2006, sv. 78A, č. 1, s. 97-103.

[14] KUMMER, K. M. et al. Biological applications of anodized TiO2 nanostructures: a review from orthopedic to stent applications. *Nanoscience and Nanotechnology Letters*, 2012, sv. 4, č. 5, s. 483-493. ISSN 1941-4900.

[15] LAI, M. et al. Surface functionalization of TiO2 nanotubes with bone morphogenetic protein 2 and its synergistic effect on the differentiation of mesenchymal stem cells. *Biomacromolecules*, 2011, sv. 12, č. 4, s. 1097-1105. ISSN 1525-7797.

[16] ZHANG, H. et al. Improved antibacterial activity and biocompatibility on vancomycin-loaded TiO2 nanotubes: in vivo and in vitro studies. *International journal of nanomedicine*, 2013, sv. 8, s. 4379.

[17] POPAT, K. C. et al. Decreased Staphylococcus epidermis adhesion and increased osteoblast functionality on antibiotic-loaded titania nanotubes. *Biomaterials*, 2007, sv. 28, č. 32, s. 4880-4888. ISSN 0142-9612.

[18] LIU, W. et al. Selenium nanoparticles incorporated into titania nanotubes inhibit bacterial growth and macrophage proliferation. *Nanoscale*, 2016, sv. 8, č. 34, s. 15783-15794.

[19] MEI, S. et al. Antibacterial effects and biocompatibility of titanium surfaces with graded silver incorporation in titania nanotubes. *Biomaterials*, 2014, sv. 35, č. 14, s. 4255-4265. ISSN 0142-9612.

[20] YANG, T. et al. Cytocompatibility and antibacterial activity of titania nanotubes incorporated with gold nanoparticles. *Colloids and Surfaces B: Biointerfaces*, 2016, sv. 145, s. 597-606. ISSN 0927-7765.

[21] LIU, W. et al. Synthesis of TiO 2 nanotubes with ZnO nanoparticles to achieve antibacterial properties and stem cell compatibility. *Nanoscale*, 2014, sv. 6, č. 15, s. 9050-9062.

[22] AHAMED, M. et al. Silver nanoparticle applications and human health. *Clinica Chimica Acta*, 2010, sv. 411, č. 23, s. 1841-1848. ISSN 0009-8981.

[23] HOYER, P. Formation of a titanium dioxide nanotube array. *Langmuir*, 1996, sv. 12, č. 6, s. 1411-1413. ISSN 0743-7463.

[24] SANDER, M. S. et al. Template-assisted fabrication of dense, aligned arrays of titania nanotubes with well-controlled dimensions on substrates. *Advanced Materials*, 2004, sv. 16, č. 22, s. 2052-2057. ISSN 0935-9648.

[25] BORBÓN-NUÑEZ, H. et al. Fabrication of hollow TiO2 nanotubes through atomic layer deposition and MWCNT templates. *Powder Technology*, 2017, sv. 308, s. 249-257. ISSN 0032-5910.

[26] KASUGA, T. et al. Formation of titanium oxide nanotube. *Langmuir*, 1998, sv. 14, č. 12, s. 3160-3163. ISSN 0743-7463.

[27] ASSEFPOUR-DEZFULY, M. et al. Oxide morphology and adhesive bonding on titanium surfaces. *Journal of materials science*, 1984, sv. 19, č. 11, s. 3626-3639. ISSN 1573-4803.

[28] LI, Y. et al. Enhanced antibacterial properties of orthopedic implants by titanium nanotube surface modification: a review of current techniques. *International journal of nanomedicine*, 2019, sv. 14, s. 7217-7236. ISSN 1178-2013

1176-9114.

[29] MACAK, J. M. et al. TiO2 nanotubes: Self-organized electrochemical formation, properties and applications. *Current Opinion in Solid State and Materials Science*, 2007, sv. 11, č. 1, s. 3-18. ISSN 1359-0286.

[30] APOLINÁRIO, A. et al. The role of the Ti surface roughness in the self-ordering of TiO2 nanotubes: a detailed study of the growth mechanism. *Journal of Materials Chemistry A*, 2014, sv. 2, č. 24, s. 9067-9078. ISSN 2050-7488.

[31] MACAK, J. M. et al. Mechanistic aspects and growth of large diameter self-organized TiO2 nanotubes. *Journal of Electroanalytical Chemistry*, 2008, sv. 621, č. 2, s. 254-266. ISSN 1572-6657.

[32] CRAWFORD, G. A. et al. Microstructure and deformation behavior of biocompatible TiO2 nanotubes on titanium substrate. *Acta Biomaterialia*, 2007, sv. 3, č. 3, s. 359-367. ISSN 1742-7061.

[33] LOCKMAN, Z. et al. Influence of anodisation voltage on the dimension of titania nanotubes. *Journal of Alloys and Compounds*, 2010, sv. 503, č. 2, s. 359-364. ISSN 0925-8388.

[34] WANG, J. a LIN, Z. Anodic Formation of Ordered TiO2 Nanotube Arrays: Effects of Electrolyte Temperature and Anodization Potential. *The Journal of Physical Chemistry C*, 2009, sv. 113, č. 10, s. 4026-4030. ISSN 1932-7447.

[35] PRIDA, V. M. et al. Temperature influence on the anodic growth of self-aligned Titanium dioxide nanotube arrays. *Journal of Magnetism and Magnetic Materials*, 2007, sv. 316, č. 2, s. 110-113. ISSN 0304-8853.

[36] BERGER, S. et al. Self-organized TiO2 nanotubes: Factors affecting their morphology and properties. *physica status solidi (b)*, 2010, sv. 247, č. 10, s. 2424-2435. ISSN 0370-1972.

[37] JHA, H. et al. Fast formation of aligned high-aspect ratio TiO2 nanotube bundles that lead to increased open circuit voltage when used in dye sensitized solar cells. *Electrochemistry Communications*, 2011, sv. 13, č. 3, s. 302-305. ISSN 1388-2481.

[38] ALBU, S. P. et al. Growth of Aligned TiO2 Bamboo-Type Nanotubes and Highly Ordered Nanolace. *Angewandte Chemie International Edition*, 2008, sv. 47, č. 10, s. 1916-1919. ISSN 1433-7851.

[39] ALBU, S. P. et al. Formation of Double-Walled TiO2 Nanotubes and Robust Anatase Membranes. *Advanced Materials*, 2008, sv. 20, č. 21, s. 4135-4139. ISSN 0935-9648.

[40] SONG, Y.-Y. a SCHMUKI, P. Modulated TiO2 nanotube stacks and their use in interference sensors. *Electrochemistry Communications*, 2010, sv. 12, č. 4, s. 579-582. ISSN 1388-2481.

[41] MIRABOLGHASEMI, H. et al. Formation of 'single walled' TiO2 nanotubes with significantly enhanced electronic properties for higher efficiency dye-sensitized solar cells. *Chemical Communications*, 2013, sv. 49, č. 20, s. 2067-2069. ISSN 1359-7345.

[42] OH, H.-J. et al. Phase transformation and photocatalytic characteristics of anodic TiO2 nanotubular film. *Journal of Physics and Chemistry of Solids*, 2013, sv. 74, č. 5, s. 708-715. ISSN 0022-3697.

[43] DAS, S. et al. Influence of annealing temperatures on the properties of low aspect-ratio TiO2 nanotube layers. *Electrochimica Acta*, 2016, sv. 213, s. 452-459. ISSN 0013-4686.

[44] COTTINEAU, T. et al. One step synthesis of niobium doped titania nanotube arrays to form (N,Nb) co-doped TiO2 with high visible light photoelectrochemical activity. *Journal of Materials Chemistry A*, 2013, sv. 1, č. 6, s. 2151-2160. ISSN 2050-7488.

[45] BENJWAL, P. a KAR, K. K. One-step synthesis of Zn doped titania nanotubes and investigation of their visible photocatalytic activity. *Materials Chemistry and Physics*, 2015, sv. 160, s. 279-288. ISSN 0254-0584.

[46] LIU, H. et al. Preparation and characterization of Zr doped TiO2 nanotube arrays on the titanium sheet and their enhanced photocatalytic activity. *Journal of Solid State Chemistry*, 2009, sv. 182, č. 12, s. 3238-3242. ISSN 0022-4596.

[47] MOMENI, M. M. et al. Fabrication and characterization of copper doped TiO2 nanotube arrays by in situ electrochemical method as efficient visible-light photocatalyst. *Ceramics International*, 2015, sv. 41, č. 7, s. 8735-8741. ISSN 0272-8842.

[48] KIM, H.-I. et al. N-doped TiO2 nanotubes coated with a thin TaOxNy layer for photoelectrochemical water splitting: dual bulk and surface modification of photoanodes. *Energy & Environmental Science*, 2015, sv. 8, č. 1, s. 247-257. ISSN 1754-5692.

[49] SZKODA, M. et al. Optimization of boron-doping process of titania nanotubes via electrochemical method toward enhanced photoactivity. *Journal of Solid State Electrochemistry*, 2016, sv. 20, č. 6, s. 1765-1774. ISSN 1433-0768.

[50] SIUZDAK, K. et al. Enhanced photoelectrochemical and photocatalytic performance of iodine-doped titania nanotube arrays. *RSC Advances*, 2015, sv. 5, č. 62, s. 50379-50391.

[51] KIM, H.-I. et al. N-doped TiO 2 nanotubes coated with a thin TaO x N y layer for photoelectrochemical water splitting: dual bulk and surface modification of photoanodes. *Energy & Environmental Science*, 2015, sv. 8, č. 1, s. 247-257.

[52] COTTINEAU, T. et al. One step synthesis of niobium doped titania nanotube arrays to form (N, Nb) co-doped TiO 2 with high visible light photoelectrochemical activity. *Journal of Materials Chemistry A*, 2013, sv. 1, č. 6, s. 2151-2160.

[53] MOLLAVALI, M. et al. Preparation of multiple-doped TiO2 nanotube arrays with nitrogen, carbon and nickel with enhanced visible light photoelectrochemical activity via single-step anodization. *International Journal of Hydrogen Energy*, 2015, sv. 40, č. 36, s. 12239-12252. ISSN 0360-3199.

[54] GEETHA, M. et al. Ti based biomaterials, the ultimate choice for orthopaedic implants–a review. *Progress in materials science*, 2009, sv. 54, č. 3, s. 397-425. ISSN 0079-6425.

[55] RAJARAMAN, T. et al. Black TiO2: A review of its properties and conflicting trends. *Chemical Engineering Journal*, 2020, sv. 389, s. 123918. ISSN 1385-8947.

[56] ASSAUD, L. et al. Atomic Layer Deposition of Pd Nanoparticles on TiO2 Nanotubes for Ethanol Electrooxidation: Synthesis and Electrochemical Properties. *ACS Applied Materials & Interfaces*, 2015, sv. 7, č. 44, s. 24533-24542. ISSN 1944-8244.

[57] NG, S. et al. ZnO Coated Anodic 1D TiO2 Nanotube Layers: Efficient Photo-Electrochemical and Gas Sensing Heterojunction. *Advanced Engineering Materials*, 2018, sv. 20, č. 2, s. 1700589. ISSN 1438-1656.

[58] ZAZPE, R. et al. Atomic Layer Deposition for Coating of High Aspect Ratio TiO2 Nanotube Layers. *Langmuir*, 2016, sv. 32, č. 41, s. 10551-10558. ISSN 0743-7463.

[59] DVORAK, F. et al. One-dimensional anodic TiO2 nanotubes coated by atomic layer deposition: Towards advanced applications. *Applied Materials Today*, 2019, sv. 14, s. 1-20. ISSN 2352-9407.

[60] BENOIT, A. et al. Decoration of TiO2 nanotube layers with WO3 nanocrystals for high-electrochromic activity. *Electrochemistry Communications*, 2009, sv. 11, č. 4, s. 728-732. ISSN 1388-2481.

[61] ROY, P. et al. Improved efficiency of TiO2 nanotubes in dye sensitized solar cells by decoration with TiO2 nanoparticles. *Electrochemistry Communications*, 2009, sv. 11, č. 5, s. 1001-1004. ISSN 1388-2481.

[62] ZHAO, L. et al. Antibacterial nano-structured titania coating incorporated with silver nanoparticles. *Biomaterials*, 2011, sv. 32, č. 24, s. 5706-5716. ISSN 0142-9612.

[63] YANG, L. et al. Fabrication of CdSe Nanoparticles Sensitized Long TiO2 Nanotube Arrays for Photocatalytic Degradation of Anthracene-9-carbonxylic Acid under Green Monochromatic Light. *The Journal of Physical Chemistry C*, 2010, sv. 114, č. 11, s. 4783-4789. ISSN 1932-7447.

[64] KANG, Y. et al. Electrochemical deposition of Co nanowire arrays into self-organized titania nanotubes. *Applied Surface Science*, 2008, sv. 254, č. 13, s. 3935-3938. ISSN 0169-4332.

[65] SCARANO, A. et al. Bacterial adhesion on commercially pure titanium and zirconium oxide disks: an in vivo human study. *Journal of periodontology*, 2004, sv. 75, č. 2, s. 292-296. ISSN 0022-3492.

[66] SALATA, O. V. Applications of nanoparticles in biology and medicine. *Journal of Nanobiotechnology*, 2004, sv. 2, č. 1, s. 3. ISSN 1477-3155.

[67] FOHLEROVA, Z. a MOZALEV, A. Tuning the response of osteoblast-like cells to the porous-alumina-assisted mixed-oxide nano-mound arrays. *J Biomed Mater Res B Appl Biomater*, 2018, sv. 106, č. 5, s. 1645-1654. ISSN 1552-4973.

[68] KUMERIA, T. et al. Advanced biopolymer-coated drug-releasing titania nanotubes (TNTs) implants with simultaneously enhanced osteoblast adhesion and antibacterial properties. *Colloids and Surfaces B: Biointerfaces*, 2015, sv. 130, s. 255-263. ISSN 0927-7765.

[69] LI, L.-H. et al. Biocompatibility of titanium implants modified by microarc oxidation and hydroxyapatite coating. *Journal of Biomedical Materials Research Part A*, 2005, sv. 73A, č. 1, s. 48-54. ISSN 1549-3296.

[70] TRAN, P. a WEBSTER, T. J. Enhanced osteoblast adhesion on nanostructured selenium compacts for anti-cancer orthopedic applications. *International journal of nanomedicine*, 2008, sv. 3, č. 3, s. 391.

[71] KIM, H.-W. et al. Hydroxyapatite coating on titanium substrate with titania buffer layer processed by sol–gel method. *Biomaterials*, 2004, sv. 25, č. 13, s. 2533-2538. ISSN 0142-9612.

[72] PARK, J.-H. et al. Bioactivity of calcium phosphate coatings prepared by electrodeposition in a modified simulated body fluid. *Materials Letters*, 2006, sv. 60, č. 21, s. 2573-2577. ISSN 0167-577X.

[73] WU, F. et al. Enhanced Biocompatibility and Antibacterial Activity of Selective Laser Melting Titanium with Zinc-Doped Micro-Nano Topography. *Journal of Nanomaterials*, 2019, sv. 2019, s. 13.

[74] LIU, X. et al. Surface modification of titanium, titanium alloys, and related materials for biomedical applications. *Materials Science and Engineering: R: Reports*, 2004, sv. 47, č. 3, s. 49-121. ISSN 0927-796X.

[75] ZHENG, C. Y. et al. Enhanced in vitro biocompatibility of ultrafine-grained titanium with hierarchical porous surface. *Applied Surface Science*, 2011, sv. 257, č. 13, s. 5634-5640. ISSN 0169-4332.

[76] RAUTRAY, T. R. et al. Surface modification of titanium and titanium alloys by ion implantation. *Journal of Biomedical Materials Research Part B: Applied Biomaterials*, 2010, sv. 93B, č. 2, s. 581-591. ISSN 1552-4973.

[77] PARK, J.-W. et al. Enhanced osteoblast response to hydrophilic strontium and/or phosphate ions-incorporated titanium oxide surfaces. *Clinical Oral Implants Research*, 2010, sv. 21, č. 4, s. 398-408. ISSN 0905-7161.

[78] ZHAO, L. et al. The influence of hierarchical hybrid micro/nano-textured titanium surface with titania nanotubes on osteoblast functions. *Biomaterials*, 2010, sv. 31, č. 19, s. 5072-5082. ISSN 0142-9612.

[79] PARK, J. et al. Narrow window in nanoscale dependent activation of endothelial cell growth and differentiation on TiO2 nanotube surfaces. *Nano letters*, 2009, sv. 9, č. 9, s. 3157-3164. ISSN 1530-6984.

[80] FU, J. et al. Mechanical regulation of cell function with geometrically modulated elastomeric substrates. *Nature methods*, 2010, sv. 7, č. 9, s. 733-736. ISSN 1548-7105

1548-7091.

[81] HOSSEINKHANI, H. et al. Osteogenic differentiation of mesenchymal stem cells in self-assembled peptide-amphiphile nanofibers. *Biomaterials*, 2006, sv. 27, č. 22, s. 4079-4086. ISSN 0142-9612.

[82] LAVENUS, S. et al. Adhesion and osteogenic differentiation of human mesenchymal stem cells on titanium nanopores. *Eur Cell Mater*, 2011, sv. 22, č. 1, s. 84-96.

[83] ZHAO, L. et al. The osteogenic activity of strontium loaded titania nanotube arrays on titanium substrates. *Biomaterials*, 2013, sv. 34, č. 1, s. 19-29. ISSN 0142-9612.

[84] CHEN, X. et al. Fabrication of selenium-deposited and chitosan-coated titania nanotubes with anticancer and antibacterial properties. *Colloids and Surfaces B: Biointerfaces*, 2013, sv. 103, s. 149-157. ISSN 0927-7765.

[85] LAN, M.-Y. et al. Both enhanced biocompatibility and antibacterial activity in Ag-decorated TiO2 nanotubes. *PLoS One*, 2013, sv. 8, č. 10, s. e75364. ISSN 1932-6203.

[86] MONTEIRO, D. R. et al. The growing importance of materials that prevent microbial adhesion: antimicrobial effect of medical devices containing silver. *International Journal of Antimicrobial Agents*, 2009, sv. 34, č. 2, s. 103-110. ISSN 0924-8579.

[87] OH, S. et al. Stem cell fate dictated solely by altered nanotube dimension. *Proceedings of the National Academy of Sciences*, 2009, sv. 106, č. 7, s. 2130-2135. ISSN 0027-8424.

[88] PARK, J. et al. Nanosize and vitality: TiO2 nanotube diameter directs cell fate. *Nano letters*, 2007, sv. 7, č. 6, s. 1686-1691. ISSN 1530-6984.

[89] BAUER, S. et al. Improved attachment of mesenchymal stem cells on super-hydrophobic TiO2 nanotubes. *Acta Biomater*, 2008, sv. 4, č. 5, s. 1576-1582. ISSN 1742-7061 (Print)

1742-7061.

[90] PARK, J. et al. TiO2 Nanotube Surfaces: 15 nm—An Optimal Length Scale of Surface Topography for Cell Adhesion and Differentiation. *Small*, 2009, sv. 5, č. 6, s. 666-671. ISSN 1613-6810.

[91] ZHANG, Y. et al. Osteoblast behaviors on titania nanotube and mesopore layers. *Regenerative biomaterials*, 2017, sv. 4, č. 2, s. 81-87. ISSN 2056-3418.

[92] YU, W. Q. et al. The effect of anatase TiO2 nanotube layers on MC3T3-E1 preosteoblast adhesion, proliferation, and differentiation. *Journal of Biomedical Materials Research Part A*, 2010, sv. 94, č. 4, s. 1012-1022. ISSN 1549-3296.

[93] LV, L. et al. The nanoscale geometry of TiO2 nanotubes influences the osteogenic differentiation of human adipose-derived stem cells by modulating H3K4 trimethylation. *Biomaterials*, 2015, sv. 39, s. 193-205. ISSN 0142-9612.

[94] SMITH, B. S. et al. Dermal fibroblast and epidermal keratinocyte functionality on titania nanotube arrays. *Acta Biomaterialia*, 2011, sv. 7, č. 6, s. 2686-2696. ISSN 1742-7061.

[95] PENG, L. et al. The effect of TiO2 nanotubes on endothelial function and smooth muscle proliferation. *Biomaterials*, 2009, sv. 30, č. 7, s. 1268-1272. ISSN 0142-9612.

[96] SMITH, B. S. et al. Hemocompatibility of titania nanotube arrays. *Journal of Biomedical Materials Research Part A*, 2010, sv. 95, č. 2, s. 350-360. ISSN 1549-3296.

[97] LI, J. et al. The hemocompatibility and the reabsorption function of TiO 2 nanotubes biomembranes. *Chinese Science Bulletin*, 2012, sv. 57, č. 16, s. 2022-2028. ISSN 1861-9541.

[98] KULKARNI, M. et al. Biomaterial surface modification of titanium and titanium alloys for medical applications. *Nanomedicine*, 2014, sv. 111, s. 111.

[99] TSUCHIYA, H. et al. Hydroxyapatite growth on anodic TiO2 nanotubes. *Journal of Biomedical Materials Research Part A: An Official Journal of The Society for Biomaterials, The Japanese Society for Biomaterials, and The Australian Society for Biomaterials and the Korean Society for Biomaterials*, 2006, sv. 77, č. 3, s. 534-541. ISSN 1549-3296.

[100] VON WILMOWSKY, C. et al. In vivo evaluation of anodic TiO2 nanotubes: an experimental study in the pig. *Journal of Biomedical Materials Research Part B: Applied Biomaterials: An Official Journal of The Society for Biomaterials, The Japanese Society for Biomaterials, and The Australian Society for Biomaterials and the Korean Society for Biomaterials*, 2009, sv. 89, č. 1, s. 165-171. ISSN 1552-4973.

[101] BAUER, S. et al. Size selective behavior of mesenchymal stem cells on ZrO2 and TiO2 nanotube arrays. *Integrative Biology*, 2009, sv. 1, č. 8-9, s. 525-532. ISSN 1757-9708.

[102] DESHMUKH, S. P. et al. Silver nanoparticles as an effective disinfectant: A review. *Materials Science and Engineering: C*, 2019, sv. 97, s. 954-965. ISSN 0928-4931.

[103] DAS, K. et al. Surface coatings for improvement of bone cell materials and antimicrobial activities of Ti implants. *Journal of Biomedical Materials Research Part B: Applied Biomaterials*, 2008, sv. 87B, č. 2, s. 455-460. ISSN 1552-4973.

[104] GUNPUTH, U. F. et al. Anodised TiO2 nanotubes as a scaffold for antibacterial silver nanoparticles on titanium implants. *Materials Science and Engineering: C*, 2018, sv. 91, s. 638-644. ISSN 0928-4931.

[105] ESFANDIARI, N. et al. Size tuning of Ag-decorated TiO2 nanotube arrays for improved bactericidal capacity of orthopedic implants. *Journal of Biomedical Materials Research Part A*, 2014, sv. 102, č. 8, s. 2625-2635. ISSN 1549-3296.

[106] MENDONÇA, G. et al. Advancing dental implant surface technology–from micron-to nanotopography. *Biomaterials*, 2008, sv. 29, č. 28, s. 3822-3835. ISSN 0142-9612.

[107] LAN, M.-Y. et al. Diameter selective behavior of human nasal epithelial cell on Ag-coated TiO2 nanotubes. *Ceramics International*, 2014, sv. 40, č. 3, s. 4745-4751. ISSN 0272-8842.

[108] TAPIERO, H. et al. The antioxidant role of selenium and seleno-compounds. *Biomedicine & Pharmacotherapy*, 2003, sv. 57, č. 3, s. 134-144. ISSN 0753-3322.

[109] EL-BAYOUMY, K. The protective role of selenium on genetic damage and on cancer. *Mutation Research/Fundamental and Molecular Mechanisms of Mutagenesis*, 2001, sv. 475, č. 1, s. 123-139. ISSN 0027-5107.

[110] TRAN, P. A. a WEBSTER, T. J. Selenium nanoparticles inhibit Staphylococcus aureus growth. *International journal of nanomedicine*, 2011, sv. 6, s. 1553.

[111] TRAN, P. A. a WEBSTER, T. J. Antimicrobial selenium nanoparticle coatings on polymeric medical devices. *Nanotechnology*, 2013, sv. 24, č. 15, s. 155101. ISSN 0957-4484

1361-6528.

[112] EL-GHAZALY, M. et al. Anti-inflammatory effect of selenium nanoparticles on the inflammation induced in irradiated rats. *Canadian journal of physiology and pharmacology*, 2016, sv. 95, č. 2, s. 101-110. ISSN 0008-4212.

[113] SHURYGINA, I. A. a SHURYGIN, M. G. Nanoparticles in Wound Healing and Regeneration. In *Metal Nanoparticles in Pharma.* Springer, 2017, s. 21-37.

[114] SHAKIBAIE, M. et al. Anti-biofilm activity of biogenic selenium nanoparticles and selenium dioxide against clinical isolates of Staphylococcus aureus, Pseudomonas aeruginosa, and Proteus mirabilis. *Journal of Trace Elements in Medicine and Biology*, 2015, sv. 29, s. 235-241. ISSN 0946-672X.

[115] HUANG, X. et al. Investigation of functional selenium nanoparticles as potent antimicrobial agents against superbugs. *Acta Biomaterialia*, 2016, sv. 30, s. 397-407. ISSN 1742-7061.

[116] FOROOTANFAR, H. et al. Antioxidant and cytotoxic effect of biologically synthesized selenium nanoparticles in comparison to selenium dioxide. *Journal of Trace Elements in Medicine and Biology*, 2014, sv. 28, č. 1, s. 75-79. ISSN 0946-672X.

[117] RAAFAT, D. a SAHL, H.-G. Chitosan and its antimicrobial potential--a critical literature survey. *Microbial biotechnology*, 2009, sv. 2, č. 2, s. 186-201. ISSN 1751-7915.

[118] ADHIKARI, H. S. a YADAV, P. N. Anticancer Activity of Chitosan, Chitosan Derivatives, and Their Mechanism of Action. *International journal of biomaterials*, 2018, sv. 2018, s. 2952085-2952085. ISSN 1687-8787

1687-8795.

[119] YAO, S. et al. Antibacterial activity and inflammation inhibition of ZnO nanoparticles embedded TiO2 nanotubes. *Nanotechnology*, 2018, sv. 29, č. 24, s. 244003. ISSN 0957-4484.

[120] GAO, A. et al. The effects of titania nanotubes with embedded silver oxide nanoparticles on bacteria and osteoblasts. *Biomaterials*, 2014, sv. 35, č. 13, s. 4223-4235. ISSN 0142-9612.

[121] LI, J. et al. Plasmonic gold nanoparticles modified titania nanotubes for antibacterial application. *Applied Physics Letters*, 2014, sv. 104, č. 26, s. 261110. ISSN 0003-6951.

[122] YANG, W. et al. Titania nanotubes dimensions-dependent protein adsorption and its effect on the growth of osteoblasts. *Journal of Biomedical Materials Research Part A*, 2014, sv. 102, č. 10, s. 3598-3608. ISSN 1549-3296.

[123] BAUER, S. et al. Covalent functionalization of TiO2 nanotube arrays with EGF and BMP-2 for modified behavior towards mesenchymal stem cells. *Integrative Biology*, 2011, sv. 3, č. 9, s. 927-936. ISSN 1757-9708.

[124] PARK, J. et al. Synergistic control of mesenchymal stem cell differentiation by nanoscale surface geometry and immobilized growth factors on TiO2 nanotubes. *Small*, 2012, sv. 8, č. 1, s. 98-107. ISSN 1613-6810.

[125] KAR, A. et al. Electrodeposition of hydroxyapatite onto nanotubular TiO2 for implant applications. *Surface and Coatings Technology*, 2006, sv. 201, č. 6, s. 3723-3731. ISSN 0257-8972.

[126] KODAMA, A. et al. Bioactivation of titanium surfaces using coatings of TiO2 nanotubes rapidly pre-loaded with synthetic hydroxyapatite. *Acta Biomaterialia*, 2009, sv. 5, č. 6, s. 2322-2330. ISSN 1742-7061.

[127] PARCHAROEN, Y. et al. Hydroxyapatite electrodeposition on anodized titanium nanotubes for orthopedic applications. *Applied Surface Science*, 2014, sv. 311, s. 54-61. ISSN 0169-4332.

[128] MA, Q. et al. Enhancement of the bioactivity of titanium oxide nanotubes by precalcification. *Materials Letters*, 2008, sv. 62, č. 17, s. 3035-3038. ISSN 0167-577X.

[129] MOTOLA, M. et al. Thin TiO2 coatings by ALD enhance the cell growth on TiO2 nanotubular and flat substrates. *ACS Applied Bio Materials*, 2020, sv. 3, č. 9, s. 6447-6456. ISSN 2576-6422.

[130] BAUER, S. et al. Improved attachment of mesenchymal stem cells on super-hydrophobic TiO2 nanotubes. *Acta Biomaterialia*, 2008, sv. 4, č. 5, s. 1576-1582. ISSN 1742-7061.

[131] YANG, Y. et al. A novel electrochemical strategy for improving blood compatibility of titanium-based biomaterials. *Colloids and Surfaces B: Biointerfaces*, 2010, sv. 79, č. 1, s. 309-313. ISSN 0927-7765.

[132] LAI, M. et al. Sustained release of melatonin from TiO2 nanotubes for modulating osteogenic differentiation of mesenchymal stem cells in vitro. *Journal of Biomaterials science, Polymer edition*, 2017, sv. 28, č. 15, s. 1651-1664. ISSN 0920-5063.

[133] LEE, Y.-H. et al. Bone regeneration around N-acetyl cysteine-loaded nanotube titanium dental implant in rat mandible. *Biomaterials*, 2013, sv. 34, č. 38, s. 10199-10208. ISSN 0142-9612.

[134] SHRESTHA, N. K. et al. Magnetically guided titania nanotubes for site-selective photocatalysis and drug release. *Angewandte Chemie International Edition*, 2009, sv. 48, č. 5, s. 969-972. ISSN 1433-7851.

[135] WANG, Q. et al. TiO2 nanotube platforms for smart drug delivery: a review. *International journal of nanomedicine*, 2016, sv. 11, s. 4819.

[136] KUNRATH, M. F. et al. Application of TiO2 nanotubes as a drug delivery system for biomedical implants: a critical overview. *ChemistrySelect*, 2018, sv. 3, č. 40, s. 11180-11189. ISSN 2365-6549.

[137] MACAK, J. M. et al. Self-organized nanotubular oxide layers on Ti-6Al-7Nb and Ti-6Al-4V formed by anodization in NH4F solutions. *Journal of Biomedical Materials Research Part A: An Official Journal of The Society for Biomaterials, The Japanese Society for Biomaterials, and The Australian Society for Biomaterials and the Korean Society for Biomaterials*, 2005, sv. 75, č. 4, s. 928-933. ISSN 1549-3296.

[138] TSUCHIYA, H. et al. Anodic oxide nanotubes on Ti alloys. *ECS Transactions*, 2007, sv. 3, č. 31, s. 365. ISSN 1938-5862.

[139] OLIVEIRA, N. T. et al. Obtaining self-organized nanotubes on biomedical Ti–Mo alloys. *Electrochemistry Communications*, 2013, sv. 35, s. 139-141. ISSN 1388-2481.

[140] GRIGORESCU, S. et al. The two step nanotube formation on TiZr as scaffolds for cell growth. *Bioelectrochemistry*, 2014, sv. 98, s. 39-45. ISSN 1567-5394.

[141] MINAGAR, S. et al. Fabrication and characterization of TiO 2–ZrO 2–ZrTiO 4 nanotubes on TiZr alloy manufactured via anodization. *Journal of Materials Chemistry B*, 2014, sv. 2, č. 1, s. 71-83.

[142] TSUCHIYA, H. et al. Anodic oxide nanotube layers on Ti–Ta alloys: Substrate composition, microstructure and self-organization on two-size scales. *Corrosion Science*, 2009, sv. 51, č. 7, s. 1528-1533. ISSN 0010-938X.

[143] HANG, R. et al. Preparation, characterization, corrosion behavior and bioactivity of Ni2O3-doped TiO2 nanotubes on NiTi alloy. *Electrochimica Acta*, 2012, sv. 70, s. 382-393. ISSN 0013-4686.

[144] DING, D. et al. Anodic fabrication and bioactivity of Nb-doped TiO2 nanotubes. *Nanotechnology*, 2009, sv. 20, č. 30, s. 305103. ISSN 0957-4484.

[145] TAIPINA, M. O. et al. A novel Ag doping Ti alloys route: Formation and antibacterial effect of the TiO2 nanotubes. *Materials Chemistry and Physics*, 2021, sv. 261, s. 124192. ISSN 0254-0584.

[146] SARRAF, M. et al. Mixed oxide nanotubes in nanomedicine: A dead-end or a bridge to the future? *Ceramics International*, 2020. ISSN 0272-8842.

[147] YENIYOL, S. et al. Antibacterial activity of As-annealed TiO2 nanotubes doped with Ag nanoparticles against periodontal pathogens. *Bioinorganic chemistry and applications*, 2014, sv. 2014. ISSN 1565-3633.

[148] LIU, H. et al. Cytocompatibility and antibacterial property of N+ ions implanted TiO2 nanotubes. *Surface and Coatings Technology*, 2019, sv. 359, s. 468-475. ISSN 0257-8972.

[149] HOU, X. et al. Antibacterial ability of Ag–TiO2 nanotubes prepared by ion implantation and anodic oxidation. *Materials Letters*, 2015, sv. 161, s. 309-312. ISSN 0167-577X.

[150] ZHANG, X. et al. A functionalized Sm/Sr doped TiO2 nanotube array on titanium implant enables exceptional bone-implant integration and also self-antibacterial activity. *Ceramics International*, 2020, sv. 46, č. 10, s. 14796-14807. ISSN 0272-8842.

[151] TRAN, P. A. a WEBSTER, T. J. Understanding the wetting properties of nanostructured selenium coatings: the role of nanostructured surface roughness and air-pocket formation. *International journal of nanomedicine*, 2013, sv. 8, s. 2001.

[152] Conference ProceedingsSTOLZOFF, M. et al. *Efficacy and mechanism of selenium nanoparticles as antibacterial agents*. Front. Bioeng. Biotechnol. Conference Abstract: 10th World Biomaterials Congress. doi: 10.3389/conf. FBIOE.

[153] GALLO, J. et al. Antibacterial Surface Treatment for Orthopaedic Implants. *International Journal of Molecular Sciences*, 2014, sv. 15, č. 8, s. 13849-13880. ISSN 1422-0067.

[154] TRAN, P. A. et al. Low cytotoxic trace element selenium nanoparticles and their differential antimicrobial properties against S. aureus and E. coli. *Nanotechnology*, 2015, sv. 27, č. 4, s. 045101. ISSN 0957-4484.

[155] BENDAS, G. a BORSIG, L. Cancer cell adhesion and metastasis: selectins, integrins, and the inhibitory potential of heparins. *International journal of cell biology*, 2012, sv. 2012. ISSN 1687-8876.

[156] PERINPANAYAGAM, H. et al. Early cell adhesion events differ between osteoporotic and non-osteoporotic osteoblasts. *Journal of orthopaedic research*, 2001, sv. 19, č. 6, s. 993-1000. ISSN 0736-0266.

[157] BLANKENBERG, S. et al. Adhesion molecules and atherosclerosis. *Atherosclerosis*, 2003, sv. 170, č. 2, s. 191-203. ISSN 0021-9150.

[158] RAYMAN, M. P. Selenium in cancer prevention: a review of the evidence and mechanism of action. *Proceedings of the Nutrition Society*, 2005, sv. 64, č. 4, s. 527-542. ISSN 1475-2719.

[159] VAZQUEZ-MUÑOZ, R. et al. Enhancement of antibiotics antimicrobial activity due to the silver nanoparticles impact on the cell membrane. *PLoS One*, 2019, sv. 14, č. 11, s. e0224904. ISSN 1932-6203.

[160] YIN, I. X. et al. The antibacterial mechanism of silver nanoparticles and its application in dentistry. *International journal of nanomedicine*, 2020, sv. 15, s. 2555.

[161] PRABHU, S. a POULOSE, E. K. Silver nanoparticles: mechanism of antimicrobial action, synthesis, medical applications, and toxicity effects. *International nano letters*, 2012, sv. 2, č. 1, s. 1-10. ISSN 2228-5326.

[162] BURKOWSKA-BUT, A. et al. Influence of stabilizers on the antimicrobial properties of silver nanoparticles introduced into natural water. *Journal of Environmental Sciences*, 2014, sv. 26, č. 3, s. 542-549. ISSN 1001-0742.

[163] BOROWIK, A. et al. The impact of surface functionalization on the biophysical properties of silver nanoparticles. *Nanomaterials*, 2019, sv. 9, č. 7, s. 973.

[164] KHATOON, Z. et al. Bacterial biofilm formation on implantable devices and approaches to its treatment and prevention. *Heliyon*, 2018, sv. 4, č. 12, s. e01067. ISSN 2405-8440.

[165] JUHNA, T. et al. Detection of Escherichia coli in biofilms from pipe samples and coupons in drinking water distribution networks. *Applied and environmental microbiology*, 2007, sv. 73, č. 22, s. 7456-7464. ISSN 0099-2240.

[166] STOCKS, S. Mechanism and use of the commercially available viability stain, BacLight. *Cytometry Part A: The Journal of the International Society for Analytical Cytology*, 2004, sv. 61, č. 2, s. 189-195. ISSN 1552-4922.

[167] ROSENBERG, M. et al. Propidium iodide staining underestimates viability of adherent bacterial cells. *Scientific reports*, 2019, sv. 9, č. 1, s. 1-12. ISSN 2045-2322.

[168] GUO, Z. et al. Fabrication of silver-incorporated TiO2 nanotubes and evaluation on its antibacterial activity. *Materials Letters*, 2014, sv. 137, s. 464-467. ISSN 0167-577X.

[169] ERCAN, B. et al. Diameter of titanium nanotubes influences anti-bacterial efficacy. *Nanotechnology*, 2011, sv. 22, č. 29, s. 295102. ISSN 0957-4484.

[170] MAZARE, A. et al. Corrosion, antibacterial activity and haemocompatibility of TiO2 nanotubes as a function of their annealing temperature. *Corrosion Science*, 2016, sv. 103, s. 215-222. ISSN 0010-938X.

[171] MAURICE, N. M. et al. Pseudomonas aeruginosa biofilms: host response and clinical implications in lung infections. *American journal of respiratory cell and molecular biology*, 2018, sv. 58, č. 4, s. 428-439. ISSN 1044-1549.

[172] HUYNH, K. A. a CHEN, K. L. Aggregation kinetics of citrate and polyvinylpyrrolidone coated silver nanoparticles in monovalent and divalent electrolyte solutions. *Environmental science & technology*, 2011, sv. 45, č. 13, s. 5564-5571. ISSN 0013-936X.

[173] QIAO, Z. et al. Silver nanoparticles with pH induced surface charge switchable properties for antibacterial and antibiofilm applications. *Journal of Materials Chemistry B*, 2019, sv. 7, č. 5, s. 830-840.

[174] NISKA, K. et al. Capping agent-dependent toxicity and antimicrobial activity of silver nanoparticles: an in vitro study. Concerns about potential application in dental practice. *International journal of medical sciences*, 2016, sv. 13, č. 10, s. 772.

[175] VAN DOORSLAER, X. et al. UV-A and UV-C induced photolytic and photocatalytic degradation of aqueous ciprofloxacin and moxifloxacin: reaction kinetics and role of adsorption. *Applied Catalysis B: Environmental*, 2011, sv. 101, č. 3-4, s. 540-547. ISSN 0926-3373.

[176] CRÉMET, L. et al. Orthopaedic-implant infections by Escherichia coli: molecular and phenotypic analysis of the causative strains. *Journal of Infection*, 2012, sv. 64, č. 2, s. 169-175. ISSN 0163-4453.

[177] VASILEV, K. Nanoengineered antibacterial coatings and materials: A perspective. *Coatings*, 2019, sv. 9, č. 10, s. 654.

[178] HUNT, P. R. et al. Bioactivity of nanosilver in Caenorhabditis elegans: Effects of size, coat, and shape. *Toxicology reports*, 2014, sv. 1, s. 923-944. ISSN 2214-7500.

[179] GenericLISTER, J. et al. *Staphylococcus aureus biofilms: recent developments in biofilm dispersal. Front Cell Infect Microbiol 4: 1–9.*

[180] SHI, C. et al. Antimicrobial effect of lipoic acid against Cronobacter sakazakii. *Food Control*, 2016, sv. 59, s. 352-358. ISSN 0956-7135.

[181] WIEGAND, C. et al. Poly (ethyleneimines) in dermal applications: biocompatibility and antimicrobial effects. *International journal of pharmaceutics*, 2013, sv. 456, č. 1, s. 165-174. ISSN 0378-5173.

[182] IVANOVA, A. et al. Layer-By-Layer Coating of Aminocellulose and Quorum Quenching Acylase on Silver Nanoparticles Synergistically Eradicate Bacteria and Their Biofilms. *Advanced Functional Materials*, 2020, sv. 30, č. 24, s. 2001284. ISSN 1616-301X.

[183] BEER, C. et al. Toxicity of silver nanoparticles—nanoparticle or silver ion? *Toxicology letters*, 2012, sv. 208, č. 3, s. 286-292. ISSN 0378-4274.

[184] FOHLEROVA, Z. et al. SiO2-Decorated Parylene C Micropillars Designed to Probe Cellular Force. *Advanced Materials Interfaces*, 2021, sv. 8, č. 6, s. 2001897. ISSN 2196-7350.

[185] LOWRY, G. V. et al. Guidance to improve the scientific value of zeta-potential measurements in nanoEHS. *Environmental Science: Nano*, 2016, sv. 3, č. 5, s. 953-965. ISSN 2051-8153.

[186] VRANDEČIĆ, K. et al. Antifungal activities of silver and selenium nanoparticles stabilized with different surface coating agents. *Pest Management Science*, 2020, sv. 76, č. 6, s. 2021-2029. ISSN 1526-498X.

[187] BI, X. et al. Super Hydrophobic Parylene-C Produced by Consecutive O2 and SF6 Plasma Treatment 2013.

[188] GUERRERO CORREA, M. et al. Antimicrobial metal-based nanoparticles: a review on their synthesis, types and antimicrobial action. *Beilstein journal of nanotechnology*, 2020, sv. 11, s. 1450-1469. ISSN 2190-4286.

[189] GEOFFRION, L. D. et al. Naked Selenium Nanoparticles for Antibacterial and Anticancer Treatments. *ACS Omega*, 2020, sv. 5, č. 6, s. 2660-2669. ISSN 2470-1343.

[190] NGUYEN, T. H. D. et al. Antibacterial properties of selenium nanoparticles and their toxicity to Caco-2 cells. *Food Control*, 2017, sv. 77, s. 17-24. ISSN 0956-7135.

[191] MENON, S. et al. Investigating the Antimicrobial Activities of the Biosynthesized Selenium Nanoparticles and Its Statistical Analysis. *BioNanoScience*, 2020, sv. 10, č. 1, s. 122-135. ISSN 2191-1649.

[192] BILEK, O. et al. Enhanced antibacterial and anticancer properties of Se-NPs decorated TiO2 nanotube film. *PloS one*, 2019, sv. 14, č. 3, s. e0214066-e0214066. ISSN 1932-6203.

[193] HUANG, T. et al. Engineering highly effective antimicrobial selenium nanoparticles through control of particle size. *Nanoscale*, 2019, sv. 11, č. 31, s. 14937-14951. ISSN 2040-3364.

[194] FILIPOVIĆ, N. et al. Comparative Study of the Antimicrobial Activity of Selenium Nanoparticles With Different Surface Chemistry and Structure. *Frontiers in bioengineering and biotechnology*, 2021, sv. 8, s. 624621-624621. ISSN 2296-4185.

[195] LI, B. et al. Self-adjusting antibacterial properties of Ag-incorporated nanotubes on micro-nanostructured Ti surfaces. *Biomaterials Science*, 2019, sv. 7, č. 10, s. 4075-4087. ISSN 2047-4830.

[196] LIU, J. et al. Nano-Modified Titanium Implant Materials: A Way Toward Improved Antibacterial Properties. *Frontiers in bioengineering and biotechnology*, 2020, sv. 8, s. 576969-576969. ISSN 2296-4185.

[197] EPAND, R. M. a EPAND, R. F. Lipid domains in bacterial membranes and the action of antimicrobial agents. *Biochimica et Biophysica Acta (BBA) - Biomembranes*, 2009, sv. 1788, č. 1, s. 289-294. ISSN 0005-2736.

[198] SHARMA, S. a CONRAD, J. C. Attachment from Flow of Escherichia coli Bacteria onto Silanized Glass Substrates. *Langmuir*, 2014, sv. 30, č. 37, s. 11147-11155. ISSN 0743-7463.

[199] GOTTENBOS, B. et al. Antimicrobial effects of positively charged surfaces on adhering Gram-positive and Gram-negative bacteria. *Journal of Antimicrobial Chemotherapy*, 2001, sv. 48, č. 1, s. 7-13. ISSN 0305-7453.

9. List of Figures

10. List of tables

11. List of used acronyms and abbreviations

AAO – Anodic aluminium oxide

APTES - 3-aminopropyltriethoxysilane

AgNPs – Silver nanoparticles

AgNPs-TNTs – Silver decorated TiO_2 nanotubes

BMP2 – Bone morphogenetic protein 2

BPEI – branched polyethyleneimine

BPEI-Ag-TNTs - TiO_2 nanotubes decorated with approximately 3-4 branched polyethyleneimine functionalized silver nanoparticles

DMEM - Dulbecco's Modified Eagle's medium

EGF – epidermalgrowth factor

FBS – Fetal bovine serum

hASCs - Human adipose-derived stem cells

HNEpC – Human nasal epithelial cell

Lipoic-acid-Ag-TNTs - TiO_2 nanotubes decorated with approximately 3-4 lipoic acid functionalized silver nanoparticles

MG-63 – Osteoblast-like cells

NIH-3T3 – Fibroblast cells

PBS - phosphate buffer saline

PEG – polyethylene glycol

PVP – polyvinylpyrrolidone

RMS- root mean squared

SEM – Scanning electron microscopy

SLA - sandblasted, large grit, acid-etched implant surface

Se-High-TNTs - TiO_2 nanotubes decorated with approximately 17 selenium nanoparticles

Se-Low-TNTs – TiO_2 nanotubes decorated with approximately 3-4 selenium nanoparticles

SeNPs – Selenium nanoparticles

TNTs - Titanium dioxide nanotubes

TiO_2 – titania, titanium dioxide

XPS – X-ray photoelectron spectroscopy

12. Co-authored publication

Modification of parylene by microstructures and selenium nanoparticles: Evaluation of bacterial and mesenchymal stem cells viability

PEKÁRKOVÁ, J.; FIALOVA, T.; BÍLEK, O., FOHLEROVÁ, Z.

The paper is currently being prepared for submission, available details can be found in the draft below.

Parylene is a commonly used polymeric protectiveness of a wide range of devices in the form of thin-film coating. Due to its excellent anticorrosion properties, it is often used as an insulator for electronic components. Further, its long-term stability and biocompatibility in the contact with bio-fluids and tissue makes this polymer excellent for biomedical applications. To date, parylene has been used as the coating of implantable sensors and transducers and orthopaedic or dental implants such as catheters, stents. Since the polymeric materials used in medicine such as polyvinylchloride (PVC), polyurethanes (PU), silicone and parylene suffer from very high bacterial colonization and infection, the effectiveness of some antimicrobial modification of polymer has been performed. Here, polyvinylpyrollidone stabilized selenium nanoparticles were synthesized and various approaches have been studied for their reproducible adsorption on parylene-C coated silicon wafer. The process of nanoparticle deposition was optimized in the nanoparticle concentration to obtain evenly distributed NPs on the flat parylene surface. Moreover, the array of parylene micropillars has been fabricated, modified with SeNPs and lately compared to the flat surface. All designed surfaces were tested against two bacterial pathogens, *Escherichia coli* (gram negative) and *Staphylococcus aureus* (gram positive) and the cytotoxicity was performed on mesenchymal stem cells.

12.1. Materials and methods

Preparation of Si wafer coated with Parylene C

5 μm thick parylene layer on Si wafer was prepared according to the following procedure: 5,5 g of parylene C was deposited on 4´´ Si wafer with orientation <100> by CVD (PDS 2010, Specialty Coating Systems (SCS), Indianapolis). In the next step, wafers with parylene layer were cut into 2×2 cm squares using Semiautomatic dicing saw ESEC 8003.

Fabrication of parylene pillars

The array of micropillars were fabricated as described previously by us with a little modification removing SiO_2 layer on the micropillars.[184] Briefly, the array was fabricated via a "top-down" process in which 10 μm thick layer of parylene C (Palmchem) was deposited on the Si wafer using the chemical vapour deposition (CVD) method. The deposition of a 500 nm thin Ti layer using the electron beam evaporation technique was

followed by standard UV photolithography using the photoresist (PR) AZ 5214E. Photolithography of PR created the pattern of hexagonally arranged features with diameter of 2 μm and center-to-center distance of 4 μm. The titanium was then etched using reactive-ion etching (RIE) in Cl_2 plasma by means of chlorine-based RIE. Finally, the wafer was placed into the ion beam etching (IBE) instrument employing pure O_2 plasma to etch the parylene C from the areas uncovered by Ti. The PR was completely removed during the IBE process and the Ti residue was additionally removed using chlorine-based RIE.

Synthesis of selenium nanoparticles

Colloidal selenium nanoparticles (SeNPs) were prepared by wet-chemical reaction according to (Gablech et al. 2021). Aqueous solution of 25 mM sodium selenite (Na_2SeO_3) was mixed with aqueous solutions of 28 mM L-cysteine ($C_3H_7NO_2S$) and 25 μM polyvinylpyrrolidone (PVP) under vigorous stirring. When the ruby red color of the mixture developed, it indicated the end of the reaction and the stirring was stopped. Afterwards, the colloidal solution was purified three times with deionized water by ultracentrifugation. SeNPs solution with final concentration of 0.2 mg/mL was subsequently diluted as follows: 0x, 5x, 10x, 20x and 50x. All chemicals were purchased from Sigma-Aldrich with chemical purity grade of per analysis (p.a.). Sodium selenite was used as a precursor of Se ions, L-cysteine as a reducing agent and polyvinylpyrrolidone with an average molecular weight of ≈ 40 000 $g \cdot mol^{-1}$ as a stabilizing agent. Nanoparticle morphology and size were characterized by STEM microscopy Verios 460L (Thermo Fisher Scientific, USA). Nanoparticle zeta potential (Zetasizer Nano ZS instrument; Malvern Instrument Ltd, UK) was measured at the condition of 25 °C and equilibrating time 0 s. Calculations considered the diminishing of particles concentration were based on Smoluchowsky model, with parameters F (κa) of 1.50. For measurement, disposable cuvettes type DTS1070 were used. The measurements were performed under the automatic setting of attenuation and voltage selection. All measurements were done in triplicates.

Decoration of parylene with nanoparticles

Si squares with parylene film were treated with O_2 plasma for 1 min to induce parylene film hydrophilicity. Then, a self-assembled monolayer (SAM) of 3-aminopropyltrimethoxysilane (APTES) was deposited using CVD. 30 μl of APTES was put on the glass slide next to the wafer and heated to 120 °C for 30 min in SAM chamber (custom-made). The adsorption of SeNPs with various concentration to the parylene film was tested and optimized for bare, plasma treated and silanized surface. Si wafer with parylene film was immersed into the petri dish with various dilutions of SeNPs solution for 90 min. Afterwards, Si wafers decorated with SeNPs were thoroughly rinse with DI water and air dried.

Surface characterization

The parylene C modification was characterized by the measurement of the contact angle (CA; Phoenix 300, SEO) by applying water drop on the surface. The CA was evaluated using Surfaceware 8 software and the statistical analysis was performed on 5 drops from each step of modified surface. The distribution of selenium nanoparticles on parylene C was characterized with scanning electron microscope (SEM, Mira II, Tescan, CZ), X-ray photoelectron spectroscopy has been used to analyse surface chemistry (XPS, AXIS Supra, Kratos Analytical Ltd, UK). XPS spectra were analyzed by a peak fitting software (CasaXPS version2.3.18PR1.0).

Antibacterial test

Antibacterial properties of SeNPs decorated parylene films (flat and micropillars) were further evaluated via colony counting method using gram-negative bacteria *Escherichia Coli* and gram-positive bacteria *Staphylococcus aureus*. Bacterial strains were cultured on Columbia blood agar 5% (Labmediaservis) at 37°C overnight. Bacterial inoculum was prepared by dilution of the bacterial colonies in Mueller Hinton broth (Sigma-Aldrich) to cell density 1-2·106 CFU·mL^{-1}. Samples were rinsed in sterile water and the bacterial inoculum was spread onto the surface, covered by sterile plastic foil, and incubated 24 hours at 37 °C. Subsequently, the samples were rinsed in PBS and adhered bacteria were de-attached by vortexing and sonication. Collected bacterial suspension was diluted in PBS by decimal dilution and selected dilutions were inoculated on PCA agar plates and incubated for 24 hours at 37 °C. Bacterial colonies grown on the plates were then counted and colony forming unit was calculated (CFU·cm^{-2}). The experiment was performed in triplicates.

Viability of mesenchymal stem cells

Mesenchymal stem cells (MSCs) isolated during a plastic surgery were cultured in MSC growth medium (Sigma Aldrich) supplemented with 5% FBS, 1% penicillin/streptomycin, and 1% L-glutamine. Cells were harvested by trypsinization in 0.25% solution of trypsin/EDTA at 80% confluence. Viability of cells were studied by tetrazolium-based assay. Proliferation of MSC cells on the samples was measured with 2,3-bis-(2-methoxy-4-nitro-5-sulfophenyl)-2H-tetrazolium-5-carboxanilide (XTT) and evaluated on days 1 and 3 after the seeding; the initial cell density was $1 \cdot 10^4$ cells per area. Briefly, the cells were cultured for a defined period and then gently washed twice with pre-heated PBS. The mixture of 150 mL culture medium and 50 mL tetrazolium dye (XTT, 1 mg·mL^{-1} in PBS, pH 7.4) was added to the samples. After 4-hour incubation, the absorbance of solution was measured at 450 nm. To image cells on the micropillars, the MSCs were fixed with 4% paraformaldehyde in PBS for 15 min, washed twice in buffer solution and permeabilized in 4% Triton-X100 solution for 1 hour. Then, the cells were washed in buffer and immunostaining of cells has been performed. The ready probe Actin-Green (Thermo Fisher) has been applied according to the manufacturer to stain actin filaments and cells were imaged at 480 nm. MSCs cells on flat

surface have been imaged by DIC mode of optical microscope. The cell surface area was measured using ImageJ software.

12.2. Results and discussion

12.2.1. Characterization of SeNPs

The morphology and size of SeNPs were determined by high resolution scanning transmission electron microscope (STEM) with an accelerating voltage of 30 kV. A 10 µl of SeNPs colloidal solution was dropped onto a carbon membrane for STEM analysis and dried at ambient temperature of 22 °C. The average particle size of SeNPs has been estimated of 60±12 nm. The stability of SeNPs was analyzed by measuring their electrokinetic Zeta (ζ) potential. ζ potential can be used as a parameter for the long-term stability prediction of the colloidal solutions.[185] In general, the solution with the absolute value of ζ potential above 30 mV can be considered as stable. The ζ potential is dependent on several factors such as concentration, charge, temperature and pH. The measured ζ potential of PVP stabilized SeNPs synthetized in this work was -31,6 ± 1,9 mV at pH 6.3 and 25 °C which correlates with similar results of PVP stabilized nanoparticles [186].

12.2.2. Preparation and characterization of SeNPs/parylene C films

The strength of nanoparticle adsorption depends mainly on the surface topography and chemical properties of both materials. In our work we initially performed the adsorption of PVP-Se-nanoparticles on bare and plasma treated flat parylene C surface. However, the SEM imaging showed no nanoparticle deposition on such surfaces (data not shown). Therefore, we decided to perform the surface functionalization of parylene C with amino-terminated silane APTES and thus provide a positively charged surface to the negatively charged PVP-Se-nanoparticles at pH ~ 7. In the preliminary characterization we performed contact angle measurements in each step of the surface modification (Fig. 2 left). The deposited “flat” parylene C (PC) with contact angle (*CA*) ~ 90° dramatically dropped to ~25° after oxygen plasma treatment making the surface hydrophilic. However, the *CA* decrease for the highly hydrophobic microstructured parylene (PC pillars) was not so dramatic. It remained in the hydrophobic region, dropping down from *CA* ~110° to 90. Silanization of plasma treated surfaces with APTES exposed the amino group on the parylene and the *CA* increased to ~ 65° and stayed almost unchanged (~90°) for the “flat” and microstructured surfaces, respectively. Subsequently, the XPS analysis was performed for the flat sample to confirm the presence of APTES and PVP-SeNPs (Fig. 2 right). Parylene C is poly(para-xylylene) in which one hydrogen atom is substituted by a chlorine atom. The wide spectrum shows the main peaks characteristic for untreated parylene C (blue line) such as C1s, Cl 2s and Cl 2p. [187] The spectrum for the APTES/SeNPs/parylene sample (orange line) showed N1s peak from the

APTES and PVP stabilizing agent, Si 2s and Si 2p peaks coming from the silane deposition and Se 3d, Se LMM peaks are characteristic for the selenium nanoparticles. Both analysis confirmed us successful functionalization and decoration of parylene C surface with APTES and SeNPs, respectively.

The same modification procedure has been performed for microstructured parylene C. However, SEM images of nanoparticle decorated surface is not shown due to the bad contrast even after the surface metallization. Nevertheless, we fabricated micropillar array of the hexagonally ordered parylene pillars with ~2 µm diameter, ~4 µm center-to-center distance, ~8 µm length and cylindrical morphology, as confirmed by a scanning electron microscopy (Figure 3 A-B, representative MSCs cell is shown on C).

After we found PVP-Se nanoparticles successfully adsorbed on the silanized surface through electrostatic interaction, we proceeded to the preparation of representative samples with variable number of decorated nanoparticles per area. Thus, we made a serial dilution of nanoparticle stock solution ranging from 0 to 1:50 and we left the solution and silanized surface to interact for 90 min. The density of nanoparticle coverage was controlled by SEM microscopy (Figure 4) and looked as follows: no dilution (~12 SeNPs·µm^{-2}), 1:5 dilutions (~9 SeNPs·µm^{-2}), 1:10 (~5 SeNPs·µm^{-2}), 1:20 (~3 SeNPs·µm^{-2}) and 1:50 dilution (~1 SeNPs·µm^{-2}). SEM images of SeNPs decorated parylene also showed that the nanoparticle size differs from that obtained by STEM microscopy. The size of nanoparticles measured from SEM images in Fig. 4 equalled about 100 ± 10 nm. This could be attributed to slight agglomeration of nanoparticles. Nevertheless, we managed to reproducibly decorate nanoparticles on amino-functionalized parylene C to obtain representative samples for further antibacterial and cytotoxicity assays.

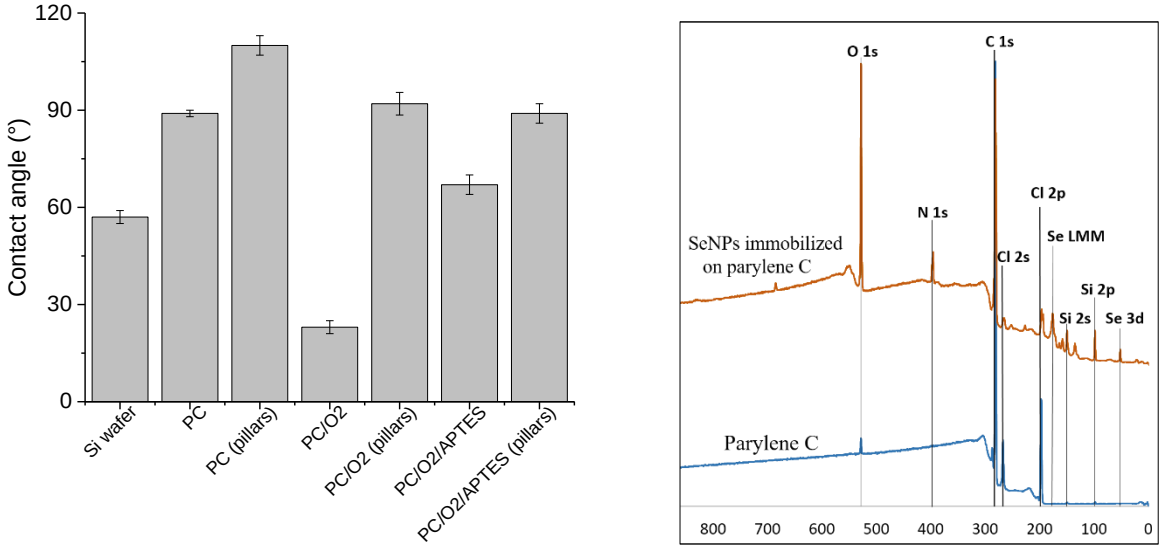

Figure 2 Contact angle measurement of the parylene – coated silicon wafer under the different surface treatment. XPS wide spectrum of parylene C coated Si wafer (blue) and

parylene surface with immobilized selenium nanoparticle via APTES silanization. X-axis represents binding energies in mV.

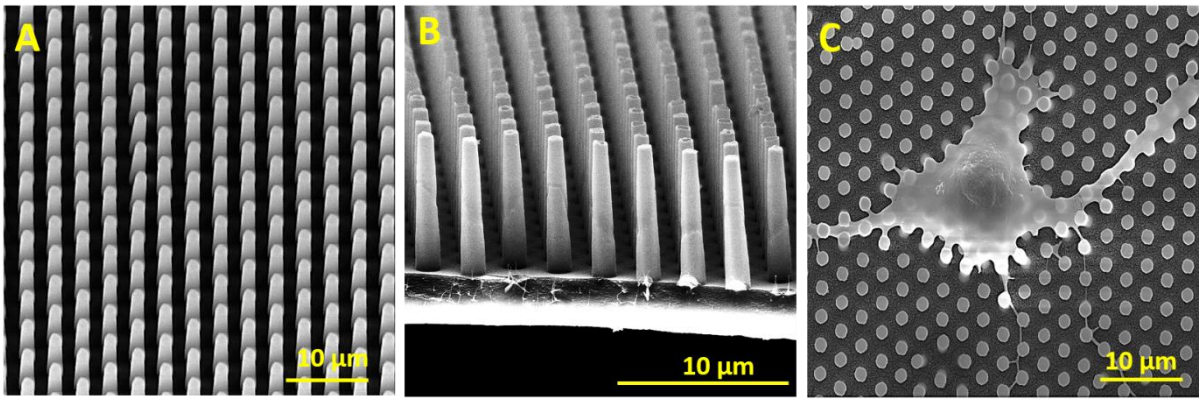

Figure 3 SEM images of the hexagonally ordered micropillars fabricated by etching of parylene C (A-B). The fixed MSCs cell laying on the micropillar substrate (C).

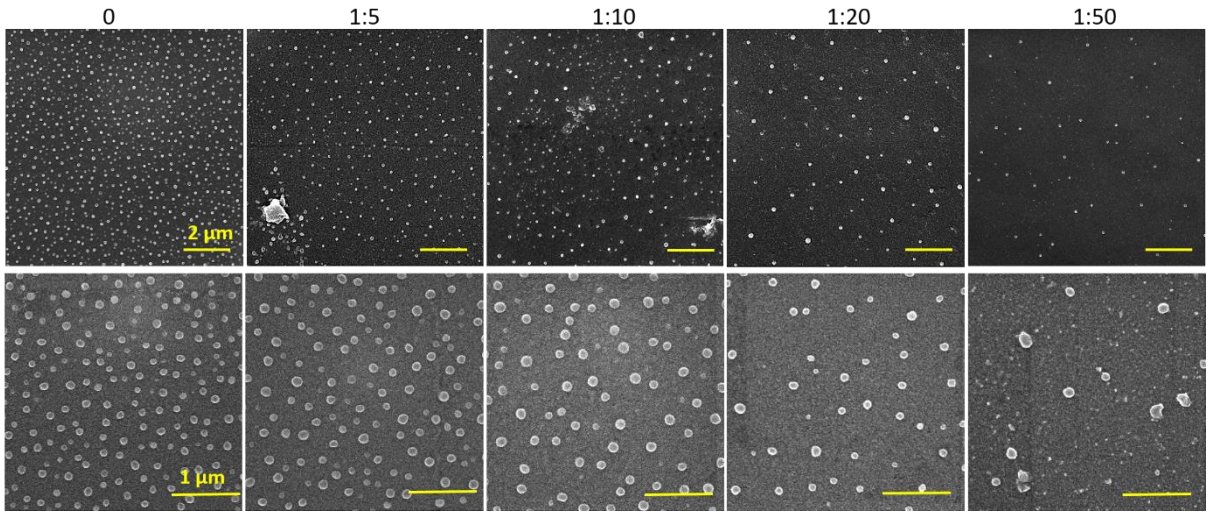

Figure 4 SEM images of SeNPs decorated parylene flat film under the different nanoparticle dilution.

12.2.3. Antibacterial properties of parylene films

Parylene C as many other medical polymers does not exhibit any significant antibacterial properties. On the other hand, some inorganic nanoparticles (Ag, Au, Se etc.) possess antibacterial action themselves.[188] Decoration of such polymeric materials with these nanoparticles have been found as one of the valid strategies for improvement of their antibacterial properties. Selenium is a trace element important for human health, which is why selenium nanoparticles are becoming an emerging nanomaterial in biomedicine. Selenium nanoparticles have been showed in many studies as the promising antimicrobial agents [189-191] . Besides, the decoration of PU, PVC and silicon [111] as well as non-polymeric

biomaterials [192] with selenium nanoparticles has increased the antibacterial properties of materials towards gram negative and gram positive bacteria in relatively positive manner. The suggested correlation between selenium nanoparticle size and antibacterial action has been studied for the range of nanoparticle size between 40 nm to 205 nm [193]. Authors showed that the best antibacterial efficiency was found for 81 nm SeNPs. Antimicrobial activity of SeNPs with different surface chemistry and structure has also been studied for several common bacterial strains.[194] Moreover, micro- and nanostructuring of hard biomaterials have also been found to have significant impact against the bacteria compared to the non-structuring ones. [195,196] Here, we studied synergistic antibacterial effect of modified parylene C polymer with both, selenium nanoparticles and microstructures in the form of micropillars. As the model of bacterial cells, we chose gram positive *S. aureu*s and gram-negative *E. coli*. Both bacteria differ from the membrane components and thus they might have different response to nano-/micro materials[197]. Figure 5 shows preliminary results from colony counting method for both bacteria after 24 hours' incubation with tested surfaces. The values are related to the initial bacterial density of 10^5 CFU·cm^{-2} (blue line) and it enables to estimate whether the surface does not exhibit any enhanced antibacterial activity or it exhibits bacteriostatic or bactericide effect. The growth of *Staphylococcus aureus* was not inhibited on any surface, the flat and microstructured, respectively as it is observed in the control experiments (Fc and Mc). Unexpectedly, selenium nanoparticles did not enhance antibacterial action of both surfaces and more importantly, the significant difference has not been observed even for the series of nanoparticle dilutions. Mechanism of antibacterial action of selenium nanoparticles is mainly the damage of the cellular membrane and the production of reactive oxygen species (ROS).[193] The possible explanation for this non-effectivity of selenium nanoparticle to act as antibacterial agents can be in the bigger nanoparticle size (~100 nm here), membrane composition of gram positive bacteria as well as positive charge on the un-decorated parylene residues which can attract the bacteria and support them in the growth. Moreover, the microstructuring did not influence *S. aureus* growth probably due to the "bigger" microstructures and pitches that made the surface favourable to bacteria colonization even in the interpillar space. Another reason for the ineffectiveness of the material on *S. aureus* may be the stronger cell wall structure of gram-positive bacteria and the spherical shape of the cocci, which allows them to resist surface irregularities more effectively. Considering the *S. aureus* and *E. coli* size of 0.5-1 μm and 1-2 μm, respectively, both bacteria can easily penetrate into the free space between pillars and the bottom of underlying substrate. However, the most of these reasons resulting in the intactness of *S. aureus* to these surfaces is caused by the combination of two or more factors. A slightly different result was obtained for gram negative *E. coli*. By comparison of the control experiments (Fc and Mc), one can observe bacteriostatic effect of both the "flat" parylene C (Fc) and the microstructured parylene (Mc). However, within the two groups (flat and microstructured surface decorated with SeNPs), no significant difference has been observed. It means, that the selenium nanoparticles, probably due to their size, did not act as antibacterial agent and more likely, the parylene itself and

microstructuring played more important role in antibacterial action towards gram negative bacteria. However, above mentioned effect of positively charged surface from the APTES functionalization of parylene has been observed to attract and support the growth of *E. coli* [198]. Here, it could contribute to the *E. coli* adhesion but not to the growth as showed in the graph. More likely, positive charge had the better impact on gram positive *S. aureus* adhesion and growth. Our results from the SeNPs non-effectivity to act as antibacterial agent is not unusual, the similar effect has been published previously.[190] We believe, that even if there can be the attraction of negatively charged bacterial membrane to positively charged surface, the SeNPs due to the size and repulsive negative charge cannot penetrate successfully the cell membrane and cause damage. Also, the different membrane composition of gram positive and gram negative bacteria can be more or less sensitive to these surfaces. It has been published previously, that both type of bacteria adhered rapidly on positively charged surface, but with no obvious growth of the gram negative bacteria, which can also correlate with our results.[199] In conclusion, our results highlight the difficulty in understanding the role bacterial cell surface characteristics to the nanoparticle resistance and biomaterial surface properties.

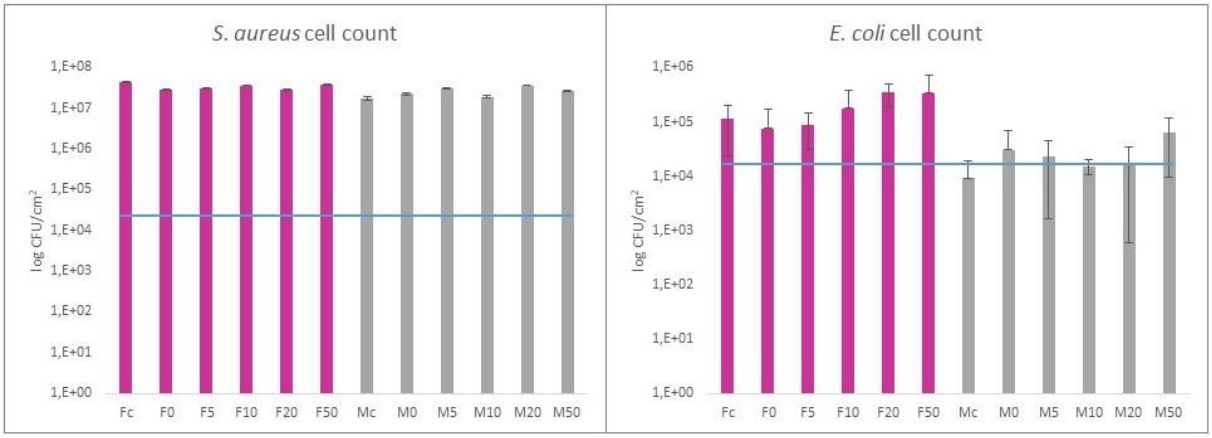

Figure 5 Colony counting method of gram-positive *S. aureus* and gram-negative *E. coli* after 24-hour incubation with the sample. The blue line indicates the initial number of bacteria deposited on the surface area. Fc and Mc means flat and micropillar surface without nanoparticles (control). F0-F50 and M0-M50 means nanoparticle dilution on flat and micropillar surface, respectively.

12.2.4. Viability of MSCs cells on parylene films

The interaction of specific medical surface with mammalian cells is the key factor in the determination of material biocompatibility. A variety of biomaterials designed, for example, to have high antibacterial activity, does not necessarily exhibit cytocompatibility to living cells. Since the nanoparticles like antibiotics can kill bacteria in a certain lower or higher dose, normal mammalian cells exposed to the same concentration of nanoparticles can also be

killed. Therefore, it is important to find some balance between effective antibacterial action and none or low cytotoxicity to normal cells and/or good effectiveness against cancer cells. Moreover, mechanical or physico-chemical micro-/nanostructuring of biomaterial surface have been suggested as the one of key factors determining the cell adhesion, proliferation, differentiation etc.(ref) In our work, we performed XTT test with mesenchymal stem cells to study the viability and proliferation of cells on all prepared surface at the day 1 and day3 (Figure 6). Fig.6A shows significant toxicity of selenium nanoparticle decorated flat parylene films compared to the undecorated parylene "control". The samples with lowest nanoparticle dilutions (1:5 and 1:10) exhibited almost 100% killing efficiency to mesenchymal stem cells even after 24 hours. The cytotoxicity was further confirmed by DIC imaging of MSCs cells by optical microscopy (Figure 7). The morphology of MSCs cells interacting with the flat parylene surfaces of high SeNPs densities (1:5 and 1:10) was mostly rounded shape due to the obvious apoptosis. MSCs cells on lower SeNPs diluted samples looked prolonged in shape and compared to the control sample, not so flattened, rectangular widespread on the surface, which is shown by the DIC contrasting mode. This could be caused by surface chemical and morphological properties inducing some stress in cells. By looking at the micropillar surface (Fig. 6B), we found it was clearly less covered by MSCs cells on SeNPs decorated surfaces. This can indicate lower adhesion preference to such microstructured surface. However, in terms of cell coverage, the microstructured control sample is comparable to flat control. On the other hand, these SeNPs decorated surfaces showed lower cytotoxicity to MSCs cells compared to the flat ones probably due the lower direct exposition of cells to nanoparticles which are also hidden in the interpillar space. Thus, the 1:10 dilution is still favourable to MSCs adhesion and proliferation. Undiluted and 1:5 diluted samples showed mostly cytotoxic effect to MSCs cells accompanied with round unspread cells attached on the surface (Fig. 8). From the 1:10 dilution upwards, the cells were well spread with a mixed prolonged and rectangular shape. MSCs cells on a control sample were rounded widespread cells, which could be attributed to a higher cell density and thus the spatial inhibition. Besides the evaluation of cell shape, we measured the cell surface area on each sample (Figure 9). We did not observe any significant difference in the cell surface area between two groups and both graphs well-corresponded with the morphological visualization captured by optical microscope.

Selenium nanoparticles have been often studied for their anticancer properties. For example, SeNPs showed a dose-dependent antibacterial effect toward Gram-negative and Gram-positive bacteria and a low cytotoxic effect to dermal fibroblasts cells at a range of concentrations up to 1 ppm while showing an anticancer effect toward human melanoma and glioblastoma cells at the same concentration range [189]. Antibacterial properties of selenium nanoparticles and their toxicity to cancerous Caco-2 cells also showed various degrees of toxicity on cells after 24 h of exposure [190]. In our previous work on SeNPs decorated titania nanotubes, we showed enhanced antibacterial properties of nanotubes and toxicity of such surfaces toward both non-cancerous and cancerous cells based on dose dependent

reaction.[192] However, our results on SeNPs-parylene C also showed dose-dependent toxicity to mesenchymal stem cells. To take in the consideration, an intensive optimization and testing of nanoparticle concentration, surface chemistry and morphology must be performed to develop surface with desired properties.

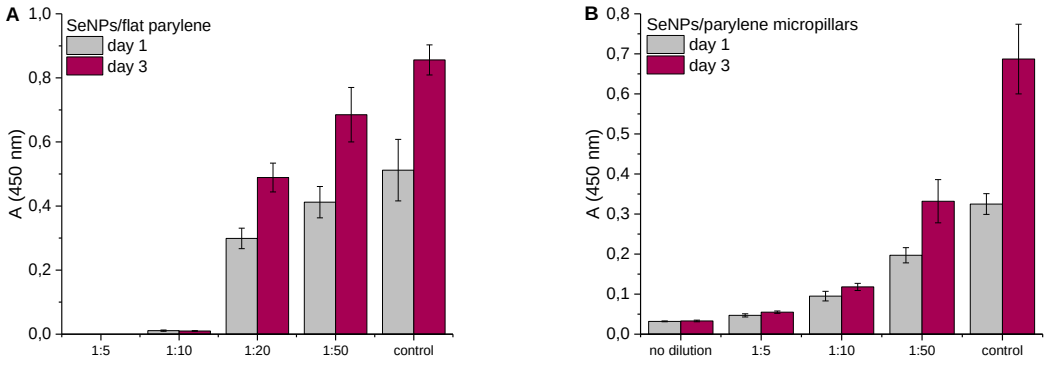

Figure 6 Proliferation assay of MSCs cells on A) selenium decorated parylene flat substrate and (B) selenium nanoparticle decorated parylene micropillars.

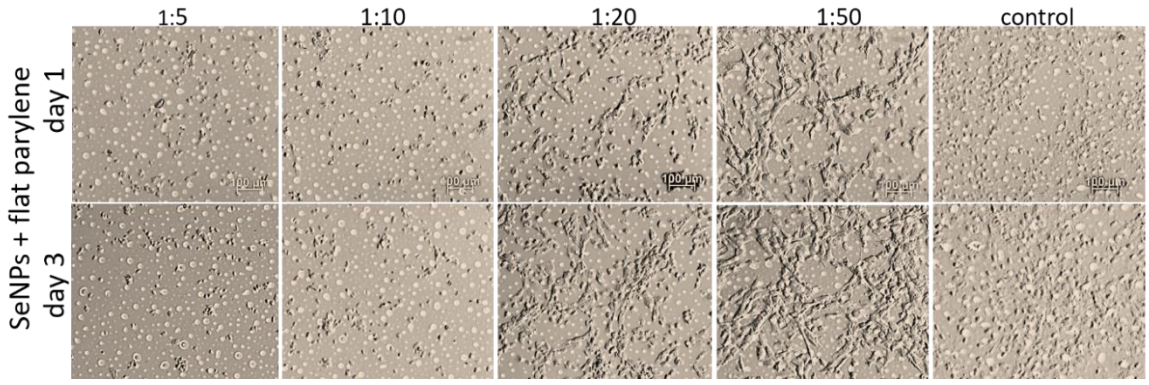

Figure 7 DIC images of adhesion and viability of MSCs cells on selenium nanoparticle decorated flat parylene substrate.

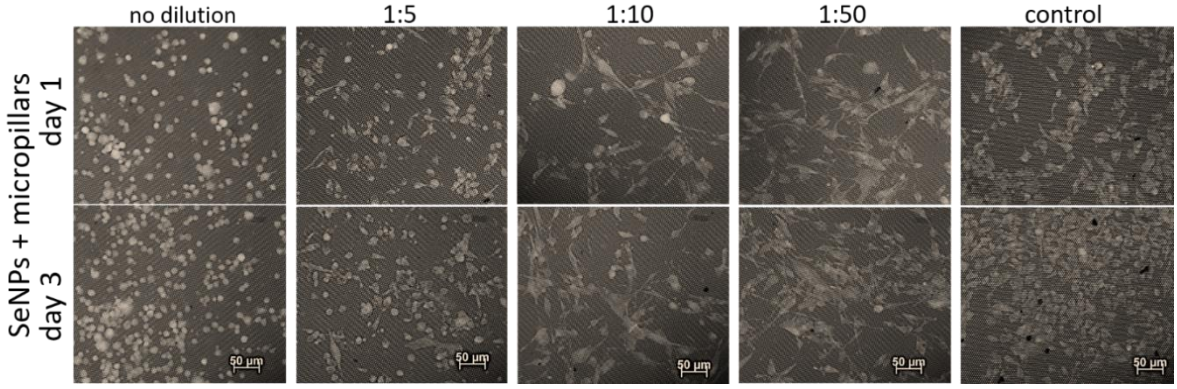

Figure 8 Recoloured fluorescence images of adhesion and viability of MSCs cells on selenium nanoparticle decorated micropillars.

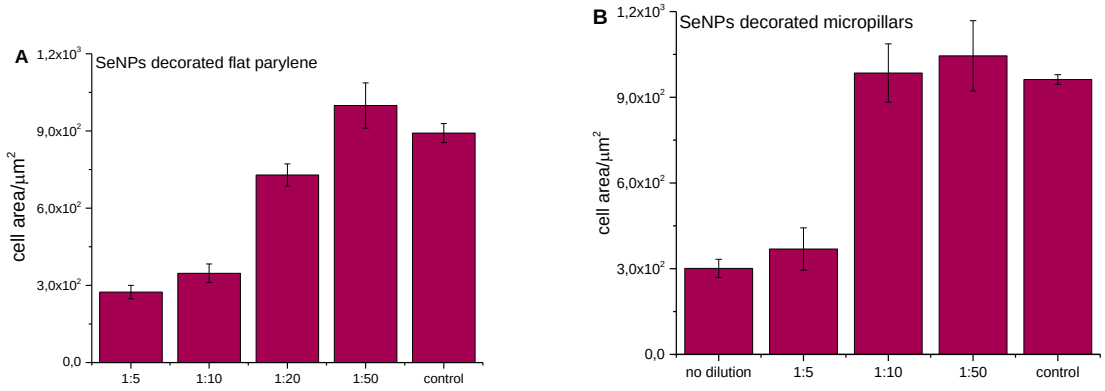

Figure 9 Cell surface area of MSCs cultured on A) selenium decorated parylene flat substrate and (B) selenium nanoparticle decorated parylene micropillars. The surface area was measured at the day1.

12.3. Conclusion

There is growing demand for the investigation and the development of new classes of antibacterial surfaces with high effectivity toward standard and antibiotic-resistant phenotypes of gram-negative and gram-positive bacteria and no toxicity to normal mammalian cells. This can be approached by finding the optimal combination of type of the material, surface chemistry and topography, additional modifications of surface as well as dose dependent utilization of nanomaterials like nanoparticles. Parylene C is widely used polymer in biomedicine, but it suffers from the low antibacterial action. Selenium nanoparticles has been proposed as a promising antibacterial agent due to the nature for the human body. Here we for the first time combine and study synergistic effect of selenium nanoparticles and the parylene C. Moreover, we performed the fabrication of parylene micropillars by plasma etching of parylene to introduced and studied antimicrobial effect and biocompatibility of "microstructured" parylene C. Our results showed almost no antibacterial effect toward *Staphylococcus aureus* while some bacteriostatic effect was observed for *Escherichia coli* on the flat and microstructured parylene, respectively. However, selenium nanoparticles did not show any antibacterial action at all samples in dose dependent experiment. Additionally, mesenchymal stem cells interaction with all designed surfaces showed cytotoxic effect at high selenium nanoparticle concentration. More work must be performed in this topic including the optimization of surface chemistry of parylene, changing the SeNPs nanoparticle size and shape or different micro- and nanotopographical features can be introduced on the surface.

13. Author publications and other outputs

PUBLICATIONS:

BÍLEK, O.; FIALOVA, T.; OTÁHAL, A.; ADAM, V.; ŠMERKOVÁ, K.; FOHLEROVÁ, Z. Antibacterial activity of AgNPs – TiO_2 nanotubes: Influence of different nanoparticle stabilizers. *RSC Advances,* 2020, roč. 1, č. 1, s. 1-10. ISSN: 2046-2069.

BÍLEK, O.; FOHLEROVÁ, Z.; HUBÁLEK, J. Enhanced antibacterial and anticancer properties of Se-NPs decorated TiO_2 nanotube film. *PLOS ONE*, 2019, roč. 1, č. 1, s. 1-9. ISSN: 1932-6203.

BÍLEK, O.; FOHLEROVÁ, Z. *The effect of selenium nanoparticles on antibacterial and cellular properties of titania nanotubes*. CEITEC PhD & Posdoc Retreat Telč 26-27 April 2018 Book of Abstracts. 1. Žerotínovo nám. 617/9, 601 77 Brno, Czech Republic: Masaryk University, 2018. ISBN: ISBN 978-80-210-8943.

ZAHRADNÍČEK, R.; BÍLEK, O.; ZDRAŽIL, L.; SOFER, Z.; LACINA, K.; HUBÁLEK, J.; FOHLEROVÁ, Z. *2D-Dichalkogenide Quantum Dots for Hydrogen Peroxide Sensing*. 2018.

CONFERENCES

PhD Retreat 2018 - Poster - Enhanced antibacterial and anticancer properties of Se-NPs decorated TiO_2 nanotube film

NANOCON 2018 - Co-authored poster - 2D-Dichalkogenide Quantum Dots for Hydrogen Peroxide Sensing

PROJECTS

Interfaculty project “Vývoj citlivého buněčného biosenzoru na bázi nanočástic z 2D materiálů pro elektrochemickou detekci H_2O_2”, FEKT/STI-J-18-5354, fellow researcher

TEACHING

2017/18 FEKT, ABSN

Teaching

2018/19 FEKT, ABSN

Teaching, innovation of the Biosensors and electronics laboratory course, revision of laboratory task instructions,

2019/20 FEKT, ABSN

Teaching, innovation of the Biosensors and electronics laboratory course – workplace schemes, theoretical introductions, added laboratory task – VOC PID, revision of laboratory task instructions, introduction of biosensor-focused thematic group projects

2020/21 FEKT, BPC-BSN

Teaching, Preparation of EN language materials for BSN course, on-line video materials and tests for BSN course